SEABED SCOUR INDUCED BY TWIN-PROPELLER SHIPS

YEW WAN TIAN

FACULTY OF ENGINEERING
UNIVERSITY OF MALAYA
KUALA LUMPUR

2017

SEABED SCOUR INDUCED BY TWIN-PROPELLER SHIPS

YEW WAN TIAN

THESIS SUBMITTED IN FULFILMENT OF THE REQUIREMENTS FOR THE DEGREE OF DOCTOR OF PHILOSOPHY

FACULTY OF ENGINEERING
UNIVERSITY OF MALAYA
KUALA LUMPUR

2017

UNIVERSITY OF MALAYA

ORIGINAL LITERARY WORK DECLARATION

Name of Candidate: Yew Wan Tian

Registration/Matric No: KHA130067

Name of Degree: Doctor of Philosophy

Title of Thesis: Seabed Scour Induced by Twin-Propeller Ship

Field of Study: Water Resources Engineering

I do solemnly and sincerely declare that:

(1) I am the sole author/writer of this Work;
(2) This Work is original;
(3) Any use of any work in which copyright exists was done by way of fair dealing and for permitted purposes and any excerpt or extract from, or reference to or reproduction of any copyright work has been disclosed expressly and sufficiently and the title of the Work and its authorship have been acknowledged in this Work;
(4) I do not have any actual knowledge nor do I ought reasonably to know that the making of this work constitutes an infringement of any copyright work;
(5) I hereby assign all and every rights in the copyright to this Work to the University of Malaya ("UM"), who henceforth shall be owner of the copyright in this Work and that any reproduction or use in any form or by any means whatsoever is prohibited without the written consent of UM having been first had and obtained;
(6) I am fully aware that if in the course of making this Work I have infringed any copyright whether intentionally or otherwise, I may be subject to legal action or any other action as may be determined by UM.

Candidate's Signature Date:

Subscribed and solemnly declared before,

Witness's Signature Date:

Name:

Designation:

ABSTRACT

To date, higher power ships are extensively used in order to fulfil the maritime trading demand. The resulting high velocity thrust produced by ship's propellers or side thrusters has seriously eroded the seabed. Ship-Twin-Propeller (STP) is a ship equipped with two propellers. It has improved powering system, handling system, ship stability, and ability to propel the ship faster as compared to single ships. These advantages have increased the demand for STP among the marine traders for higher profitability and efficiency. This study involves experimental and virtual simulation works. Laboratory experiments were designed to investigate the axial velocity profile of selected rotating STP and the resulting scouring actions; whereas, the Computational Fluid Dynamic (CFD) model simulation was used to observe and estimate scouring pattern. The existing theory and experimental results were mostly derived from plain jet and single rotating propeller. This study has enhanced the understanding on the scour mechanisms and relationships of STP's velocities impingement on the seabed. The asymptotic scour induced by STP profile was defined in four stages, which are (i) initial stage, (ii) developing stage, (iii) merging stage and (iv) asymptotic stage. An equation is proposed to relate between the parameter, namely the densimetric Froude number, the clearance ratio and the reference time scale for the prediction of maximum scour depth and also the maximum scour location. The proposed equations were found to be highly correlated with the observed parameters. Moreover, the proposed CFD and experiment model have given representative data in graphical method to simulate the scouring pattern at different sections for better scour estimation and visualisation. Therefore, it is able to assist design engineers and port authorities in designing the protection structure against scour erosion. Moreover, this will also help in designing the bathymetry level, so that the designed level would be maintained to minimise the dredging or filling sediments costs.

ABSTRAK

Setakat ini, kapal-kapal yang berkuasa tinggi telah digunakan secara menyeluruh bagi memenuhi permintaan perdagangan maritim. Halaju tinggi yang terhasil daripada kipas kapal telah menghasilkan suatu kuasa yang kuat sehingga dapat menghakiskan dasar laut secara serius. *Ship-Twin-Propeller* (STP) yang merupakan sesebuah kapal yang dilengkapi dengan dua buah kipas kapal. Ia menpunyai system penjana yang kuat, pengendalian dan stabiliti yang baik, dan dapat menggerakkan kapal dengan halaju yang lebih cepat berbanding dengan kapal yang dilengkapi dengan satu kipas sahaja. Kelebihan STP ini telah menggalakkan penggunaan STP oleh peniaga-peniaga marin untuk mendapatkan lebih untungan. Kajian ini melibatkan experimentasi dan kerja-kerja simulasi. Experimentasi telah direka bentuk untuk mengajikan profile halaju paksi and corak kerokan yang dikeluarkan oleh STP. Manakala, modal *Computer Fluid Dynamic* (CFD) hanya menumpukan kajian terhadap corak dan penganggaran kerokan yang dijanakan oleh STP. Teori-teori dan keputusan terkini hanya diperolehi daripada kapal yang dilengkapi oleh satu unit kipas sahaja. Oleh itu, kajian ini dapat meningkatkan pemahaman mekanisme dan perkaitan antara halaju yang diperolehi oleh STP atas kerokan yang dibuat atas dasar laut. Profile *asymptotic* yang telah disebabkan oleh STP menpunyai empat peringkat, iaitu, (i) peringkat awal, (ii) peringkat pembangunan, (iii) peringkat penggabungan dan (iv)peringkat *asymptotic*. Suatu persamaan telah dicadangkan atas hubungan antara nombor Froude, nisbah perlepasan dan skala masa yang dirujukan untuk menjangkakan maksima kedalaman korekan dan lokasinya. Korelasi antara persamaan yang dicadangi dengan data-data yang diperhatikan daripada experimentasi adalah tinggi. Cadangan model daripada CFD dan experimentasi dapat memberi corak kerokan yang tepat untuk menganggarkan dan menggambarkan kerokan yang diperolehi oleh STP. Dengan ini, jurutera dan pihak berkuasa perlabuhan dapat merekabentuk struktur perlindungan terhadap kerokan secara efektif dan masalah yang

sedia ada tidak akan merunsing. Selain itu, tahap batimetri pun dapat direkabentukan supaya kos pengorekan dan pengisian sedimen dapat diminimasikan.

ACKNOWLEDGEMENTS

It was a tough and crucial time for me to complete this project in time, within budget and also with quality. However, without all of the supports and guidance from them, I would not have succeeded. Hence, I would like to give a sincere appreciation to them for their helping hands.

I am highly indebted to both my beloved supervisors Professor Dato' Ir' Dr. Roslan bin Hashim and Associate Professor Dr. Ng Khai Ching for their guidance, continuous supervision, provision of necessary information in regards to the project, as well as their financial support (HIR-47 grant) in completing the project from the beginning up to the submission of thesis.

I would like to express my gratitude towards my beloved parents, Yew Chong Hooi and Thun Kooi Lan, for their kind encouragement and moral support which assisted me in the completion of this project without any worries.

I would like to express my special gratitude and thanks to my project colleagues, Mr. Chen Long, Mr. Ng Kai Wern, Miss Cindy Soon, Mrs Aalisha Bhatia and Mr. Termizi for giving me motivation and helping me from zero to the completion of report.

Not to be forgotten, I would like to thank my friends, especially Miss Yeong Li-Lin for assisting and motivating me in order to complete this project.

Last but not least, my thankfulness also goes to all people who have willingly helped me out with their abilities.

TABLE OF CONTENTS

LIST OF FIGURES

LIST OF TABLES

LIST OF SYMBOLS AND ABBREVIATIONS

A	:	Area of cross section $\frac{\pi D^2}{4}$
A_m	:	Maximum scour area
b_o	:	Nozzle hydraulic radius
C	:	Clearance
C_t	:	Thrust coefficient
C_μ	:	Empirical constant
c	:	Chord length
D_h	:	Propeller hub diameter
D_L	:	Initial beam thickness
D_j	:	Jet diameter
D_o	:	Initial diameter of the slip stream.
D_p	:	Propeller diameter
d	:	Particle size
d_{50}	:	Sediment mean size
d_f	:	Fringe separation
E	:	Beam expansion
E	:	Energy
F	:	Lens' focal length
$\vec{F}$	:	Body force
F_g	:	Resulting hydrodynamic lift force
F_o	:	Densimetric Froude number
f_D	:	Doppler frequency
f_{peak}	:	Peak beat frequency
G	:	Weight of single particle

g	:	Gravitational force, $9.81 m/s^2$
H	:	Water depth
h	:	Height of ridge
h_d	:	Helical distance from the blade leading edge to rake datum line
h_t	:	Helical distance from the blade leading edge to the position of maximum thickness
I	:	Turbulent intensity component
k	:	Empirical constant
K	:	Modulus of bulk viscosity
k_{eff}	:	Effective thermal conductivity
L	:	Length of the water line level on the ship
L_m	:	Length term depending on propeller blade area ratio
L_s	:	Scour hole length
m	:	Metre
mm	:	Millimetre
N	:	Number of blades
N	:	Number of propellers
N_f	:	Number of fringe
n	:	Propeller rotational speed in revolutions per second
p	:	Face pitch of propeller blade
Q_m	:	Maximum scour volume
q	:	Water discharge per unit channel width
q_b	:	Bed load discharge per unit channel width
Re_{flow}	:	Reynolds number of flow
R_{ej}	:	Reynolds number
Re_{prop}	:	Reynolds number of propeller

R_h	:	Radius of hub (m)
R_{mo}	:	Position of efflux velocity (m)
R_p	:	Radius of propeller (m)
r	:	Radial distance in the jet measured from the propeller axis
r/R_p	:	Radial distance
s	:	Specific gravity of sediments
T	:	Propeller thrust
t	:	Time variable (s)
t_h	:	Thickness of the section
U	:	Time average velocity, ship's velocity, mean velocity
U_f	:	Undisturbed bed shear velocity
U_{max}	:	Maximum velocity
U_{mean}	:	Root mean square velocity
U_o	:	Efflux velocity
u_x	:	x-component particle velocity
u'	:	x-velocity components
V_A	:	Advance speed of ship
V_D	:	Velocity of fluid
V_{ref}	:	Mean flow velocity
w	:	Width of scour hole
w_r	:	Width of ridge
w'	:	z-velocity components
v'	:	y-velocity components
$\vec{v}$	:	Velocity vector
υ	:	Kinematic viscosity of fluid
X	:	Scour distance from the propeller/jet

X_m	:	Maximum scour distance from the propeller/jet
X_s	:	Scour location
X_w	:	Propeller to quay wall distance
x/D_p	:	Dimensional distance
y_o	:	Offset height, from the centre of propeller to the seabed
Z_b	:	Distance of propeller axis to the fairway bottom
α	:	Volume fraction
α_a	:	Expansion angle
α_s	:	Swirl constant
α^*	:	Coefficient to damp the turbulence viscosity
β	:	Propeller blade area ratio
γ	:	Unit weight of water
γ_s	:	Unit weight of sediment
$\boldsymbol{\epsilon}$	:	Dissipation rate of energy
ε	:	Scour depth
ε_m	:	Maximum scour at any time, unconfined
ε_{ma}	:	Relative unconfined scour depth measured from propeller axis
ε_{mc}	:	Maximum scour at any time, confined
θ	:	Hydrodynamic lift angle
θ_a	:	Angle between two laser beams
θ_{cr}	:	Critical tractive value of Shield parameter
θ_L	:	Angle between two laser beams
θ_s	:	Shield parameter
λ	:	Fringe length
μ	:	Phase viscosity
μ_t	:	Turbulence viscosity

ρ	:	Density of water
ρ_b	:	Bulk density
ρ_d	:	Dry density
ρ_s	:	Density of soil
$\Delta\rho$	:	Difference between density of soil and water
τ	:	Tractive force
τ_c	:	Critical tractive force
φ	:	Angle between the between the direction flow and up flow tangent of downstream of the sediment support
Γ	:	Empirical constant
Ψ	:	Angle of friction
Ω	:	Swirl characteristic
Ω	:	Empirical constant

LIST OF APPENDICES

CHAPTER 1: INTRODUCTION

Overview

The background of study of ship's propeller wash induced seabed scour pattern since it is first study in 1950s, were discussed briefly. Gaps and the need for further studies of ship-twin-propeller are also highlighted in this chapter. The section of problem statement gives an insight on the impact of ship's propeller wash induced seabed scour pattern and the need for remedial actions. The objectives of this study are stated to ensure readers have a clear understanding on what the author wished to achieve. Scope, limitation and significance of study are discussed to give an overview on the details of this study, including its boundary conditions. The importance and needs in investigating on ship-twin-propeller's wash for the design of coastal structures and bathymetry are also highlighted. Nevertheless, brief outline of all chapters in this study are also specified in this chapter.

1.1 Background of Study

To date, ships with higher power are extensively used in order to fulfil the maritime trading demand. The resulting high velocity thrust driven by ship's propellers or side thrusters had produced high erosive power which had significant impact on the seabed.

Ship-Twin-Propeller, in general, refers to a ship equipped with two propellers. It has improved powering system, handling system, ship stability, and ability to propel the ship faster compared to single ship's propeller (Kim et al., 2007). These advantages have increased the demand for ship-twin-propeller among the marine traders for higher profitability and efficiency. By general terminology as stated in Hamill (1987), "wash" is the forces exerted by propellers jet which impinged the seabed and caused scour. Scouring creates negative consequences such as soil erosion in the coastal regions, especially close to the port structures. Therefore, the necessity to identify the

relationship between the jets and the scour formation led to the importance in conducting an experimental research.

The understanding of the fluid flows within the ship's propeller wash and its resulting seabed scouring are key factors in the marine structure and bathymetry designs. Whitehouse (1998) and Gaythwaite (2004) highlighted the potential damages made by ship's propeller wash induced scour in their book. Previous researches such as Hamill (1987), Hamill et al. (1999) and Hong et al. (2013) had discussed on single propeller induced scour. They gave insights into theories and methodologies in predicting maximum scour depth and single ship's propeller jet characteristics by investigating a single rotating propeller. However, there are limited published literature in regards to scour induced by ship-twin-propeller's jets.

This study involves experimental and numerical simulation works. Laboratory experiments were designed to investigate the axial velocity profile of selected rotating ship-twin-propeller and its resulting scouring actions; whereas the CFD model simulation was focused only on the model setup for the observation and estimation of the scour pattern induced by ship-twin-propeller's wash. Both methods were conducted in bollard pull conditions, whereby there was no significant velocity and consequent hull effects. The existing theory and experimental results were mostly derived from plain jet and single rotating propeller. Therefore, in order to acquire accurate results of ship-twin-propeller wash induced scour, large amount of tests are required to examine on various propeller rotating speed and the clearances between the propeller tip and the sediment layer.

1.2 Problem Statement

The size and speed of marine transport have increased tremendously to improve its manoeuvrability in order to transport larger amount of goods around the world. The

usage of ship-twin-propeller becomes common to achieve the design speed for ships, leading to an improvement in ship manoeuvring frequencies. As a result, the risk of scour attacked by ships' propellers wash at ports has inevitably increased. Moreover, the damage due to ships' propeller wash could be maximised when the under keel clearances between the ship and seabed are low. The small keel clearances may cause damages and failures along the coastal structures attributed to the significant impact from ship's propeller wash. Therefore, the seabed scouring theory and the jet velocity distribution from the ship's propeller jet is vital for the estimation of the scouring impacts induced by ship's propellers jet.

Since the past decades, studies on single rotational propeller were initiated after several problems of ship's propellers wash induced seabed scouring had been encountered in the 19th century. A list of affected ports in Europe and United Kingdom, have been summarised by Hamill et al. (1999) as the following,

i. Larne Harbour, Northern Ireland
ii. Stockholm port, Sweden
iii. Elizabeth port, South Africa
iv. French ports, French
v. British ports, United Kingdom

Beforehand, the potential damages of ship's propeller wash were also highlighted in Hamill and Johnston (1993), Whitehouse (1998), and subsequently in Sumer and Fredsøe (2002). Since then, single propeller ships have caused problematic consequences along the coastal line, and more problems are expected as technology advances. The development from single propeller to twin propellers will certainly increase the occurrence of scour if it is not studied and designed for the coastal protection.

To date, data on the scour profile and pattern induced from ship-twin-propeller's jet have yet to be discussed. Only the manoeuvring ability and advantages of ship-twin-propeller were highlighted in literature (Kim et al, 2007; Abramowicz-Gerigk, 2008; Dubbioso and Viviani, 2012). Therefore, due to the advancement of technology, it is essential to study the ship-twin-propeller's wash induced scouring, particularly on its scour pattern, depth and maximum scour location. This study is important in designing the protection system to counter the problems due to the scour erosion induced from ship-twin-propeller's jet.

1.3 Objectives

This study aims to improve the understanding of ship-twin-propeller wash induced scour. We hypothesise that the above problem can be solved by conducting a series of experiment and numerical simulation in order to reveal the insights of scour formation. Therefore, the objectives of current study are stated as below,

i) To identify the source and pattern of axial velocity impinging the seabed which was induced by ship-twin-propeller's wash.

ii) To determine the temporal development of scour induced by ship-twin-propeller's wash by investigating the seabed scouring pattern.

iii) Simulation of seabed scour pattern induced by ship-twin-propeller's wash

1.4 Scope and Limitation of Study

All research works and simulations were done in University of Malaya (UM), Kuala Lumpur. The numerical works were done using CFD software known as Gambit and Fluent. The numerical works were used to study the seabed scour pattern induced by ship-twin-propeller's wash through the Volume of Fluid (VOF) method. The CFD works were then compared with the validated experimental data. The experimental

works were carried out to study the axial velocity profile induced by ship-twin-propeller's wash and the resulting scouring pattern. The axial velocity profiles including the decay profiles and the profile of axial velocity thrust were extracted at efflux plane. Axial velocity was chosen to be studied as it is the most significant force induced by ship's propeller wash (Hamill et al., 1999; Lam et al., 2010). From the literature done by Hamill (1987), Yüsel et al., (2005) and Cihan et al., (2011), the non-cohesive soil type seabed was more vulnerable in reacting with the forces impinging on the seabed. Therefore, only non-cohesive soil was used for both experimental works and numerical simulations. On the other hand, several preliminary tests were completed before the actual experiments in order to ensure the accuracy of the experiment methodologies. A single unit of 2D and 3D ship's propeller induced scour were done using VOF method and compared with experimental works. This was performed to validate the VOF method in the estimation and visualisation of the scour pattern before the accurate simulation was run. The VOF simulation will only give insights on the formed scour pattern and simulate the velocity thrusts washing the sediment layer. Detailed constraints and descriptions of simulation can be referred to Section 3.8.4.

The experiment was carried out in the Hydraulic laboratory in UM. This laboratory is located on the ground floor of UM, which has high pressure water supply required for the water tank filling. However, available space for the allocation of tank in the laboratory was limited to 3.2 m in terms of length and 1.3 m in terms of width. Therefore, the maximum tank size was restricted to length of 3.0 m and width of 1.2 m, where the leftover space was used for the walkway and equipment placing. Consequently, the range of propeller speed, size and the space between two propellers were restricted due to the limitation of the tank size. The range of speed and other parameters used in this study are further discussed in Chapter 3.

1.5 Significance of Study

Results of this study has enhanced the understanding on the mechanisms of the scour formation on the seabed surface, which is important for design engineers and port authorities to design the protection structure against scour erosion. Moreover, the proposed coefficient and equation from the current study will improve the design of protection unit by considering the ship-twin-propeller's wash as one of the key factors in protection design. This also helps in the designation of the bathymetry level, so that the designed level would be maintained in order to minimise the dredging or filling sediments costs. The proposed CFD model and experimental methods will give representative data in graphical method to simulate the different sections of scouring pattern for better scour estimation and visualisation. Therefore, engineers and port authorities will be able to predict the scour impacts induced by ship-twin-propellers in cost and time effective manner.

1.6 Thesis Outline

In this chapter, background of study was presented to provide an overview of the research. The problem statement was discussed thoroughly to further understand the need of the current study. Three objectives were proposed for the current study as outlined in section 1.3. The scope and limitations of this research have also been discussed based on the physical, environmental and technical limitations.

Chapter 2 contains a summary of the previous works that had been carried out by other researchers on the analysis of the characteristics of ship's propeller wash and the resulting scour process which led to severe scour impacts. Findings to date have given insights into theories and methodologies on the estimation of maximum scour depth and the single ship's propeller jet characteristics for situation with and without the present of berth structures.

In Chapter 3, the design of experiment and CFD model were proposed based on previous literature and constrained limitations. Experimental setup has taken into consideration several factors such as the experimental tank design, the ship-twin-propellers design and its locations, the rotational speed as well as clearances between propellers and seabed. For CFD model, the selection of software and the theory of VOF method were discussed. The data acquisition steps were discussed in this chapter to ensure the repeatability of the experiment and CFD model.

Chapter 4 records all the data acquisition results from both experiment and simulation works and all the obtained results were discussed thoroughly. Conclusions and recommendations for future studies were discussed in Chapter 5.

CHAPTER 2: LITERATURE REVIEW

Overview

A rotating ship's propeller draws water, accelerates and then discharges the water downstream to propel a ship. The water discharged with a high velocity flow, which is capable to scour the bed if it is uncheck (Lam et al., 2011b). The scouring action of ship's propeller wash will result in the erosion of seabed sediments. As the manoeuvring activities increases and the under-keel clearances remain small, the erosion of seabed sediments will increase (Hamill, 1987). For example, when the ship moors at the same port or bathymetry with its stern predominantly facing the coastal line, it leads to possible coastal structure failure and even costly remedial works. To date, it is common in practice for ship-twin-propellers to improve the maritime trading efficiency. Therefore it is necessary to improve the understanding of erosive power induced by ship-twin-propeller's wash and the resulting scouring actions, particularly to assist engineers in designing any structures with adequate scour protection towards possible scour areas. In this chapter, works carried out by other researchers on wash produced by plain jets and single propeller's jets are summarised. Literatures revealed that limited amount of published works were done in relation to ship-twin-propeller's wash induced scour.

2.1 Theory of Seabed Scouring: Sediment Transport

Occurrence of seabed scouring is resulted from the transport of seabed sediments by moving water column in combination of two general load modes including: bed load and suspended load. Bed load is known as the soil particles that are moving in contact with the bed in the form of jumping (saltation), rolling and sliding. Therefore, bed load is only able to be transported by the forces exerted on the seabed layer. Suspended load is moved by the water column and is suspended by the turbulence of water. This load

will settle down when the turbulence intensity in the water column decreases. The total load is the sum of bed load and suspended load. Theoretically, there are two main approaches to determine the total load. As stated in Chang et al. (1965), one of it is by computing the bed load and suspended load separately, whereas the other approach is to calculate the sum of total load without computing the bed load and suspended load separately.

Since the ship's propeller wash induced seabed scouring only happens when the under-keel clearance is low, it is expected that sedimentation will be largely transported in the form of bed load. Therefore, bed load theory should be used as the fundamental theory in the determination of sediment transport induced by ship-twin-propeller's jet.

2.1.1 Bed Loads Theories

When the moving water flow exceeds the resisting forces of the sediment particles, the water column will affect the positioning of these sediment particles. Hamill (1987) has described the detachment of a single sediment grain as shown in figure 2.1. The relationship between the moving water and sediment detachment can be obtained through,

$$\frac{F_g}{G} > \frac{\sin(\varphi+\Psi)}{\cos[\theta-(\varphi+\Psi)]} \tag{2.1}$$

Where, F_g is the resulting hydrodynamic lift forces, G is the weight of single particle, θ is the hydrodynamic lift angle, φ is the angle between the direction flow and up flow tangent of downstream of the sediment support and Ψ is the angle of friction of the particle.

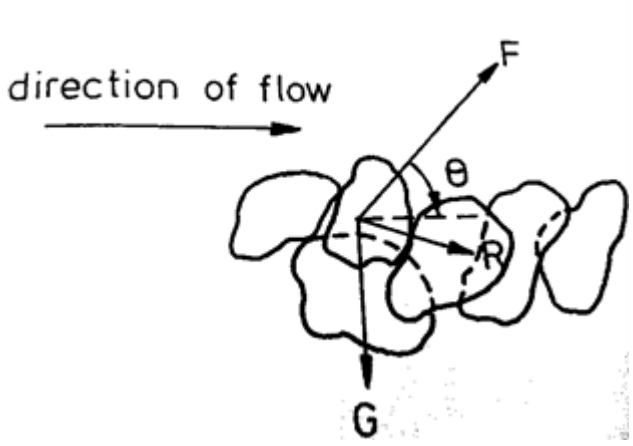

Figure 2.1: Forces acting on cohesion-less grain *(Hamill, 1987)*

Bed load theories are classified according to its calculation methods which are shear stress method and probabilistic method. Shear stress method has been stated in DuBoys (1879), which proposed the equation below to predict the movement of sediment particles along the bed:

$$q_b = \frac{0.173}{d^{\frac{3}{4}}}\tau(\tau - \tau_c) \tag{2.2}$$

Where, q_b is total bed-load discharge in $(ft^3/s)/ft.$, d is particle size in millimetres, τ is tractive force acting along the bed and τ_c is critical tractive force along the bed. The range of τ_c is highly dependent with the type of bed particles, for example, typical fine silt would have a τ_c value of 0.05 N/m^2. DuBoys (1879) equation was obtained through small laboratory flumes with a small range of particle variation, thus the application on field condition remains limited. In later works, equation [2.2] has been further improved by Shields (1936), Kalinske (1947) and Chang et al. (1967). Shield (1936) equation is dimensionally homogeneous and is applicable to any unit systems. Moreover, it is advantageous due to its ability to measure flow conditions with sediment transport greater than zero. The equation proposed by Shield (1936) is written in the form,

$$\frac{q_b\gamma_s}{q\gamma S} = 10\frac{\tau-\tau_c}{(\gamma_s-\gamma)d} \tag{2.3}$$

Where, γ_s is the unit weight of sediment, γ is the unit weight of water. For probabilistic method, Einstein (1942, 1950) has stated two main criteria which are: (i) the critical

criterion for incipient motion is avoided and (ii) the bed-load transport is related to the fluctuation in turbulent flow rather than the average values exerted by the flow on sediment particles. Therefore the beginning and end of sediment motion are expressed in terms of probability.

2.2 The Concept of Scour

Sumer and Fredsøe (2002) has provided an insight on the concept of scour in their works. It was stated that the formation of the scour hole was due to sediment transport. This sediment transport has been modifying the boundary between the land and sea, altering and reshaping the seabed morphology. There are two main categories for seabed scour, which are local scour and global scour. Local scour occurs at a specific area due to sudden change in parameters that are associated to moving water, while the occurrence of global scour is attributed to the combined actions of all parameters formed by all nearby local scours. From previous literature (Blaauw et al., 1978; Hamill, 1987), it has been found that the study of scour development caused by ship propellers is similar to the formation of local scour. Therefore, the concept of local scour should be understood in the determination of sediment transport caused by ship-twin-propeller's jet.

Local scour is classified into two categories:

(i) Clear water scour, and

(ii) Live-bed scour

Clear water scour arises when no sediment motion occurs at the upstream region, which is when the undisturbed Shield parameter, θ_s is less than the critical tractive value of the Shield parameter, θ_{cr}. Shield parameter is defined as $\theta = \frac{U_f^2}{g(s-1)d}$, where U_f is the undisturbed bed shear velocity, g is the gravity force, s is the specific gravity of sediment and d is the sediment grain size. When the undisturbed Shield parameter is

larger than the critical tractive value, the live-bed scour occurs. The examples of scour patterns with functional of time for clear water scour and live-bed scour are shown in Figure 2.2.

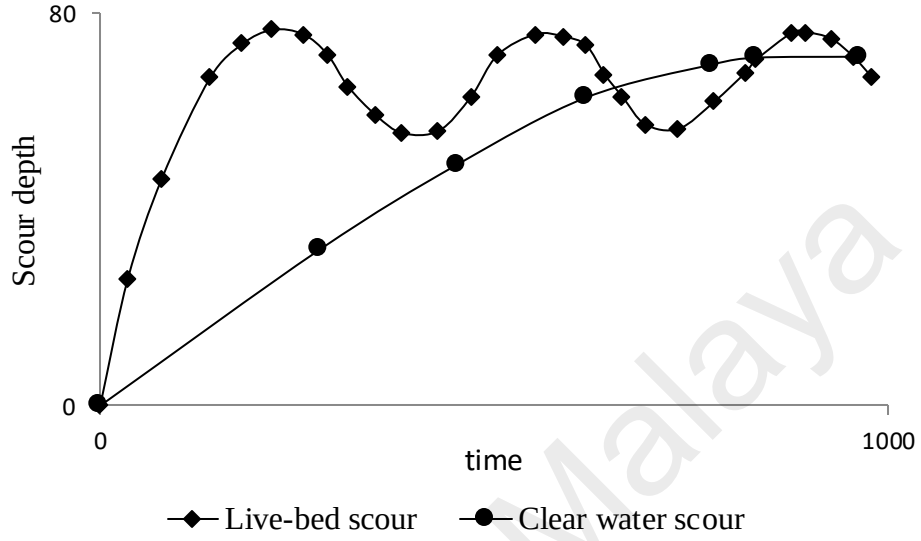

Figure 2.2: Examples of scour patterns with the functional of time

Hamill (1987) highlighted that the clear water scouring action can be further categorised into two periods which are: (i) the concentration of local flow in vertical development of scour hole, and (ii) the concentration of scour size decreased and distributed horizontally. Then, the concentration of local flow remains constant and stabilises the scour profile, until an equilibrium scour profile is reached. Equilibrium scour profile is also known as asymptotic state scour profile, where there is minimal or no changes on the maximum scour depth as compared to the selected previous accurate value (Hamill, 1987). Therefore, the time scale of scour process is important as the scour depth develops with time until it reaches the equilibrium state.

The literature review shown that various studies on the scour analysis by the plain jet and single ship's propeller wash had been carried out. However, there is no study on scouring actions induced by ship-twin-propeller's jets.

2.2.1 Scour from Plain Jet

Scour from plain jet consider the flows under barriers or gates, these flows have high potentials to cause scour due to its high velocity thrust and turbulent intensity flow. Plain jets exert a two-dimensional flow, which are generally being classified into wall jets and surface jets. Hoffmans and Verheij (2011) defined wall jets as jets with the characteristics of high near-bed velocities and high turbulence intensities, whereas surface jets have the characteristics of low near-bed velocities. The summary of the different jet forms is shown in Figure 2.3.

The process of the jet scour cycle is also described in detail by Balachandar et al. (2000) as shown in Figure 2.4. This cycle indicates the beginning of the scour, followed by the digging process induced by the jet velocity flow. As it achieves the maximum digging level, the filling phase begins and continues up to the maximum filling level. The whole process is repeated until the scour formation reaches the equilibrium state.

Mohamed and McCorquodale (1992) identified the two stages of local scour caused by wall jets, which are: (i) short term scour that occurs rapidly at the initial stage and (ii) long term scour that occurs progressively after a long duration. They found that the short term scour is associated with regimes of attached jet, moving jump, wave jump and inverted jump, whereas the long term scour is associated with surface jet and plunging jump.

The scour parameters that govern the scour process from the wall jet had been clearly described by Sui et al. (2008), as shown in Figure 2.5. The given description on the scour parameters are: b_o is the nozzle hydraulic radius divided by 4, ε_m is the maximum scour depth, x_m is location of maximum scour depth, L_s is the scour hole length, H is the depth of water, h is the height of ridge, w is the width of scour hole and w_r is the width of ridge.

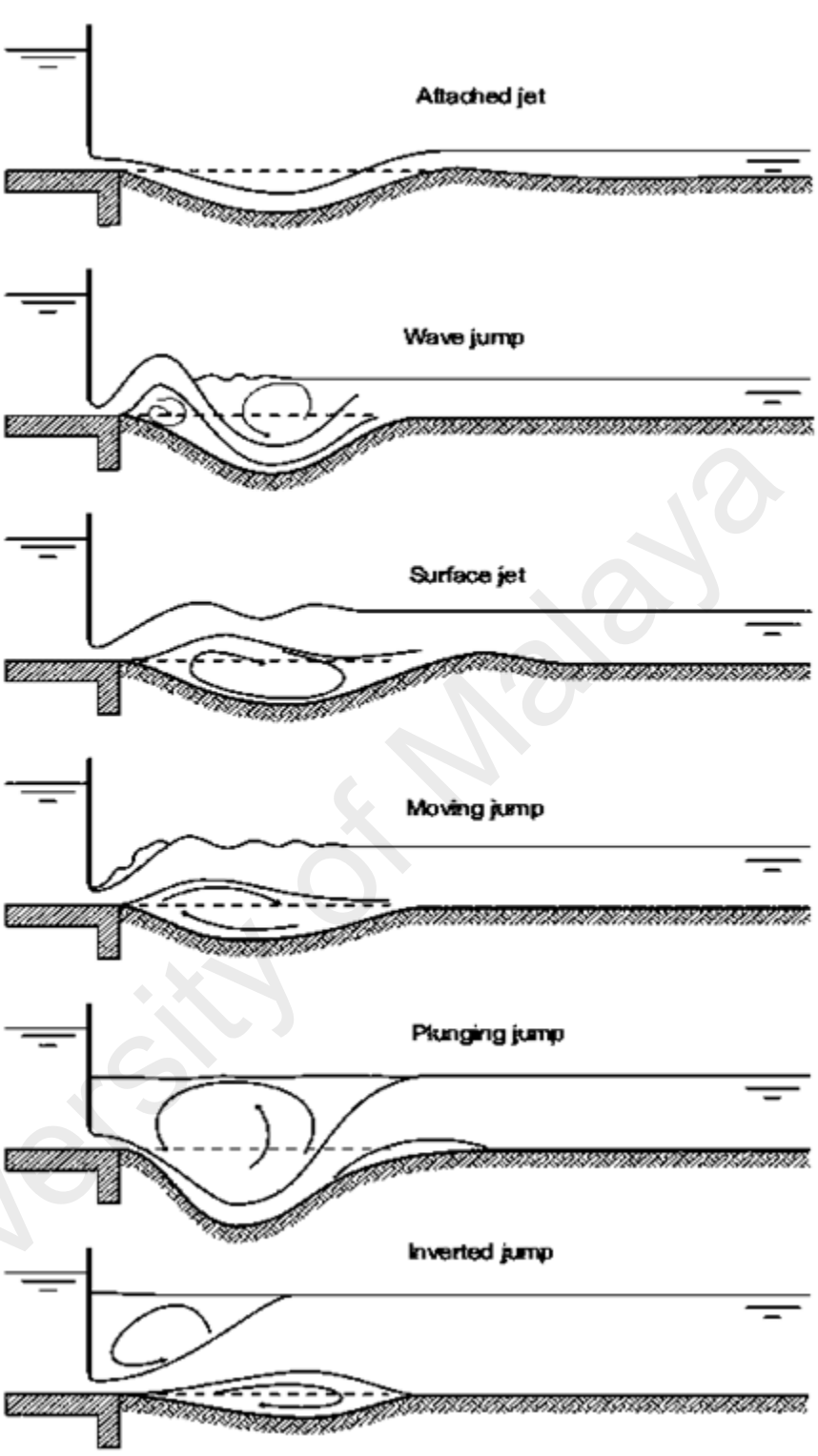

Figure 2.3: Different jet forms (a)attached jet; (b)wave jump; (c)surface jet; (d)moving jump; (e)plunging jump and (f)inverted jump *(Hoffmans and Verheij, 2011)*

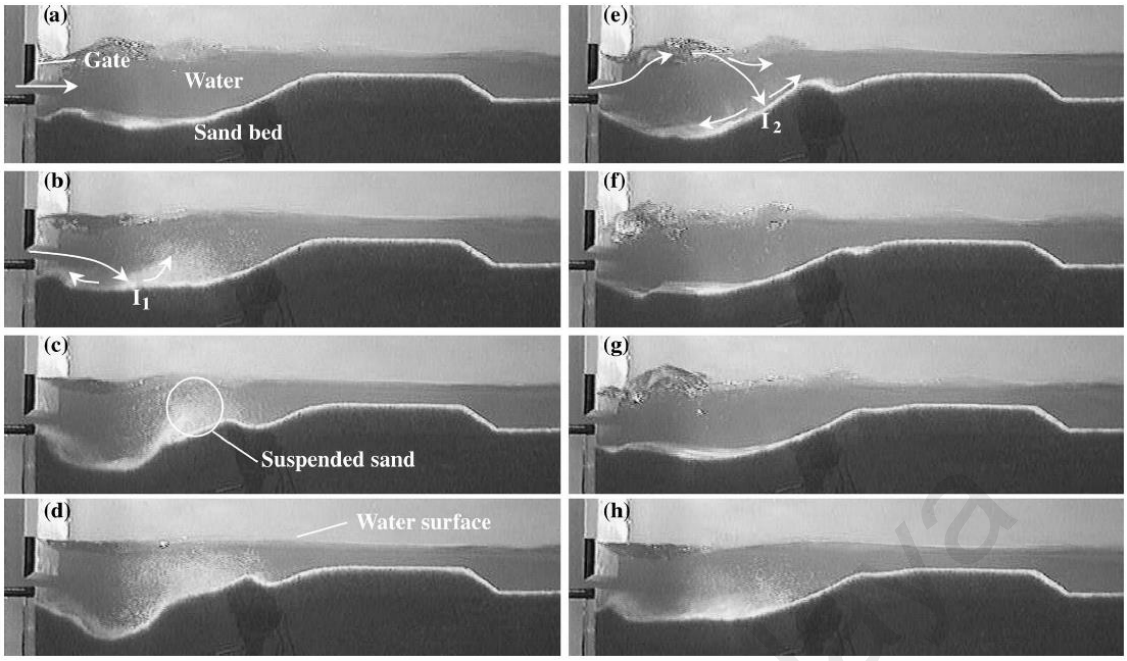

Figure 2.4: Process of the jet scour cycle: (a) scour begins; (b) digging phase commences; (c) digging continues; (d) maximum digging; (e) filling phase begins; (g) maximum fill; (h) reoccurrence of digging phase. *(Balachandar et al., 2000)*

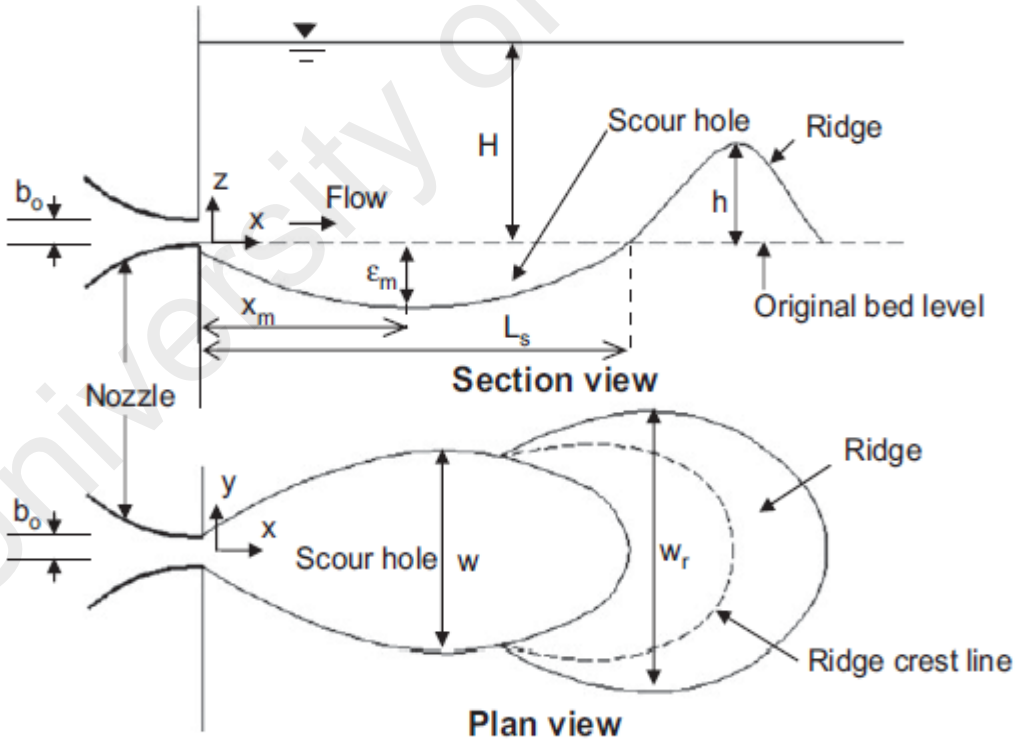

Figure 2.5: Geometry for scour induced by wall jet *(Sui et al., 2008)*

2.2.2 Scour Induced by Single Propeller

The scour from single propeller is relatively similar to plain jet, but the consideration on the direction of forces has been increased from two-dimensional to three-dimensional. The additional dimensional force input for single rotating propeller jet increased the complexity of scour analysis as compared to wall jets. Researchers have done their work in analysing the single ship's propeller wash induced scour which require methodologies with higher complexity as compared to plain jet. Early works by Blaauw et al. (1978), Verhey et al. (1987) and Hamill (1988) initiated the investigations of scouring action on fine sand induced by single ship's propeller wash for the port location without the present of berth structures. Hamill et al. (1999) also extended his studies and presented the scouring patterns on propeller wash scour near quay wall.

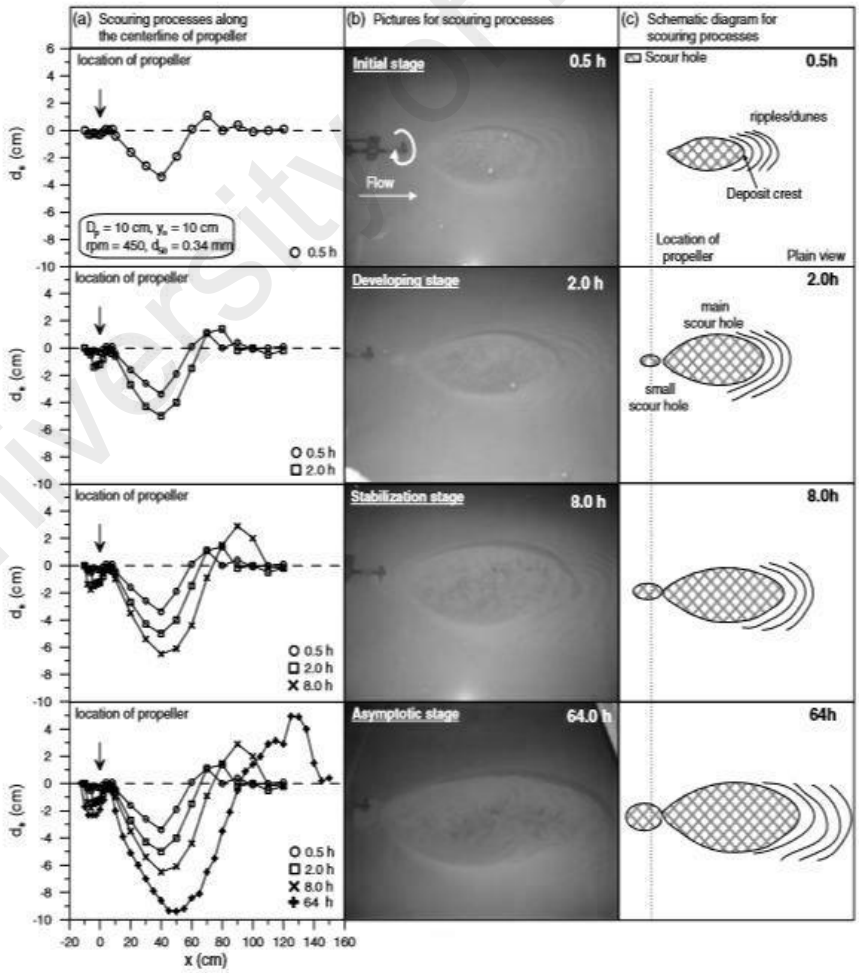

Figure 2.6: Scour pattern induced by single ship's propeller wash *(Hong et al., 2013)*

To date, Hong et al. (2013) investigated the development of scour hole using a rotating ship's propeller jet through the experimental works and proposed the scour patterns as shown in Figure 2.6. Hong et al. (2013) divided the development of scouring profile into four stages, known as: (i) initial stage, (ii) developing stage, (iii) stabilisation stage and (iv) asymptotic stage. The asymptotic scour profile, which is the final scour profile, comprises a small scour hole beneath the propeller, a primary scour hole and the deposition mound. Andrew (2013) also investigated the single ship propeller geometry measured by the point gauge manually using a coordinate system. This geometry is useful for the repetition of experiment. The 14 survey characteristic scour points have been labelled from P1 to P14, as stated in Figure 2.7.

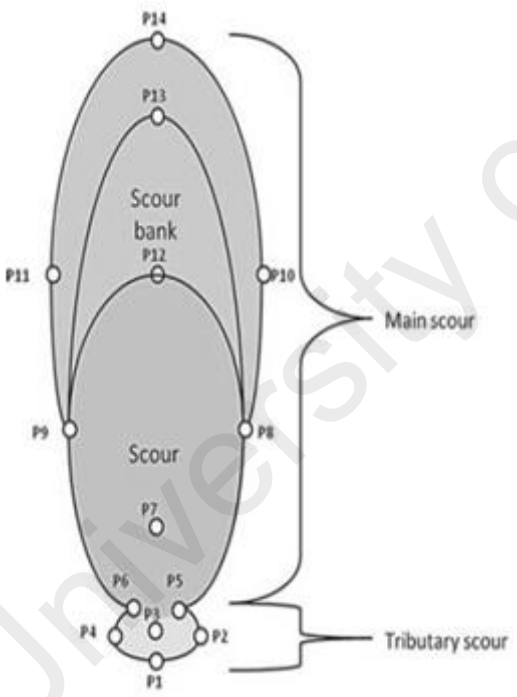

P1:Start of tributary scour
P2: Port side of tributary scour
P3: Deepest point of tributary scour
P4: Starboard side of tributary scour
P5: Port side of transition to main scour
P6: Starboard side of transition to main scour
P7: Scour depth
P8: Beginning of scour ridge (port side)
P9: Beginning of scour ridge (starboard side)
P10: Port side of scour ridge
P11: Starboard side of scour ridge
P12: Beginning of scour ridge
P13: Scour ridge height
P14: End of scour ridge

Figure 2.7: Scour geometry from a single ship's propeller jet *(Andrew, 2013)*

On the other hand, Johnston et al. (2013) proposed that there are different scouring zone, which are: (i) the zone prior to jet impact, (ii) the zone of boundary layer development and (iii) the zone of developed boundary layer flow. The zone prior to jet

impact is more vulnerable to ship's propeller wash due to the higher expansion rate of the bottom stream of a propeller jet as compared to the upper stream. Therefore, an increase in the clearance height will result in an increase in expansion angle, α. The expansion angle was derived and proposed by Johnston et al. (2013) based on the clearance, C, as shown below,

$$\alpha = 66 \times 10^{-3} C + 8.3 \tag{2.4}$$

The figure of three zones indicated by Johnston et al. (2013) is shown in Figure 2.8. Although there are many works in regards to the investigation on scouring actions of single ship's propeller wash, there is limited works related to scouring actions of ship-twin-propeller's wash. As such, further research is required.

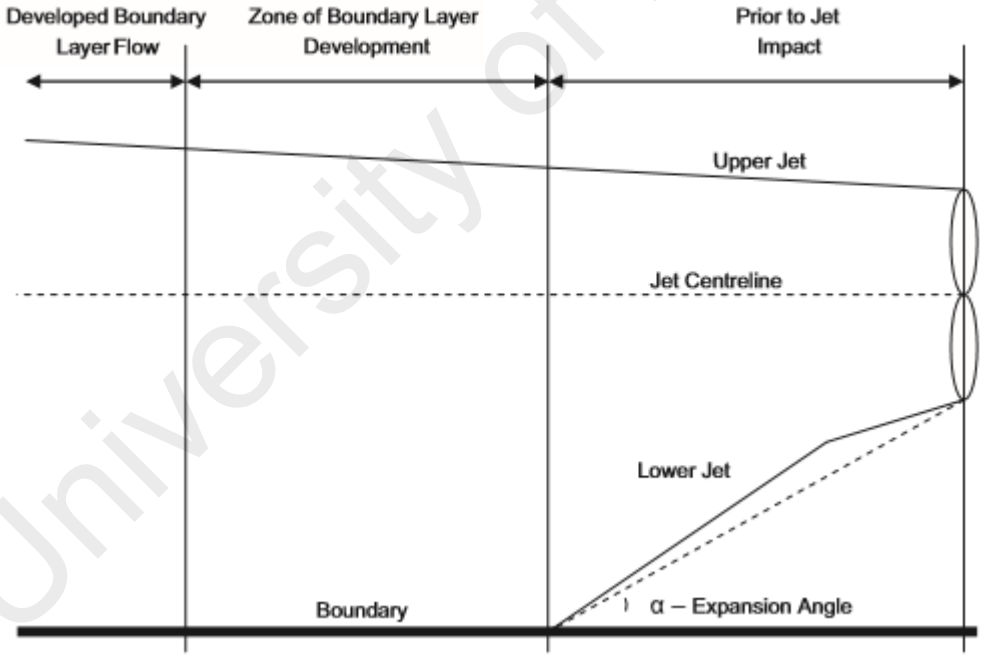

Figure 2.8: Boundary zone of propeller jet expansion *(Johnston et al., 2013)*

2.2.3 Hyper-concentrated Flow

When the ship docks at the port, it is usually near bollard pull condition, which resulted in low clearance depth between the ship's propeller and the seabed. Thus, this condition prepared a shallow water aspect in analysis which will be eventually causes

the occurrence of hyper-concentrated flow, as firstly mentioned and defined by Pierson (2005). According to Pierson (2005), hyper-concentrated flow is the mixture of water and sediments flow where water flow remains as the main driving forces for the push of sediment transport. Hyper-concentrated flow does not process characteristics of non-Newtonian flow e.g. high viscosity fluid. As such, the sediment transportation process induced by ship propeller's wash is considered as a hyper-concentrated flow.

2.3 Maximum Scour Depth and Scour with Functional Time Model

Modelling time scale of maximum scour depth has been established and proposed by previous researchers. Research works in the past decades were summarised by Sumer and Fredsøe (2002). The model time scales for maximum scour depth focused on the scour around the piles, pier structures, and pipeline. However, works related to the model time scale of ship-twin-propeller's wash induced scour are limited.

Early works on establishing the functional time model in finding the maximum depth of plain jet scour has been stated in Rajaratnam and Berry (1977). Rajaratnam and Berry (1977) proposed the dimensional equation of maximum scour depth in any time through,

$$\frac{\varepsilon_m}{d} = f_1\left[F_o, \frac{U_o d}{v}, \frac{D_p}{d_{50}}\right] \tag{2.5}$$

Where, $F_o = \frac{U_o}{\sqrt{gD\frac{\Delta\rho}{\rho_s}}}$ is a densimetric Froude Number. The densimetric Froude number, Fo, is considered as the most significant factor in affecting the maximum scour depth (Hamill, 1987; Hamill et al., 1999; Hong et al., 2013). Further details on the evaluation of F_o are discussed in Chapter 3 and 4. Moreover, they concluded that the effect of fluid viscosity on the growth of jet can be neglected, if the Reynolds number of jet, [$\frac{U_o d}{v}$] is larger than $1x10^4$. Thus, equation [2.5] can be reduced to,

$$\frac{\varepsilon_m}{d} = f_2\left[F_o, \frac{D_p}{d_{50}}\right] \tag{2.6}$$

The asymptotic state of scour profile was plotted with ($\frac{\varepsilon}{\varepsilon_m}$) versus ($\frac{X}{X_m}$) and a sine curve was obtained in good agreement to the actual scour geometry.

Verhey (1983) then studied the scour depth, scour area and scour volume based on the approach adopted by Rajaratnam (1981) in his studies on circular water jets. Three corresponding equations on scour depth, area and volume, have been proposed with limited range of $0.1m<d_{50}<0.3m$,

$$\frac{\varepsilon_m}{Z_b} = 4x10^{-3}\left[\frac{F_o}{Z_b/D_p}\right]^{2.9} \tag{2.7}$$

$$\frac{A_m}{Z_b^2} = 9x10^{-3}\left[\frac{F_o}{Z_b/D_p}\right]^{3.9} \tag{2.8}$$

$$\frac{Q_m}{Z_b^2} = 8x10^{-6}\left[\frac{F_o}{Z_b/D_p}\right]^{6.8} \tag{2.9}$$

Where, Z_b is the distance of propeller axis to the fairway bottom and D_o is the initial diameter of the slip stream. Moreover, Verhey (1983) also suggested that the scaling effect due to viscosity were negligible if Reynolds number for both propellers and flow were larger than 7×10^4 and 3×10^3, respectively. The Reynolds number for both propellers and flow can be calculated in the form of:

$$Re_{prop} = \frac{nD_p L_m}{v} \tag{2.10}$$

$$Re_{flow} = \frac{V_o D_p}{v} \tag{2.11}$$

Later works including Hamill (1988), Hamill et al., (1999) and Hong et al., (2013) proposed the maximum scour equation based on single rotating propeller. Hamill (1988)

first proposed the dimensional analysis for maximum scour depth by considering the efflux velocity, $U_o = nD_p\sqrt{C_t}$ (Blaauw et al., 1978), which can be written as follows:

$$\frac{\varepsilon_m}{D_p} = f_2\left[F_o, \frac{D_p}{d_{50}}, \frac{C}{d_{50}}\right] \tag{2.12}$$

Hamill (1988) indicated that the maximum scour depth profile is dependent on the three main characteristics: (i) the densimetric Froude number; (ii) the ratio of propeller diameter to mean sediment size; and (iii) the ratio of clearance to the mean sediment grain size. Hamill (1988) also proposed the logarithmic function of time for the maximum scour depth profile where the time, t is in seconds, the resulting scour depth in millimetres, mm, U_o in millimetres per second and d_{50}, D_p and C in metres. It is shown in the form of,

$$\varepsilon_m = \Omega[\ln(t)]^{\Gamma} \tag{2.13}$$

where,

$$\Gamma = 4.113\left(\frac{C}{d_{50}}\right)^{0.742}\left(\frac{D_p}{d_{50}}\right)^{-0.522} F_0^{-0.682}$$

$$\Omega = 6.9\text{x}10^{-4}\left(\frac{C}{d_{50}}\right)^{-4.63}\left(\frac{D_p}{d_{50}}\right)^{3.58} F_0^{4.535}$$

Hamill et al., (1999) then improved his proposed equation [2.13], by considering a constant value of k=38.97 and two new correlations for the parameters of Ω and Γ. However, the improved equation is limited to the range of $0.5D_p<C<2.5D_p$ of unconfined condition, which is written as follow:

$$\varepsilon_m = k\Omega[\ln(t)]^{\Gamma} \tag{2.14}$$

where,

$$\Gamma = \left(\frac{C}{d_{50}}\right)^{0.94}\left(\frac{D_p}{d_{50}}\right)^{-0.48} F_0^{-0.53}$$

$$\Omega = \Gamma^{-6.38}$$

Hamill et al. (1999) also proposed an equation to determine the distance from propeller to maximum scour depth for unconfined wash, X_{mu}, which has regression, R^2 of 0.99.

$$X_m = F_o^{0.94} C \tag{2.15}$$

On the other hand, Hamill et al. (1999) studied on the scouring action by propeller wash in the confined condition. It was found that the confined condition has developed the same profile with the unconfined condition, but with the consideration of additional erosion near the wall. Therefore the confined scour profile calculation is the sum of unconfined scour profile and erosion near wall. This indicates that the confined scour profile has larger scour impacts compared to unconfined scour profile. Hence the proposed confined scour equation after taking into consideration the distance between propeller and quay wall in unit meter(s) can be obtained through:

$$\frac{\varepsilon_{mc} - \varepsilon_m}{\varepsilon_{ma}} + 1 = 1.18\left(\frac{X_w}{X_m}\right)^{-0.2} \tag{2.16}$$

However, unconfined scour profile remains as the key factor to observe and identify the erosive power of ship's propeller wash. In order to identify the ship-twin-propeller's wash, studies on unconfined scour profile should be conducted. Hong et al. (2013) estimated the time dependent maximum scour depth by considering the offset height ratio, $\frac{y_o}{D_p}$. The proposed equation is limited to the offset height ratio of $0.5 < \frac{y_o}{D_p} < 2.87$ and densimetric Froude number of $5.55 < F_o < 11.1$, written in the form of,

$$\frac{\varepsilon_m}{D_p} = k_1\left[\log_{10}\left(\frac{U_o t}{D_p}\right) - k_2\right]^{k_3} \tag{2.17}$$

where,

$$k_1 = 0.014F_o^{1.120}\left(\frac{y_o}{D_p}\right)^{-1.740}\left(\frac{y_o}{d_{50}}\right)^{-0.170}$$

$$k_2 = 1.882F_o^{-0.009}\left(\frac{y_o}{D_p}\right)^{2.302}\left(\frac{y_o}{d_{50}}\right)^{-0.441}$$

$$k_3 = 2.477F_o^{-0.073}\left(\frac{y_o}{D_p}\right)^{0.53}\left(\frac{y_o}{d_{50}}\right)^{-0.045}$$

Where, k is the empirical constants proposed by Hong et al., (2013). Findings to date exhibited the works on jet scour and single ship's propeller wash induced scour, but no conclusion has been drawn on the rate of development of ship-twin-propeller wash induced scour. Hence, this study will focus on the ship-twin-propeller wash induced scour. Moreover, since seabed scouring actions are highly dominated by the velocity from the propeller wash, the theory of the ship propeller velocity distribution will be investigated in order to provide a sound basis for the development of scouring actions from ship-twin-propeller wash.

2.4 Theory of Ship's Propeller Velocity Distribution

Whitehouse (1998), Sumer and Fredsøe (2002) and Gaythwaite (2004) emphasised the need of investigation on velocity distribution of ship's propeller jet as the initial step to predict the scouring impacts by the ship's propeller jet. The investigation on velocity distribution of plain jet was initiated by Albertson et al. (1950). The investigation was based on the fundamental of Axial Momentum Theory, which was proposed by Froude with reference to Rankine's investigation in 19th century. As a result, the Axial Momentum Theory became the fundamental of all subsequent works related to the investigation on velocity distributions of plain jets and later for ship's propeller jets.

Several researchers have used the actual rotating ship's propeller to compensate the limitation on the investigation of plain jet. However, limited works were reported on ship-twin-propeller's manoeuvring ability and velocity distribution profile of ship-twin-propeller jets at the cross section of ship (Kim et al, 2007; Abramowicz-Gerigk, 2008; Dubbioso and Viviani, 2012; BAW, 2010; PIANC, 2015). Since the principle of rotating ship-twin-propeller jets is similar to rotating single propeller jet, the fundamental of plain jets and single ship's propeller jet will be reported.

2.4.1 Plain Jet

The velocity distribution of a plain jet was investigated by Albertson et al. (1950) using a plain water tube with assumptions of axial momentum theory. As consequence, the characteristic of ship's propeller using a plain jet is proposed based on the following assumptions:

(i) The propeller is represented by an ideal actuator disc of equivalent diameter as shown in figure 2.9.

(ii) The disc consists of an infinite number of rotating blades, rotating at an infinite speed.

(iii) There is negligible thickness of the disc in the axial direction.

(iv) The disc is submerged in an ideal fluid.

(v) All elements of fluid passing through the disc undergo pressure that increases at an equivalent rate.

(vi) The energy supplied to the disc is, in turn, supplied to the fluid without any rotational effects being induced.

Figure 2.9 shows the propeller represented as an actuator disc. The upstream of the velocity and pressure are represented by V_A and P_A respectively. A minimum distance between section *A* and *D* is required to allow the occurrence of uniform and axial flow. As the flow approaches the propeller disc at section *B*, acceleration occurs at the

upstream side of the disc due to the reduction of pressure at *B* (P_B). The negligible thickness of the disc causes the velocity at section *B* (V_B) and *C* (V_C) to be equal. This leads to the energy supplied to the system when the fluid passes through the disc and enter into Section *D*. As a result, the Bernoulli's equation cannot be applied between Section *B* and *C*. However, Bernoulli's equation can be applied between section *A* and *B*, as well as between section *C* and *D*. The changes of momentum due to the disc have resulted in a net thrust of the fluid. Based on the expression of this thrust, equations for the velocities predictions have been developed by several authors, and are further discussed in section 2.4.4.1. In Figure 2.9, *P* represents pressure and *V* represents velocity.

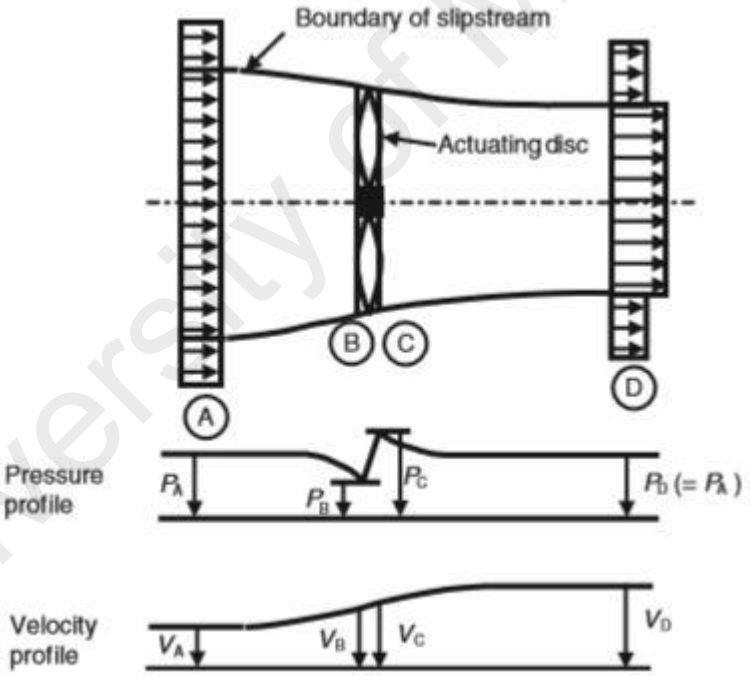

Figure 2.9: Ideal actuator disc representing propeller *(Hamill et al., 2004)*

2.4.2 Limitation of Axial Momentum Theory

The axial momentum theory, which is also known as Froude's number theory, has its limitations on the applicability for analysing a ship's propeller jet. Hamill et al. (2004) highlighted the inadequacies of the application of the axial momentum theory as follows:

(i) The propeller is idealised as a disc with an infinite number of blades rotating at an infinite speed, which does not agree with the propeller design. The propeller is normally designed with three to six blades, and the speed of rotation is carefully chosen to provide the maximum efficiency when in service.

(ii) It is not practical to have the disc which has negligible thickness in axial direction. The propeller must have a pitch in its plane in order to meet the operational efficiency.

(iii) The disc is approximately same on either side is incorrect, with sizable differences (in order of a factor of 20) being measured by Hamill et al., (2004).

(iv) The assumption of "pressure increases at an equivalent rate" is invalid. The blades on a ship's propeller have significant pressure changes in both pitch and area within a three-dimensional space.

(v) The assumption on "without any rotational effects being induced" is also flawed. The three-dimensional profile of the blade produces three directional velocity components, namely axial, radial and tangential velocity components.

These shortfalls in the theory have led to several modifications to the theoretical efflux equation in an attempt to consider the propeller characteristic (Hamill et al., 2004). Thus, further investigation on the calculation of efflux velocity forces induced by single ship's propeller jet has been carried out by several researchers, and the propeller characteristics were taken into consideration. The semi-empirical equations were proposed to compensate the flaws of existing theories, which is discussed in section 2.4.4.2.

2.4.3 Differences between the Phrases: Zone of Flow Establishment and Zone of Established Flow

Albertson et al. (1950) suggested categorising the flow of a ship's propeller jet into two distinct zones: (i) a zone of flow establishment and (ii) a zone of established flow, as shown in Figure 2.10. The schematic view of zone of flow establishment from an orifice jet is shown in Figure 2.11. It is assumed that a potential wash exists within the zone, while the efflux velocity of jet maintained (V_{max}=V_o). The lateral section of potential central core diminishes due to the velocity discontinuity of the jets and surrounding fluid. Thus, the lateral mixing progress is continuously decelerating the fluid flow of the jet, while the overall breath of the jet increases. The overall breath continuously increases until the mixing process penetrates the centreline of the jet. The flow of jet becomes stable when it reaches the zone of established flow.

The schematic view of zone of established flow from an orifice jet is shown in Figure 2.12. From the previous zone, zone of flow establishment, the contraction which was due to turbulent mixing between the potential core and the surrounding fluid, caused the decay in velocity. In this zone, the maximum velocity began to decay along the rotation axis (V_{max}<V_o). This diffusion process continues without any essential changes in character (Steward et al., 1991). Subsequently, the surrounding fluid balances along with the reduction of jet velocity. Moreover, the plain water jet is asymmetrical with the entire jet, which resulted in the plain water jet being mirrored along the central axis (Hamill, 1987). Albertson et al. (1950) also reported that the angle of diffusion in the zone of established flow is larger than the angle in the zone of flow establishment. Further investigation carried out by Brewster (1997) reported that the differences of the angle may be due to the varied diffusion process within these two zones.

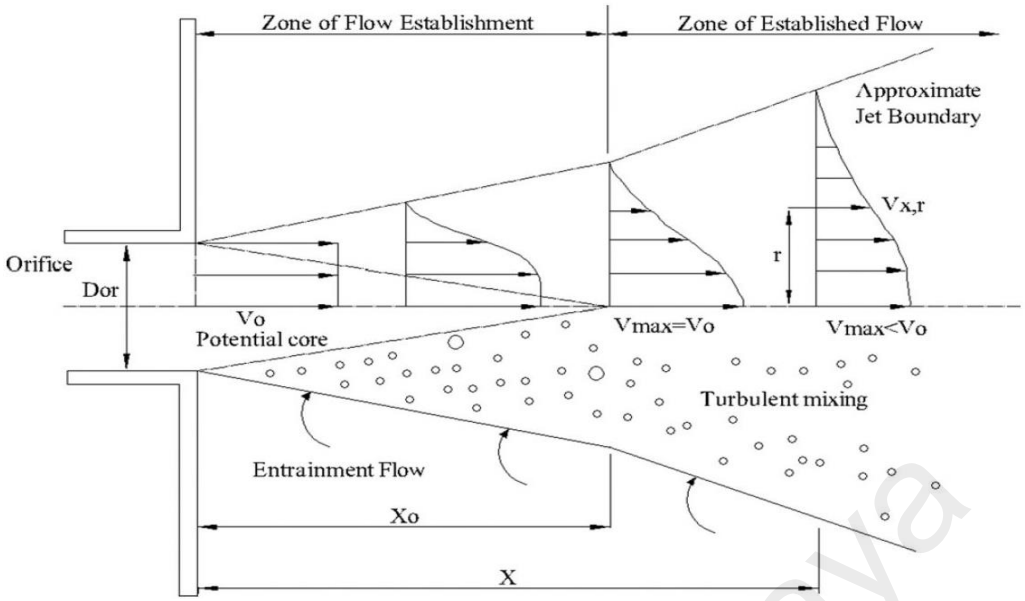

Figure 2.10: Schematic view of two zone flows from an orifice jet *(Albertson et al., 1950)*

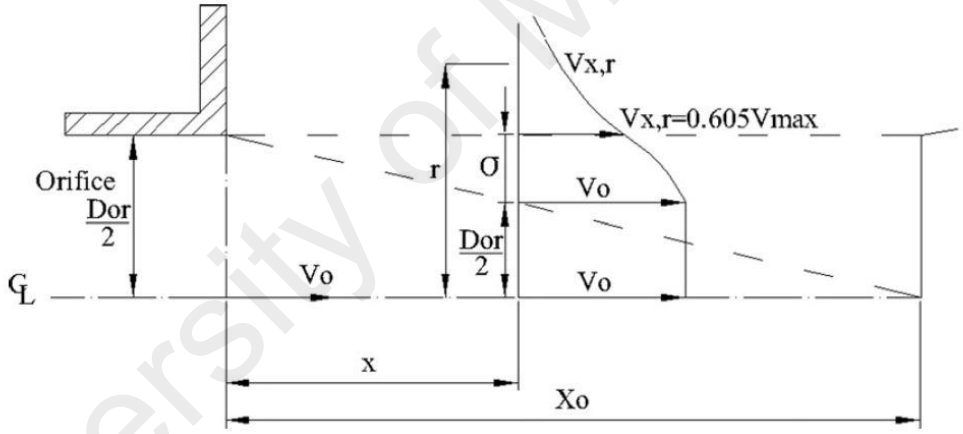

Figure 2.11: Schematic view of zone of flow establishment from an orifice jet *(Albertson et al., 1950)*

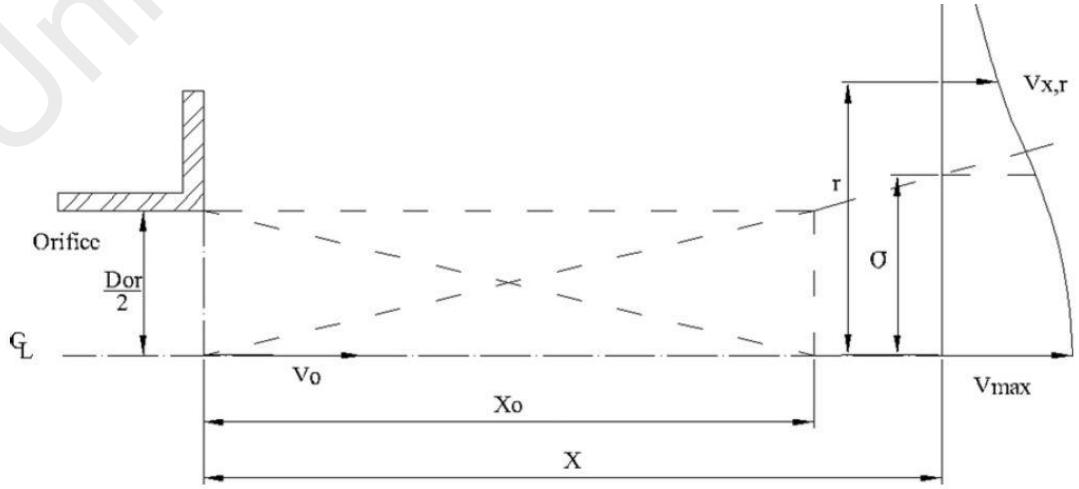

Figure 2.12: Schematic view of zone of established flow from an orifice jet *(Albertson et al., 1950)*

The fundamental theory of the characteristic of these two zones has improved the understanding on velocity distributions of the ship's propeller jet induced scour. This theory is important especially in predicting the occurrence of maximum velocity (efflux velocity), which leads to the prediction on maximum scour depth. It is therefore believed that the maximum scour depth will occur at the zone of flow establishment, based on Figure 2.11. Thus, the zone of flow establishment will be given high attention in the prediction of efflux velocity of ship-twin-propeller wash in current study.

2.4.4 Single Ship's Propeller Jet

Ship's propeller jet has a complex flow field which induced high velocity jet while its hull induced turbulent wakes (Hamill, 1987). Moreover, Prosser (1986) highlighted that the effect of ship's propeller geometry on the propeller jet is insignificant when the ship is stationary or manoeuvring at low speeds. The investigation of ship's propeller wash has been developed thoroughly from the investigation of plain jet to a three-dimensional propeller. A few researchers have highlighted on the prediction of axial, radial and tangential velocity of components, which is discussed in the following sections.

2.4.4.1 Efflux Velocity Based On Axial Momentum Theory

Efflux velocity is the maximum velocity induced by ship's propeller jet in the axial direction. Lam et al., (2010) indicated that the efflux velocity is the main contributor to velocity magnitude. Therefore, due to the large contribution made by axial velocity towards the seabed scouring, other earlier researchers were solely interested in research on axial velocity. Fuehrer and Römisch (1977) mentioned that efflux velocity (U_o) is the maximum velocity at the face of propeller. In the event of ships being manoeuvred, the speed of the ship is very low and the influence of the propeller at slipstream is assumed to have zero speed in advance (U_o=V_D), where V_D is the velocity of net thrust produced by the jets based on axial momentum theory.

Steward (1992) proposed an equation to predict the net thrust from a propeller based on axial momentum theory. The proposed equation is shown as below,

$$T = \frac{1}{2}\rho_w A(v_D^2 - v_A^2) \tag{2.18}$$

Where, T is the propeller thrust, ρ is the density of fluid, A is the area of the cross section of $\frac{\pi D^2}{4}$, V_D represents the velocity of fluid, V_A is the advance speed of ship, C_t is the thrust coefficient measured from the propeller and n is the speed of rotation of propeller in revolutions per second. Hamill (1987) reported that the propeller thrust, T is dependent on D_p, n, ρ, μ, K, V_A, as written below,

$$T=f\ \{C_t, D_p, n, \rho, \mu, K, V_A\}$$

Where, D is the propeller diameter, μ is the water viscosity and K is the modulus of bulk viscosity. By using dimensional analysis, it is reported in the form of,

$$T = C_t \rho n^2 D_p^4 f[\frac{U}{D_p^2 n}, \frac{K}{\rho D_p^2 n^2}, \frac{V_A}{n D_p}] \tag{2.19}$$

Where, $\frac{U}{D_p^2 n}$ is the reciprocal of Reynolds number, $\frac{K}{\rho D_p^2 n^2}$ is the combination of speed of sound and speed of the blade tip, and $\frac{V_A}{n D_p}$ is the distributed acceleration per revolution. In short, the dimensional analysis of the propeller thrust is written in the form of,

$$T = C_t \rho n^2 D_p^4 \tag{2.20}$$

Hence, by associating equations [2.18] and [2.20] for the prediction of propeller thrust, it is showed as,

$$\frac{1}{2}\rho_w A(v_D^2 - v_A^2) = C_t \rho n^2 D_p^4 \tag{2.21}$$

By substituting, the A=$\frac{\pi D^2}{4}$, V_A=0 (for zero or low advance speed), it results in,

$$\frac{\pi}{8}(v_D^2) = C_t n^2 D_p^2 \tag{2.22}$$

By rearranging the equation, it is shown in the form of,

$$V_D = 1.59 n D_p \sqrt{C_t} \tag{2.23}$$

Since, V_D=U_o, thus the equation is written as follows,

$$U_o = 1.59 n D_p \sqrt{C_t} \tag{2.24}$$

However, Fuehrer et al., (1987) has highlighted that the equation [2.24] has an approximate error of ±20%. Hamill et al., (2004) also proposed the limitations of the assumptions of axial momentum theory (refer to section 2.4.2). Consequently, the need of understanding and validating the flaws of axial momentum theory through semi-empirical methods was therefore highlighted in Hamill (1987), Steward (1992) and Hashmi (1993). A comprehensive description of the semi-empirical method for the prediction of efflux velocity is discussed in the next section.

2.4.4.2 Efflux Velocity Based On Semi-Empirical Equations

The efflux velocity is the maximum velocity taken from a time average velocity distribution along the initial propeller plane and is denoted by U_o (Ryan, 2002). The accuracy of the entire jet relies on the accurate prediction of efflux velocity (Steward, 1992). The summary of the efflux equations proposed by several researchers is shown in Table 2.1.

Table 2.1: Summary of semi-empirical equations

Source	Equations
Hamill (1987)	$U_o = 1.33 n D_p \sqrt{C_t}$
Steward (1992)	$U_o = \varsigma n D_p \sqrt{C_t}$ where, $\varsigma = D_p^{-0.0686} P'^{1.51} \beta^{-0.323}$; $P' = 1.0$; $\beta = 0.47$
Hashmi (1993)	$U_o = E_o n D_p \sqrt{C_t}$ where, $E_o = \left(\frac{D_p}{D_h}\right)^{-0.403} C_t^{-1.79} \beta^{0.744}$, $D_h = 14.92mm$

Hamill (1987) initiated the prediction of the efflux velocity using experimental method by replacing the plain jet with a single ship's propeller jet. A lower coefficient was proposed compared to axial momentum theory for the prediction of efflux velocity and is shown in Table 2.1.

Steward (1992) then furthered the investigation on efflux velocity by using two types of rotating propellers to conduct similar series of experiments. A new coefficient, ς was proposed based on the geometry characteristic of the propeller. The proposed equation of efflux velocity calculation is shown in Table 2.1. D_p must be a dimensional term, while the remaining is non-dimensional. The P' is the ratio of propeller pitch to propeller diameter, and β is the blade area ratio of the propeller used.

Hashmi (1993) then refined the efflux equation by using the non-dimensioning propeller diameter with the division of propeller hub diameter. The proposed equations and coefficients are written as follows,

$$U_o = E_o n D_p \sqrt{C_t} \tag{2.25}$$

where,

$$E_o = \left(\frac{D_p}{D_h}\right)^{-0.403} C_t^{-1.79} \beta^{0.744};$$

$$D_h = 14.92mm$$

2.4.4.3 Position of Efflux Velocity

Albertson et al. (1950) believed that the position of the maximum efflux velocity of a plain jet is at the rotation axis. However, this statement is not applicable for rotating ship's propeller, which had been proven by Berger et al. (1981), Steward (1992) and McGarvey (1996). Therefore a new proposed equation is as below,

$$R_{mo} = 0.67(R_p - R_h) \quad (2.26)$$

This equation proposed by Berger et al. (1981) is well accepted and validated by Steward (1992) and McGarvey (1996). Several researchers such as Prosser (1986), Hamill (1987) and Lam et al. (2010) have modified and refined equation [2.28] with experimental approach. The summary of the equations used for the prediction of position of efflux velocity is shown in Table 2.2.

Table 2.2 Summary of equations for the prediction of position of efflux velocity

Source	Equations
Berger et al. (1981)	$R_{mo} = 0.67(R_p - R_h)$
Prosser (1986)	$R_{mo} = 0.6(R_p - R_h)$
Hamill (1987)	$R_{mo} = 0.7(R_p - R_h)$
Steward (1992)	Agree with Berger et al. (1981)
McGarvey (1996)	Agree with Berger et al. (1981)
Lam et al. (2010)	$R_{mo} = 0.74(R_p - R_h)$

2.4.4.4 Radial and Tangential Velocity

Lam et al. (2010) mentioned that the tangential and radial velocity had contributed to the rotation and diffusion of the propeller, respectively. The tangential velocity is the second largest contributor to the total velocity flow of the maximum velocity, accounted for 82% of the maximum axial velocity at the initial plane. This is followed by the radial velocity, which is the third largest velocity contributor accounted for 14% of the maximum axial velocity at the initial plane. For example, when the maximum velocity equals to 3.0 m/s, the tangential velocity would be 2.46 m/s and the radial velocity would be 0.14m/s, giving the velocity thrust in their respective dimension.

The tangential velocity has two peaks with two axisymmetric sides (Lam et al., 2010). Petersson et al. (1996) and Brewster (1997) reported that the tangential velocity profile has two peaks between the rotation axis and jet boundary. The first peak corresponds to the joint of the hub and propeller blades, while the second peak is near to the propeller

tip. Petersson et al. (1996) suggested that the first peak is located at the radial distance of r/R_p=0.15, and the second peak located at r/R_p=0.65. Subsequently, Brewster (1997) proposed that these two peaks are located at r/R_p= 0.3 and r/R_p= 0.8 at the initial efflux plane. Lam et al. (2010) believed the two velocity peaks occurs at r/R_p= 0.13 and r/R_p= 0.66. The difference in positions of peaks is approximately 2~22%, thus further investigation on its characteristics is required.

According to Lam et al. (2010), radial velocity has similar number of peaks with tangential velocity. McGrarvey (1996) and Lam et al. (2010) reported that the radial velocity of ship's propeller jet increased from the hub to a peak velocity and thereafter decreased towards the blade tip. Brewster (1997) found that a portion of flow was directed towards the rotation axis to penetrate the low velocity core, which has been validated by Lam et al. (2010).

2.5 Concept of Turbulent Jet Model

The turbulent fluid motion is an irregular condition of flow in which various quantities of turbulent fluid showed a random variation in time and space coordination. The statistically distinct average values can be discerned as revealed by Hinze (1975). Hamill (1987) said that the movement of any fluid is governed by two key factors, namely gravity and viscosity, which are associated with the inertial forces of the flow. Since the velocities induced by ship's propeller jet are largely horizontal flows, the viscosity character is clinched as the major dependent factor of the speed of flow. This viscosity can be sub-categorised into laminar, transient and turbulent flows. Turbulent flow occurs when the viscosity relative to inertial forces is weak. Therefore, the turbulent flow from a ship's propeller jet is water particles moved in irregular paths neither smooth nor fixed, and the combination remains as a representation of forward motion of jet (Hamill, 1987).

The effect of viscosity relative to inertial forces of the flow can be represented by Reynolds number. Since the turbulent flow increases with the Reynolds number, it is dependent to the Reynolds number. However, the impact on velocity thrust by characteristic of turbulent jet is minimum, compared to axial velocity (Hamill, 1987). Abramovich (1963) concluded that transverse components of turbulent jet are minor and can be disregarded in engineering problems involving jet theory.

2.6 Decay of Axial Velocity within the Zone of Flow Establishment of A Single Propeller

As discussed in section 2.4.3, the zone of flow establishment of single rotating ship's propeller is different from plain jet. Hamill (1987) stated that the zone of flow establishment has two peak values at the lateral distribution of axial velocity. Hamill (1987) initiated the research on the decay of maximum axial velocity in the zone of flow establishment. He indicated that there is no maximum axial velocity decay up to the distance of $0.35x/D_p$, as the decay of axial velocity only initiated after this point.

The length of zone of flow establishment is defined by the position where two peaks of flow are combined into a single peak positioned at the rotation axis (Steward, 1992). Therefore, the decay continues up to a point where the two peaks velocity profile join into a single peak after several propeller diameters downstream. The length of zone of flow establishment proposed by several researchers have been summarised in Table 2.3.

Table 2.3: Summary of suggested length of Zone of Flow Establishment by previous researchers

Source	Length of Zone	Acquisition method
Albertson et al. (1950)	$x/D_p = 6.20$	Prediction
Blaauw & van de Kaa (1978)	$x/D_p = 2.18$	Measurement
Fuehrer et al. (1987)	$x/D_p = 2.60$	Measurement
Verhey (1983)	$x/D_p = 2.77$	Measurement
Hamill (1987)	$x/D_p = 2.00$	Measurement
Steward (1992)	$x/D_p = 3.25$	Measurement
Lam et al. (2012a)	$x/D_p = 3.68$	Measurement

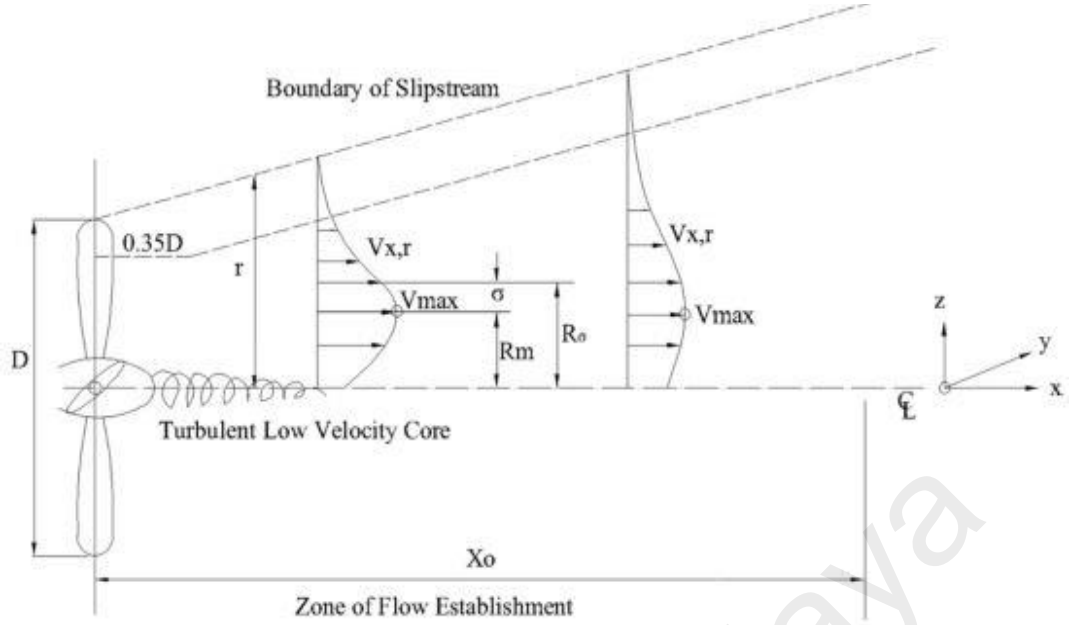

Figure 2.13: Schematic view of propeller jet in the zone of flow establishment *(Hamill, 1987)*

Albertson et al. (1950) proposed the ratio of maximum velocity to efflux velocity as,

$$\frac{U_{max}}{U_o} = 1 \tag{2.27}$$

Hamill (1987) found that equation [2.27] is only valid up to the distance of x/D_p=0.35 from the propeller plane as shown in Figure 2.13. From then onwards, the maximum velocity begins to decay steadily along the propeller jet. The maximum velocity at the downstream can be calculated using the equation below,

$$\frac{U_{max}}{U_o} = 0.87\left(\frac{x}{D_p}\right)^{-(\beta/4)} \tag{2.28}$$

Steward (1992) then continued the work and proposed the longitudinal length for the zone of flow establishment to be x/D_p=3.25, and suggested an equation to determine the maximum velocity decaying from the propeller plane within the zone of flow establishment, as written in the form of,

$$\frac{U_{max}}{U_o} = 1.0172 - 0.1835\left(\frac{x}{D_p}\right) \tag{2.29}$$

Several researchers such as Fuehrer and Römisch (1977), Blaauw and van de Kaa (1978), Berger et al. (1981), Verhey (1983), Steward (1992) and Hashmi (1993) carried out researches on the formulas to predict the flow velocity decay. The summary of the equations and evolution of velocity decay are shown in Table 2.4.

On the other hand, Johnston et al. (2013) suggested that the development of a propeller wash is influenced by the boundary and the axial velocity only increases rapidly before reaching the boundary or seabed. Subsequently, the axial velocity reduces due to the influence of the boundary. It is proposed that the high turbulence still exists at the boundary of the jet, but with slow return supply flow due to the suppression by the boundary. Moreover, Johnston et al. (2013) proposed that the maximum axial velocity close to the boundary level at lower clearance height was lower compared to higher clearance heights.

2.7 Influence of Ship Design

The design of ship geometry will influence the flow pattern when the stern of ship approaches the inlet of a propeller during ship manoeuvring. However, when the ship is stationary or manoeuvred at a low speed, these effects are insignificant as the flow of propeller will be relatively undisturbed by the hull (Hamill, 1987).

Table 2.4: Summary of equations based on flow velocity decay

Source	Length of zone of flow establishment	Equations	Descriptions
Albertson et al. (1950)	$0 \leq x/D_j < 6.2$	$\frac{U_{max}}{U_o} = 1$	Maximum velocity is constant within entire zone up to $x/D_p = 6.2$
	$x/D_j \geq 6.2$	$\frac{U_{max}}{U_o} = \frac{1}{2C}(\frac{x}{D_p})$ where, $C = 0.018$ and $D_j = D_p$	Maximum velocity is constant within entire zone up to $x/D_p = 2.6$
Fuehrer and Römisch (1977)	$x/D_p \geq 2.6$	$\frac{U_{max}}{U_o} = 2.6(\frac{x}{D_p})^{-1.0}$	Maximum velocity is constant within entire zone up to $x/D_p = 2.8$
Blaauw and van de Kaa (1978)	$x/D_p \geq 2.8$	$\frac{U_{max}}{U_o} = 2.8(\frac{x}{D_p})^{-1.0}$	Maximum axial velocity is constant close to propeller up to $x/D_p = 1.0$, but not entire zone
Berger et al. (1981)	$x/D_p \geq 1.0$	$\frac{U_{max}}{U_o} = 1.025(\frac{x}{D_p})^{-0.6}$	Maximum axial velocity is constant close to propeller up to $x/D_p = 1.5$, but not entire zone
Verhey (1983)	$x/D_p \geq 1.5$	$\frac{U_{max}}{U_o} = 1.275(\frac{x}{D_p})^{-0.7}$	Maximum axial velocity is constant close to propeller up to $x/D_p = 0.35$, but not entire zone
Hamill (1987)	$0 \leq x/D_p < 0.35$	$\frac{U_{max}}{U_o} = 1$	No constant maximum axial velocity close to propeller
	$0.35 \leq x/D_p < 2$	$\frac{U_{max}}{U_o} = 0.87(\frac{x}{D_p})^{-\frac{\beta}{4}}$	
	$x/D_p \geq 2$	$\frac{U_{max}}{U_o} = A'(\frac{x}{D_p})^{B'}$ where, $A' = -11/4C_t + 6.65\beta + +2.16P'$; $B' = -(1.0C_t)^{-0.216}\beta^{1.024}P'^{-1.0}$	
Steward (1992)	$0 \leq x/D_p < 3.25$	$\frac{U_{max}}{U_o} = 1.0172 - 0.1835(\frac{x}{D_p})$	
	$x/D_p \geq 3.25$	$\frac{U_{max}}{U_o} = 0.543 - 0.0281(\frac{x}{D_p})$	
Hashmi (1993)	$x/D_p \geq 3.25$ up to $x/D_p = 16$	$\frac{U_{max}}{U_o} = 0.638e^{(-0.097\frac{x}{D_p})}$	Use exponential equation

2.7.1 Influence of Propeller Geometry

The propeller geometry can be differentiated in terms of propeller diameter, number of blades, blade area ratio, mean pitch ratio, and thrust coefficient. The influence of ship's propeller geometry remained unknown (Lam et al., 2012b). Thus, Lam et al. (2012b) proposed a series of equations to predict the efflux velocity with different propeller geometry, as shown in Table 2.5. However, the variations between different geometries are less than 5%.

Table 2.5: Proposed equation with different propeller geometry *(Lam et al., 2012b)*

Propeller	Source	Proposed Equation
Propeller-76	Experimental	$U_o = 1.71nD_p\sqrt{C_t}$
Propeller-76	Numerical	$U_o = 1.46nD_p\sqrt{C_t}$
Propeller-131	Experimental	$U_o = 1.61nD_p\sqrt{C_t}$
Propeller-131	Numerical	$U_o = 1.41nD_p\sqrt{C_t}$
Both propeller	Experimental	$U_o = 1.65nD_p\sqrt{C_t}$
Both propeller	Numerical	$U_o = 1.41nD_p\sqrt{C_t}$
Modified four-bladed propeller-76	Numerical	$U_o = 1.48nD_p\sqrt{C_t}$
Modified five-bladed propeller-76	Numerical	$U_o = 0.89nD_p\sqrt{C_t}$

2.8 Ship-Twin-Propeller's Jets

The application of ship-twin-propeller has been given attention as it is essential to promote efficiency of the ship manoeuvring ability, particularly for large container ships. Limited studies on investigation aspects and behaviours of ship-twin-propeller were carried out, especially on its hydrodynamic properties. Abramowicz-Gerigk (2008) studied the ship-twin-propeller ferry fluid flow during self-berthing based on experimental works. Kim et al. (2007) also studied the manoeuvrability of large container ship equipped with ship-twin-propeller and twin rudders using mathematical model. Both Abramowicz-Gerigk (2008) and Kim et al. (2007) used horizontal planar motion mechanism (HPMM) test and computer simulation with four degree of freedom

mathematical model. It was found that the vertical centre of hydrodynamic forces acting on the hull for ship-twin-propeller is smaller than single propeller ship. Moreover, ship-twin-propeller has better linear directional stability compared to single propeller ship.

Dubbioso and Viviani (2012) investigated the stern appendages effect of manoeuvring models of twin screw ships using semi-empirical method. Coraddu et al. (2013) then further improved their research on ship-twin-propeller ship manoeuvrability by investigating the asymmetric propeller behaviour by means of free running models. The design of twin-propeller is relatively similar with single propeller when fixed pitch propeller is used. The difference between right-handed and left-handed propeller are both used for propeller propulsion in different ship system design as stated in Techet (2004). Moreover, the typical range between twin-propeller ships are also approximately 1.0 to $1.5D_p$ as stated in aforementioned literatures. Therefore, in viewing the geometry of twin fixed pitch propeller are relatively similar (Stoye, 2011), therefore the further design explanation will not be described in detailed. Further reading can be referred to aforementioned literatures. However, understanding of ship-twin-propeller's hydrodynamic properties in bollard pull condition and induced scour pattern remained unknown. The usage of ship-twin-propeller has been applied to all large ships for maritime activities. Therefore, it is important to observe the trend of ship-twin-propeller jets velocity distribution and the scouring impacts.

2.9 Computer Fluid Dynamic (CFD) Simulation

CFD simulation is a type of numerical simulation based on computational method, which uses software instead of laboratory work. Therefore, reliability of results is mainly dependent on the interpretation of experts. However, its advantages include cost effectiveness, less time consuming, lower risk and space efficiency, as compared to the scaled experimental setup. The reliability of computational study is proven by a few successful simulation cases. For example, Lam et al., (2012b; 2012c; 2012d)

investigated the efflux velocity and turbulence intensity of ship's propeller wash by using Fluent CFD. Other relevant research on CFD can be found in Hamill et al. (1998) on influence of rudder on bed velocity produced by ship's propeller wash; Johnston et al. (1985), Lee et al. (1988), Lee et al. (2003), Kang et al. (2008) and Kang et al. (2011) on the simulation of single or twin-propeller ship incorporated with single or twin rudder system using mathematical model.

2.9.1 Turbulence Model Considered In Simulation

The turbulence forces in the water are resulted from high velocity of water current. In CFD software, turbulence model is used to predict the turbulent flow of water in steady state by using time-average equations, which commonly known as Navier-Strokes equations (RANS). To date, there are turbulence models used to predict the turbulent flow according to the characteristic of fluid flow and problem cases. Thus, the selection of turbulence model for numerical simulations requires detailed literature reviews on the type of problems. According to Lam et al. (2012c), the turbulence models used in numerical simulations including standard k-ε, RNG k-ε, realizable k-ε, standard k-ω, SST k-ω and the Spalart-Allmaras turbulence models, are from Boussinesq family. Hinze (1975) stated that the Boussinesq hypothesis is the Reynolds stresses in proportion to the mean strain rate with a scalar property of eddy viscosity. Thus, the Reynolds stress can be solved by predicting the eddy viscosity and through Reynolds Stress Models (RSM).

2.9.1.1 Standard k-ε Turbulence Model

Standard k-ε turbulence model is a well-established turbulence model, which uses two equations to solve the model (Launder and Spalding, 1972). The two equations are used to determine the length scales and turbulent velocity in the model. The solving steps are based on the assumption that the rate of production and dissipation of

turbulence flows are in near-balance energy transfer (Lam et al. 2012c). The dissipation rate of energy, ϵ can be predicted using the following equation,

$$\epsilon = \frac{k^{3/2}}{l} \tag{2.30}$$

Where, k is the kinetic energy of the flow, l is the length scale, whereas the turbulence viscosity, μ_t is estimated based on Prandtl mixing length model,

$$\mu_{t0} = \rho C_\mu \frac{k^2}{\varepsilon} \tag{2.31}$$

Where, C_μ represents an empirical constant and ρ is the density of the flow. Therefore, the standard k-ε model is deemed as a well validated model in the ship's propeller jet prediction. Lam et al. (2012c) also recommended that standard k-ε turbulence model is a robust, economic and suitable model to predict the turbulence intensity within the flow field induced by a ship's propeller in a reasonably accurate range.

2.9.1.2 RNG k-ε Turbulence Model

The RNG k-ε turbulence model is a model to improve the standard k-ε model using statistical mechanics approach known as renormalisation group theory (Choudhury, 1993). Thus, the model is able to enhance the accuracy in prediction of flows with high strain and swirling flows. The prediction is done by adding a swirl constant into the standard k-ε model, which forms the following equation,

$$\mu_t = \mu_{t0} f(\alpha_s, \Omega, \frac{k}{\varepsilon}) \tag{2.32}$$

Where μ_{t0} represents the turbulence viscosity value without the swirl modification calculated by using equation [2.31]; α_s is a swirl constant that has different value according to the level; and Ω is the swirl characteristic evaluated within the Fluent software.

2.9.1.3 Realizable k-ε Turbulence Model

Instead of using statistical mechanics approach, another turbulence model based on mathematical approach, the Realizable k-ε turbulence model was also proposed. As it is a mathematical approach, the ability to predict the spreading rate of the plane or round jet is better than standard k-ε turbulence model. This indicates that it is likely to have a better estimation on rotating flows, strong adverse pressure gradient imposed boundary layers, separation flows and recirculation flows (Shih and Liou, 1995). However, it will produce non-physical turbulent viscosities in the situation where the computational domain contains rotor and stators, as the rotating of rotor of computational domain might unduly affect the term (Lam et al., 2012c). Hence, caution should be taken when this model is associated with the rotating model (Fluent User Manual, 2003).

2.9.1.4 Standard k-ω Turbulence Model

Wilcox (1998) introduced the standard k-ω turbulence model to overcome the deficiencies of the standard k-ε model at walls, which has low Reynolds number. Thus, the standard k-ε model which is a high Reynolds number model, is not able to estimate the value near a wall accurately. Moreover, this model is likely to predict well the spreading rate of the shear flow for wake, mixing layers and jets, and overcome the limitation of k-ε turbulence model in the estimation of shear flow (Wilcox, 1998). The standard k-ω turbulence model is based on the transport equation which considers the turbulence kinetic energy, k and the dissipation rate, ω. Thus, the turbulent viscosity, μ_t can be predicted using the following,

$$\mu_t = \alpha^* \frac{\rho^k}{\omega} \tag{2.33}$$

Where, α* is a coefficient used to damp the turbulent viscosity causing a correction of low Reynolds number. Further description on the use of α* shall be referred to the Fluent User Manual (2003).

2.9.1.5 Spalart-Allmaras Model

The Spalart-Allmaras model is a simple model for the simulation with a coarse mesh, developed by Spalart and Allmaras (1992). This turbulence model contains only one equation, unlike previous mentioned models that have two equations. It is suitable when the accuracy of turbulent flow computation is not critical. It is also able to give relative estimation on the initial stage of simulation as the requirement of computational power is lower compared to previous mentioned models. According to Lam et al. (2012c), this model gives a good prediction on wall-bounded flows and boundary layers subjected to adverse flow gradients.

2.9.1.6 Reynolds Stress Model (RSM)

This model abandons the eddy viscosity model and resolves the Reynolds stress by using RANS equations (Launder and Reece, 1975). This indicates that a two-dimensional simulation requires five equations, while a three-dimensional simulation requires seven equations. According to Launder and Reece (1975), this model is able to solve complex flows due to its ability to reflect the effects of rotational, swirling and rapid changes in strain rate. However, the accuracy of the prediction using RSM is restricted by the closure of assumption employed (Lam et al., 2012c). Thus, it does not always predict better results compared to other turbulence models.

2.9.2 Turbulent Intensity

Pantan (1984) defined turbulent intensity in terms of root mean square (RMS) for each velocity components. The equations for each velocity components are shown below,

$$I_x = \frac{\sqrt{(u'u'}}{V_{ref}} ; I_y = \frac{\sqrt{(v'v'}}{V_{ref}} ; I_z = \frac{\sqrt{(w'w'}}{V_{ref}} \quad (2.34)$$

Where, I_x, I_y and I_z are representing the x-component, y-component and z-component of turbulent intensity respectively, V_{ref} is the mean flow velocity, and $\sqrt{(u'u'}$, $\sqrt{(v'v'}$ and $\sqrt{(w'w'}$ are the x-component, y-component and z-component of turbulent fluctuations.

2.10 Summary

Based on literature review, it has been found that there is no experimental works carried out for ship-twin-propeller's wash and its resulting scour. It is therefore decided that investigation on the ship-twin-propeller's wash induced scour should be carried out. In order to improve the understanding of ship-twin-propeller wash and its resulting scour, it was decided that the flow field produced by a ship-twin-propeller has to be investigated, particularly on the axial velocity profile. Moreover, the efflux velocity from the propeller for all later works was calculated based on equation [2.24]. Therefore the experiment of ship-twin-propeller induced scour was initially conducted to compare with single propeller prior to proposing any coefficient or correlation based on equation [2.24]. As a result, a series of experiments was planned based on various keel clearances and rotational speeds.

CHAPTER 3:METHODOLOGY

Overview

The current study is designed to investigate the velocity profiles of selected rotating ship-twin-propellers and resulting scouring actions. An experiment model and a Computational Fluid Dynamic (CFD) model were set up to assist the data observation for the formation of scour pattern. Software and hardware were also required to measure, store and analyse the data. A thorough literature review revealed that there are minimal works consist of ship-twin-propeller's velocity profiles, particularly on the rotating axial velocities and the resulting scouring profile. Literature revealed that the existing theories and experimental results were mostly derived from plain jet and single rotating propeller. Therefore, the erosive power induced by ship-twin-propeller's wash was studied in order to establish the relationships for their distribution of velocities and the scour development with time. Large amount of experiments were required for various rotating speeds and clearances between the propeller tip and the sediment layer.

3.1 Work procedure

A flowchart indicating the overall procedures is shown in Figure 3.1. Methodologies used in this study are based on three objectives as stated in Chapter 1. First objective, "To identify the source and pattern of axial velocity impinging the seabed which was induced by ship-twin-propeller's wash". Experiment equipment such as a tank, a ship-twin-propeller, a shaft, an electrical system and other necessary equipment are required to set up and run the experiment smoothly. A Laser Doppler Anemometry (LDA) system was used to acquire the axial velocity profile of the ship-twin-propeller jet.

To achieve second objective, which is "To determine the temporal development of scour induced by ship-twin-propeller's wash by investigating the seabed scouring pattern", the same experiment setup as the first objective was used. An additional layer of sediment was added, and the seabed scouring pattern was observed and tabulated with adequate equipment.

In order to achieve the third objective, which is "Simulation of seabed scour pattern induced by ship-twin-propeller's wash", a CFD model has been established. The CFD model uses similar initial and boundary conditions with the experiment of scour investigation. The correlation of both experiments and simulation setups will be inter-correlated and compared.

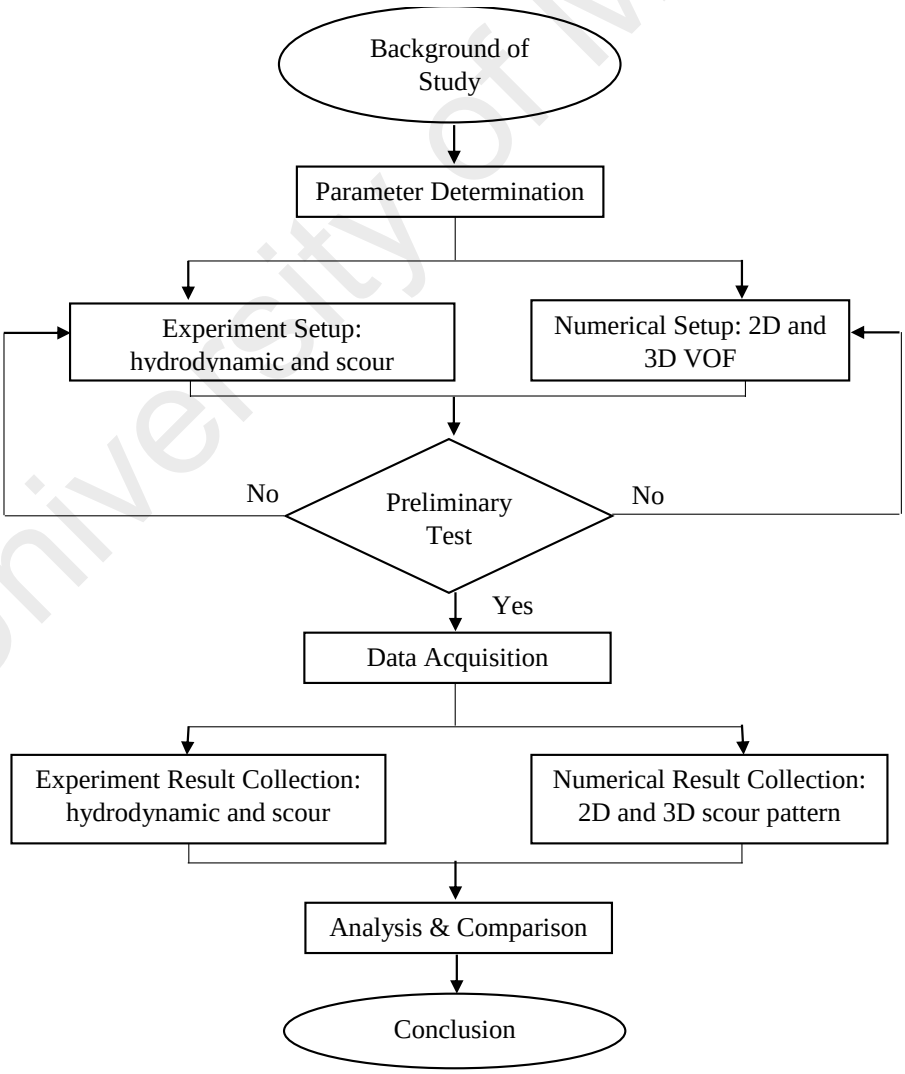

Figure 3.1: Flowchart of current study

3.2 Configuration and validation

Configuration is a set of values of all parameters used in an experiment. It is useful when it is required to run experiments in multiple modes.

Experiment

In current study, a ship-twin-propeller was rotated in the same direction (clockwise) for the investigation. Distance between both propellers was set to $1.0D_p$ (one propeller diameter). A series of experiment was run under three sets of velocity which were 400rpm, 500rpm and 600rpm. Validation on the current investigation has been made using two approaches: (i) to measure one side of the propeller with the other side turned off (SP) and (ii) to measure one side of the propeller with the other side turned on (TP). Both results were compared with previous literature for validation purposes.

For scouring observation, three different clearances, specifically $0.31D_p$, $0.5D_p$ and 0.64Dp, were used in this study. These clearances were run in three different modes of speeds, which are 400rpm, 500rpm and 600rpm. Each set of experiment was scheduled to run for a total of 64 hours or until it achieved the asymptotic state of scour. Asymptotic stage is the stage that has minimal or no further changes on the scour geometry profile as compared to previous chosen accuracy scour value (Hamill, 1987). Since, it is using trial and error method for some of the validation experiments, it is hard to specify an exact number of experiments to be conducted. Therefore, excluding the trial and error experiments, there would be a total of thirty nine sets of final experiments for hydrodynamic acquisition and twenty seven sets of final experiments for scour observation.

Simulation

VOF method is being used in current study. The capability of current VOF to predict scour profile was validated by experiment data of scour profile induced by single ship's

propeller jet, both two-dimensionally (2D) and three-dimensionally (3D). The scour pattern that was produced by single ship's propeller jet, was then validated using the results from previous literature. Then, the simulation for ship-twin-propeller's induced scour was run using the same setting as the experiment set up to observe and validate the scour pattern. Therefore, the series of simulation is similar to the experiment configuration in estimating the scour pattern.

3.3 Experimental tank

A tank was required to study the velocity profile and its resulting scouring actions of ship-twin-propeller's wash. The efflux velocity of ship-twin-propeller's wash, which is the maximum velocity speed that falls in the length of zone of flow establishment, was also investigated.

Since there was no existing tank in the hydraulic laboratory of University Malaya. A new tank with dimension of 3000mm×1200mm was proposed due to limited laboratory space as stated in Chapter 1. It was made of acrylic material that gave the transparent property, which was needed for the scanning equipment. The tank was designed with a depth of 1000mm for the water level to be maintained at 700mm depth, while leaving 300mm freeboard. Table 3.1 shows the specifications of the proposed tank. Due to the limited available space in the laboratory, it is not possible for an extension in the dimension of tank. Thus, the range of diameters for ship-twin-propeller was restricted.

The study on efflux velocity by Hamill (1987) was carried out using two propellers with diameters of 154mm and 61mm, respectively. He found that the length of zone of flow establishment of both propellers in two-dimensional falls within the range, less than $2.0\frac{X}{D_p}$, which is diameter range of two propellers (where X is the distance from the propeller and D_p is the propeller diameter). Lam et al. (2012a) then further investigated the efflux velocity profile with a small propeller in three-dimensional space. It was

found that the length of zone of flow establishment was approximately $3.68\frac{X}{D_p}$. Therefore, a tank with 3000mm in length, with propeller shaft and rig is set to a calculative distance from the edge of tank. The choices of size of propeller geometry were limited and are discussed further in the later sections. However, the range of adequate propeller diameters remained for further investigation, particularly on larger propeller sizes.

Table 3.1: Proposed tank specification

Tank Specifications	
Material used	Acrylic
Shape	Rectangular
Dimension	3000mm × 1200mm × 1000mm
Thickness	25mm
Equipment allocation	Hydraulic Lab

Figure 3.2: Custom made tank

The water tank was specially made by our research team in Malaysia. Two acrylic boards of 2400mm×1000mm×25mm and three acrylic boards of 1200mm×1000mm× 25mm were purchased. There were no acrylic boards of 3000mm×1000mm×25mm in the market. Thus, one of 1200mm×1000mm×25mm board was cut into two equally sized boards, which were then joined with the two 2400mm×1000mm×25mm boards to

form a total length of 3000mm. The tank was reinforced with stainless steel screws of 7mm diameter and 20mm diameter. All joints were sealed with acetic silicon sealer (VT-201) before and after the reinforcement to prevent water leakage. The successive made tank is shown in Figure 3.2.

3.4 Ship-twin-propeller design

Since the past few decades, maritime ships with single propeller has been slowly replaced with ship-twin-propeller due to the demand for trading efficiency as stated in Kim et al. (2007). Moreover, ships equipped with ship-twin-propeller have better acceleration and manoeuvring abilities, handling power and stability effects as compared to ships with single propeller as mentioned in Dubbioso and Viviani (2012). Furthermore, Kim et al. (2007) mentioned ship-twin-propeller has better linear directional stability, coarse keeping and changing ability. With these advantages, ship-twin-propeller had become popular in the maritime transport these days.

The main differences between single and ship-twin-propeller are the forces and the force coverage areas induced by propellers. The jet produced by ship-twin-propeller has created new coverage areas, which will have a vast difference as compared to previous literature. As a result, the scour area, depth and volume induced by ship-twin-propeller's wash were remained unknown and it is vital for them to be investigated. Therefore, in the following sections, methodologies for the investigation on ship-twin-propeller's wash and its resulting scouring actions were reported.

3.4.1 Terminology

The typical cross section of a ship's propeller blade showing some propeller's characteristics is shown in Figure 3.3. It is useful to define some of the specific terms associate with propellers that will be used throughout the thesis in reference to Hamill

(1987) and EN-ISO-3715-1 (2004). All terms used in this current study are described as below:

i. Blade area ratio: the area of propeller with non-dimensional value which can be calculated by dividing the blade area over the disc area.
ii. Blade back: the suction side of propeller.
iii. Blade face: the pressure side of propeller.
iv. Blade number: the number of blades on the propeller.
v. Blade root: the fillet area, where the blade is attached to the hub.
vi. Blade tip: the maximum distance from the centre of hub.
vii. Develop blade area: the sum of face areas of all the blades.
viii. Disc area: the area of the rotating propeller tips that is normal to the propeller axis.
ix. Leading edge: the edge when the rotating propeller producing ahead thrust.
x. Projected area: the area of the plane of projected blade, which normal to the propeller axis.
xi. Pitch ratio: is the distance of the line representing the helicoidally surface that will advance during one rotation. It can be calculated by dividing the pitch of the blade over the propeller diameter. The pitch of the blade is varies with the radius of propeller.
xii. Trailing edge: the other edge of leading edge.

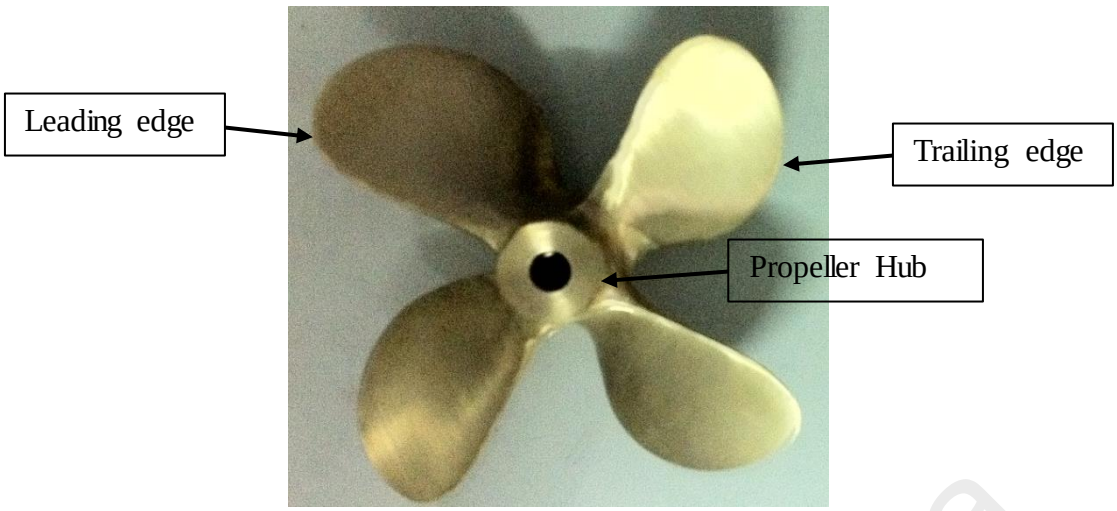

Figure 3.3: Typical cross section of a ship's propeller blade

3.4.2 Small scale propeller

As the experiment tank space was limited, the range of propeller used for current investigation was hence limited. The ideal location for the propeller rig was set to a ratio between 0.2 and 0.3 from the edge of tank (refer to section 3.4.4). In current study, the proposed length from the propeller was $6.5\frac{X}{D_p}$, which was double of the distance proposed by Steward (1992). The purposed length was doubled after taking into consideration the flow by ship-twin-propeller wash which may have an impact on a lengthier area. Hence, only propellers with D_p <300mm are adequate for efflux velocity investigation. However for the scouring actions, Hong et al (2013) studied a range of propellers with diameters between 60mm and 210mm, and suggested that the propeller wash impacts up to a length of $10D_p$. By using the same setting as aforementioned, range of propellers with $D_p \leq 230$mm is adequate for scouring action investigation.

According to Prosser (1986), the number of blades will affect the propeller efficiency. A smaller number of blades will improve the propeller efficiency whereas higher number of blades will allow propeller to take larger loads. This experiment will be run in bollard pull condition, in other words in zero advance speed. Consequently, the effects on the number of blades have been reduced to minimal as investigated by

Prosser (1986) in such condition. The propeller selected from a range of propellers available was, propeller number HP6.393.001.0, which is hereafter termed as Propeller-1 (P1). The coefficient of thrust has been worked out using the formula of $C_t = {}^{T}/_{\rho n^2 D_p^4}$, where T is the maximum thrust of this model, ρ is the fluid density, n is speed in the revolutions per seconds, and D_p is the diameter of propeller. The characteristics and picture of P1 were shown in Table 3.2 and Figure 3.4 respectively.

Table 3.2: Characteristics of propeller

Characteristics	**Propeller-1 (P1)**
Number of blades, N	3
Propeller diameter, D_p	220mm
Pitch ratio, P'	1
Thrust coefficient, Ct	0.64

Figure 3.4: Propeller-1

3.4.3 Powering of Propeller

Based on previous literature as stated in Section 2.4.4, it was found that the propeller geometry is negligible when the propeller is in zero advance speed. Therefore, the frame to hold the trailing motor does not have to represent the ship hull (Hamill, 1987). A simple shaft of 1300mm width × 1050mm height was coupled with a horizontal beam of 40mm width × 75mm height (see Figure 3.5).

Two propeller trailing motors, manufactured by Ningbo Haibo Machinery Co. Ltd. were used to power P1. The trailing motor systems have variable speed controls where the minimum angular speed is 1700rpm and maximum speed is 2100rpm, when it is placed underwater. However, the initial designed speed was too high to power the propellers, where stable velocity flow is unobtainable. It is therefore decided to add an inverter to lower the range of speed. The inverter had successively reduced the range of speed to a minimum of 300rpm and maximum of 1200rpm when it is placed underwater. The range of speed was measured by tachometer. These trailing motors were clamped to the shaft, and each trailing motors were equipped with one unit of calcium battery as a backup in the event of power shortage in the laboratory. The arrangement of motors is shown in Figure 3.6.

Figure 3.5: Designed shaft

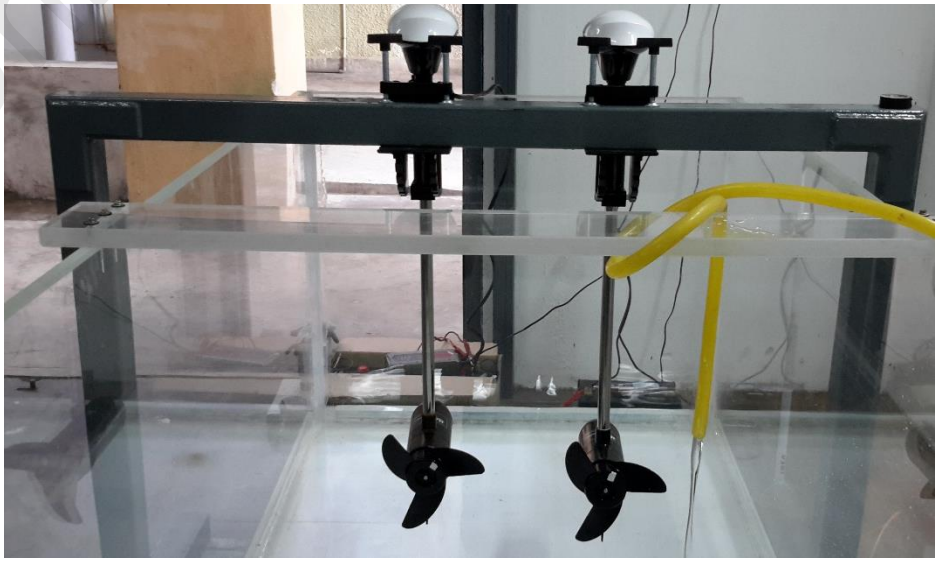

Figure 3.6: Arrangement of motor for P1

3.4.4 Location of propeller shaft and jet

Propeller shaft location was selected on a trial and error basis in order to balance between the distance of the jet and the fluid return. Based on Hamill (1987), the best location for the propeller shaft is proportional between 0.2 and 0.3 of the length of the experimental tank, when measured from the edge. The location of the propeller shaft for this experiment was therefore decided to be benchmarked against Hamill (1987), which was set between 600mm and 900mm from the edge of the tank depending on the chosen propeller size. Location of ship-twin-propeller jets, P1 was fixed at 350mm from the bottom of the tank, close to the centre of water level, leaving 350mm water freeboard.

Preliminary tests were carried out to observe the physical flow and the return flow of the ship-twin-propeller jet. The circulation effect of water within the tank has been shown to be insignificant to the propeller's jet expansion. However, it was found that the return flow has a tendency to cause defects on the jet and frequent instability. Therefore, a baffle was introduced to resolve the instability of return flow and it was able to separate the flow from the forward moment. The baffle was placed at the other edge of the tank, away from the ship-twin-propeller. The location of baffle is shown in Figure 3.6. With the baffle in place, a steady jet of preliminary speed was constantly produced. Thus, the speed for propeller to run in the actual experiment was then determined.

Figure 3.7: Location of baffle

3.4.5 Speed of rotation

The maximum speed of motor has caused the propeller to be overheated and propeller shaft to be dislocated. Thus, for safety precaution, the maximum speed to be used was limited to 900rpm.

Based on previous literature as stated in Qurrain (1994) Hamill (1987), it was found that the typical speed for manoeuvring a ship with propeller diameter of 1600mm was approximately 6 revolutions per second. For a ship, the Froude number is represented by,

$$F_r = \frac{U}{\sqrt{gL}} \tag{3.1}$$

Where, U is the ship's velocity, g is the gravitational forces and L is the length of the water line level on the ship. With the similar approach, the length was replaced by the propeller diameter. As g equals to 1 for the ratio in prototype and model, the Froudian scaling equation is as below,

$$F_o = \frac{U}{\sqrt{D_p}} \tag{3.2}$$

By equating both propeller model and its prototype, the equation is written in the form,

$$\frac{U_1}{\sqrt{D_{p1}}} = \frac{U_2}{\sqrt{D_{p2}}} \tag{3.3}$$

According to a survey on British ports and harbours by Qurrain (1994), the typical propeller size which may cause seabed scouring, lies within the range of 1.5m to 3m in diameter with approximately 200rpm of operating speed. In this study, a typical ship propeller with diameter of 2500 mm and a coefficient of thrust, C_t of 0.35 with a speed of 200rpm, was used as a prototype for P1. By substituting these parameters into the

efflux velocity equation which was proposed by Fuehrer and Römisch (1977), the equation below was obtained,

$$U_o = 1.59nD\sqrt{C_t} \tag{3.4}$$

$$U_o = 7.84\ m/s$$

By taking Froudian scaling equation into consideration, the necessary speed to obtain a similar efflux velocity was 2.33 m/s, and both propellers should run under the minimal speed of 500 rpm. Therefore, the angular speed to investigate velocity measurement was set to 400rpm, 500rpm and 600rpm, in order to observe the variations of different velocity profiles.

3.4.6 Rotation direction of ship-twin-propeller

The ship-twin-propeller is constrained to rotate in one direction, i.e. clockwise (towards the right hand side), and is in the form to allow free expansion. The ship-twin-propellers rotate in the same right-handed direction when the ship is in the process of parking or docking towards the port side. This is attributed to the pulling gear case in the same direction and supporting the twin screw ship to roll over to the port side, as discussed with the port technicians. For investigation on the forces exerted by twin screw ship under bollard pull condition (in zero advance speed), the right-handed ship-twin-propeller system shall be investigated first, when the ship docks at the port. Moreover, the effects of the tank bottom and water boundaries were found not to be hindered towards the expansion of the unconfined jet. According to Hamill et al. (1999), a distance of $10.00D_p$ is required for the experiment setup in order to allow free expansion for propeller flow. Therefore, the circulation effect of the water within the tank for current setup was found to be insignificant towards the jet expansion.

3.5 Velocity measurements

The velocity measurements were designed using grid dimension. The diameter of P1 was 220mm, the grid dimensions were set to 10mm×10mm for both horizontal and vertical grid as shown in Figure 3.8. The horizontal grid was used to obtain the velocity decay of the axial velocity flow, while the vertical grid was used to obtain the efflux velocity exerted by the propeller jet near to the propeller's plane. A proposed measurement line has been identified (as shown in Figure 3.9) to measure the axial velocity of the plane x-z. The experimental hardware and software used in this study are discussed in section 3.5.1. LDA system was suggested to be used as data acquisition method, which has been discussed in section 3.5.1.1.

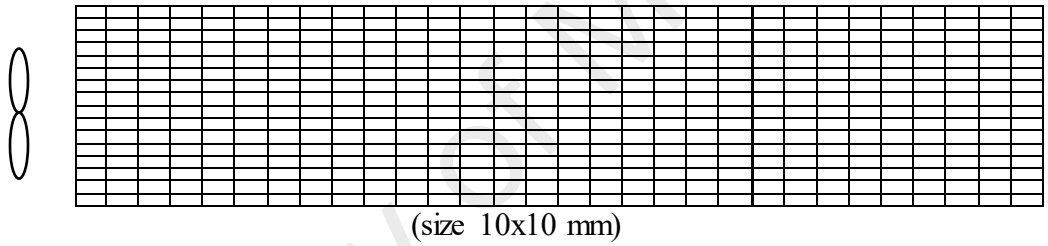

Figure 3.8: Schematic diagram of proposed experimental grids for measurement

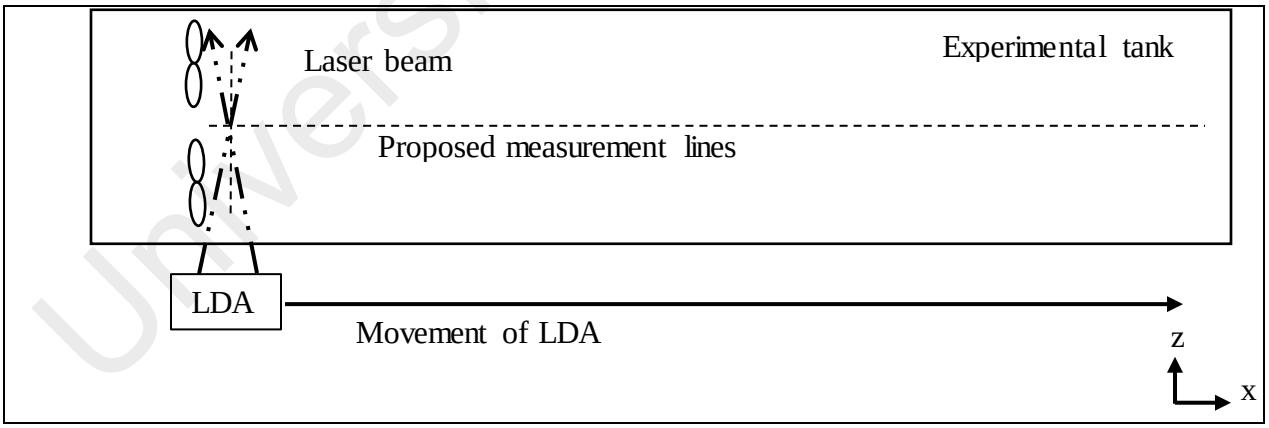

Figure 3.9: Schematic diagram of proposed measurement line for axial velocity flow for ship-twin-propeller's jet

3.5.1 Experimental hardware and software

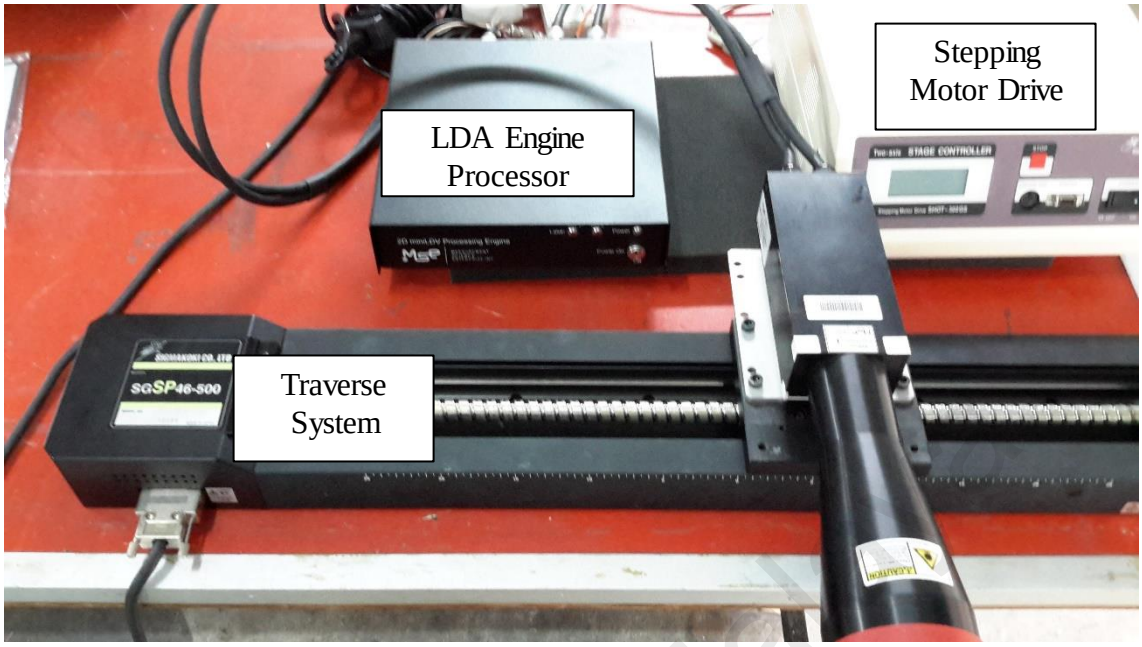

Figure 3.10: Physical image of LDA hardware system

As mentioned earlier, the experimental hardware used for this study includes experimental tank, P1 propellers, inverter, and motors to run the propellers, as well as chargers for the motors' backup batteries during the event of power shortage. LDA hardware system was also prepared for scanning purposes. This laser hardware system includes a traverse system coded SGSP46-500, which 500 denotes that the travel distance of the traverse system for the movement of the laser beam was limited to 500mm. A dual channel Laser Doppler Velocimetry (LDV) to disperse laser was coded as GSL 2D-400. A two-dimensional (2D) LDV processing engine is used to process the laser data for both channels. Both channels are able to acquire two dimensional results simultaneously, for instance, x and y direction of results. A stage controller known as Stepping Motor Drive SHOT-320GS was also used for the progressive data acquisition. The physical image of the LDA hardware system is shown in Figure 3.10.

The experimental software used in this study were basic software such as Microsoft Office, and a scanning software named 3D Burst processor Acquisition Manager, which were used with the scanning hardware. This software allows user to input settings on the

LDA system and obtain data from it. The theories on LDA system have been described in detail in section 3.5.1.1. In addition, Hamill et al. (2004) proposed an equation for the usage of LDA in relation to the geometric characteristic. Therefore their methodology is used as a reference in this current study. The equation proposed by Hamill et al. (2004) is as below,

$$\frac{U_o}{Nnr} = 1.261 - 0.974\left(\frac{p}{r}\right) + 0.733\left(\frac{c}{r}\right) + 18.53\left(\frac{t_h}{r}\right) + 5.028\left(\frac{h_d}{r}\right) + 0.106\left(\frac{p}{r}\right)^2 - 7.277\left(\frac{h_d}{r}\right)^2 - 4.093\left(\frac{h_t}{c}\right)^2 \quad (3.5)$$

3.5.1.1 Scanning software theory: Laser Doppler Anemometry (LDA)

LDA is also known as Laser Doppler Velocimetry (LDV). As mentioned in Keenan and Chapin (2009), LDA is a well-understood and accurate method to detect and measure the velocity of small particles suspended in a liquid medium. The principle of LDA is splitting a single laser beam into two beams that focus on a same focal point. These two beams shared the same intensity and created an elliptical cross sectional area, which is also known as a two-beam intersection zone (Figure 3.11). This region has interference patterns, which are uniformed light and dark fringes. In reference to Figure 3.11, d_z represents the diameter measured at the z axis, d_x is the diameter measured at the x axis and d_f is the fringe separation. The calculation of d_f and the number of fringe, N_f are written in the form (Jensen, 2004),

$$d_f = \frac{\lambda}{2\sin\left(\frac{\theta}{2}\right)} \quad (3.6)$$

$$N_f = \frac{8Ftan\left(\frac{\theta}{2}\right)}{\pi E D_L} \quad (3.7)$$

Where, D_L is the initial beam thickness, E is the beam expansion and F is the lens' focal length. The number of fringes is essential to estimate the LDA results reliability. The

higher number of fringes will give higher number of periods in the recorded signal to estimate the Doppler frequency.

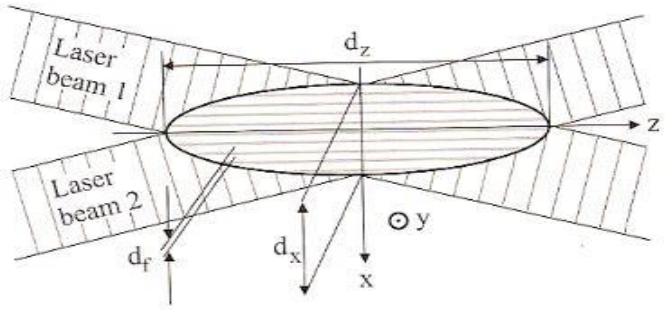

Figure 3.11: Fringing pattern observed from the two incident beams *(Keenan and Chapin, 2009)*

Doppler Effect

The particle with constant velocity will then pass through the fringe and create a Doppler shift, which is the difference between the frequency of scattered light and the frequency of the laser beam. Measurement of Doppler shift will be able to estimate the velocity of the particles passing through the fringe. However, due to the incapability of LDA in capturing and measuring the large frequency of Doppler shift, LDA focuses merely on the measurement of the beat frequency. Then, the photodiode will predict and calculate the velocity particles since the Doppler shift is linearly proportional to the velocity particles.

As the frequency of the Doppler shift is proportional to the velocity, it is important to know the beat frequency or the Doppler frequency for the particular component for velocity estimation. Keenan and Chapin (2009) suggested that the calculation of peak beat frequency and mean velocity can be obtained through,

$$U = \frac{f_{peak}\lambda}{2\sin(\frac{\theta_a}{2})} \tag{3.8}$$

Where, U is the mean velocity, f_{peak} is the peak beat frequency, λ is the fringe length and θ_a is the angle between two laser beams. In simple words, the calculation of velocity is done by multiplying the fringe spacing with the frequency intensity.

Jensen (2004) mentioned the estimation of the Doppler frequency and velocity of particular component can be calculated in the form of,

$$f_D = \frac{2\sin(\frac{\theta_a}{2})}{\lambda} u_x \quad (3.9)$$

Where, u_x is the particle velocity of the x-component, f_D is the Doppler frequency.

Characteristics of LDA

According to Jensen (2004), LDA has few advantages compared to other similar functions tools which are as below:

- Non-Contact Optical Measurement: It can sense the velocity without disturbing the flow in the measuring volume. It only requires a transparent medium and a suitable concentration of seeding.
- No Calibration and Drift: It has absolute linearity in response to fluid velocity. The measurement is based on the stability and linearity of optical electromagnetic waves and unaffected by temperature and pressure variables.
- Well-Defined Directional Response: The measuring direction is defined by the optical system, so the angular response is thus unambiguously defined.
- High Spatial and Temporal Resolution: This temporal resolution is usually limited by the concentration of seeding rather than the measuring equipment itself.
- Multi-Component Bi-Directional Measurements: This bi-directional shift allows two way measurements. Acoustic-optical frequency shift allows measurement on reverse flow velocities.

The chosen seeding particles used in the current study was Titanium Dioxide (TiO_2). This is due to the capability of TiO_2 to be well scattered in the liquid medium whilst optimising the particle surface properties and relative refractive index.

3.5.2 Propeller characterisation for validation

Validation was done for the confirmation of the current experiment with reference to particular requirements. Therefore, the single propeller characterisation was done along the efflux plane and compared with previous literature in two conditions: (i) measure one of the propeller with the other propeller remained off and (ii) measure one of the propeller with the other propeller on. The schematic view of propeller jet in the efflux plane for single propeller will be plotted and rendered to compare with the schematic view as shown in Figure 2.12. The comparison results on the characterisation are further discussed in chapter 4 and 5.

3.5.3 Experiment scaling

The scaling of experiment model was based on Verhey (1983), where the scaling effects due to the viscosity were negligible if the Reynolds number of flow (Re_{flow}) and Reynolds number of propeller (Re_{prop}) were greater than $3x10^3$ and $7x10^4$, respectively. The Reynolds numbers can be calculated using the following equations:

$$Re_{flow} = \frac{U_o D_p}{v} \tag{3.10}$$

$$Re_{prop} = \frac{nL_m D_p}{v} \tag{3.11}$$

Where L_m is the length term depending on β defined by Blaauw and van de Kaa (1978),

$$L_m = \beta D_p \pi \left[2N\left(1 - \frac{D_h}{D_p}\right)\right]^{-1} \tag{3.12}$$

U_o is the efflux velocity; D_p is the diameter of propeller; D_h is the diameter of hub; v is the kinematic viscosity of fluid (kinematic viscosity of water at 27°C $8.54x10^{-7}m^2/s$); *n* is the number of revolution per seconds and N is the number of blades. In addition, according to Rajaratnam (1981), the scale effect was neglected when the viscosity is higher than 1×10^4. The Re_{flow} ranges between 3.6×10^5 and 5.3×10^5 and Re_{prop} ranges between 1.8×10^5 and 2.7×10^5 for current study. Considering the Reynolds number for the current experiment is higher than $3x10^3$ and $7x10^4$, respectively, the scaling effect due to fluid viscosity is negligible in the current study.

3.5.4 Sampling for axial velocity acquisition from LDA

The sampling bias is computed by LDA system using the equation of $U_{mean}=1.96\times\sqrt{\frac{\overline{u'^2}}{N_s}}$, where, $\sqrt{\overline{u'^2}}$, is the root mean square of the velocity component, and N_s is the sample size. The confidence limit was set to 95% for velocity acquisition. The LDA user manual advised to use a large sample size to increase the accuracy for the acquired results. The number of samples obtained in this study was in the range of 3695 to 18995, with an average of 5289 samples at each measurement point. Therefore, the sampling bias of current investigation is approximately 0.05m/s based on the confidence limit calculated by LDA system.

3.5.5 Experiment procedure for axial velocity investigation

The experiment began by filling clean water to the tank, which is colourless without sediments. This was required for the data acquisition process. Therefore, a filter system was setup to filter all the water supply connected to the water tank. The connections between pipes and filter system were ensured to be tight and leak-proof. The water was filled to the designed height, with a minimum water level of one propeller diameter height from the tip of the propeller blade. Moreover, to prevent the breeding of

mosquito larva, a pesticide named ABATE 1-SG was poured into water tank according to its concentration level without disturbing the data acquisition process.

After filling in the water, baffle plane was inserted to the tank with the alignment of 30 degrees from the horizontal plane of the water tank, as shown in Figure 3.7. The LDA system was setup with USB connections of (i) LDV processor, (ii) stepping motor device and (iii) traverse system connected to computer ports. The system for data acquisition was arranged according to Figure 3.10. The ship-twin-propeller with inverter was switched on and left to run until the voltage reading stabilised. This was to ensure that the constant voltage has been supplied to the rotor of ship-twin-propeller before the acquisition starts. Each velocity measurement was repeated to obtain several sets of data. Thereafter, all readings were averaged and tabulated in Microsoft Excel for graph plotting.

3.6 Scour development

Scour development in time relation was observed to monitor the changes in shape and pattern of scour induced by ship-twin-propeller's wash. Apart from the rotational speed of the ship-twin-propeller, Hamill (1987) stated the other factors that will influence the scour development, as follows:

(i) Sediment size; and

(ii) Clearance between surface sediment and propeller tip.

Therefore, considerations on the choice of sediment and bed clearances used were discussed in the following sections.

3.6.1 Choice of sediment

'Single grain size' sediment was suggested by Hamill (1987) to be used in the experiment in order to allow all sediments to travel at similar velocity. The uniform sand was supplied by University of Malaya Geotechnical Engineering Laboratory. The

average value of bulk density and mean sediment size, d_{50} were also tested in the laboratory. It was estimated that a minimum of 1750 kg of sand, with bulk density of 1600 kg/m^3, will be required for the experiment. Moreover, the average range of d_{50} required for sand lies between 0.9mm and 1.0 mm.

3.6.2 Choice of bed clearances

The bed clearance is the distance between propeller tips and the surface layer of the sediment. The clearance ratio is the value of the bed clearance divided by the propeller diameter. It was decided to test the impacts on ship-twin-propellers wash at three different bed clearances. For propeller-1 (P1), depth of 70mm, 110mm and 140mm were chosen and given the clearance ratio of 0.31, 0.5 and 0.64D_p, respectively. By combining the experiment for propellers and sediments, a data series comprising three speeds (400rpm, 500rpm and 600rpm) were tested on these three clearance ratios.

3.6.2.1 Properties of sediment

The particle size of sediment along the coast is one of the major concerns that determine the transportation of sediment. Therefore, the properties of sediment, particularly the mean sediment size, d_{50}, were studied prior to the scour experiment. Two types of sediments were tested before the final sediment size was chosen.

A grain-size analysis test was performed using the Sieve Method in accordance to BS 1377: Part 2: 1990, to determine the mean sediment size, d_{50} for current experiment. Three tests were conducted. Sand 1 (*S1*) and Sand 2 (*S2*) were tested individually, where sand 3 (*S3*) was a mixture of *S1* and *S2* with the ratio of 1:1. The final sediment used in current analysis was then decided. The examples of the sieve analysis test performed in current investigation were shown in Table 3.3 and Figure 3.12.

Table 3.3: Example of Sieve Analysis Data

Sieve Size (mm)	Sieve Weight (g)	Sieve-Sample Weight (g)	Weight Retained (g)	Cumulative Weight Retained (g)	Percent Retained (%)	Cumulative Percent Retained (%)	Percent Passing (%)
2.000	410.0	410.0	0.0	0.0	0.00	0.0	100.0
1.180	390.0	500.0	110.0	110.0	0.21	21.2	78.8
1.000	395.0	550.0	155.0	265.0	0.51	51.0	49.0
0.707	325.0	580.0	255.0	520.0	1.00	100.0	0.0
0.425	315.0	315.0	0.0	520.0	1.00	100.0	0.0
0.300	295.0	295.0	0.0	520.0	1.00	100.0	0.0
0.250	305.0	305.0	0.0	520.0	1.00	100.0	0.0
0.180	300.0	300.0	0.0	520.0	1.00	100.0	0.0
0.150	305.0	305.0	0.0	520.0	1.00	100.0	0.0
0.000	275.0	275.0	0.0	520.0	1.00	100.0	0.0

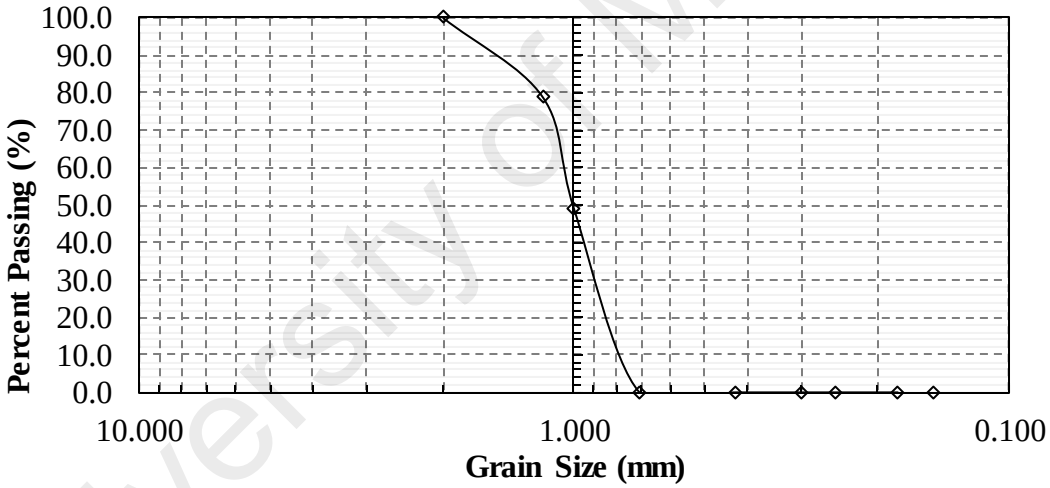

Figure 3.12: Sieve Analysis Graph for current measurement, *S1*

After performing the sieve analysis test, the geometric standard deviation was calculated based on the equation written in the form of, $\sigma_g = \sqrt{d_{84}/d_{16}}$. The σ_g of coarse sand, fine sand and coarse fine sand were 1.35, 1.48 and 1.88 respectively. Their mean sediment sizes, d_{50}, were 1mm, 0.32mm and 0.45mm respectively. *S1* was uniform soil, while *S2* and *S3* soil were not uniform. Therefore only *S1* soil was appropriate for experiment.

It is good to know that current experiment only considered one type of soil sediment size. Reason being the sediment trend is believed and agreed with previous literature that the finer the particle the scour would be more severe due to the bed load is lighter as per literature or vice versa.

3.6.2.2 Soil relative density

Apart from sediment grain size, sediment density will also have an impact on the sediment transportation based on the dependent factor of densimetric Froude number, F_o, as previously mentioned in Chapter 2. Therefore, a standard Proctor test was performed on chosen soil, *S1*, in accordance with BS 1377: Part 4: 1990 to determine bulk (ρ_b) and dry (ρ_d) density of *S1* soil. The results of bulk and dry density of *S1* were 1590 kg/m^3 and 1553 kg/m^3, respectively. The properties of chosen soil *S1* are shown in Table 3.4.

Table 3.4: Properties of experimental sediment, *S1*

	d_{50} (mm)	ρ_b (kg/m^3)	ρ_d (kg/m^3)
S1	1.0	1600	1553

3.6.3 Scour geometry properties

The scour geometry profiles are affected by experiment variables. Current investigation had limited the experiment variables for precise analysis on these parameters. The main factors which determined the maximum scour depth are,

(i) The efflux velocity from ship-twin-propeller's wash, and

(ii) The clearance between the tip of propeller and the surface of sand bed.

Efflux velocity is the maximum velocity from ship-twin-propeller's wash. As such, only efflux velocity is considered in determining the maximum scour depth. Moreover, distances between propeller's tips and the surface of sand bed will also have a strong impact on the maximum scour results as stated by Hamill, (1987) and Hong et al.,

(2013). Therefore, the clearance is also a major parameter in determining the maximum scour depth.

3.6.4 Experiment procedure for scour investigation

The sand in the experiment was levelled to obtain a flat-bed for observation purposes, prior to the commencement of each experiment. The water filling process had to be done slowly and carefully to avoid disturbance on the levelled sand bed. In order to take the readings with the presents of water, a depth gauge was used. Paper rulers were attached around the top of the tank for position reading. The scour geometry readings were taken at intervals twice as long as the previous reading, starting from 15 minutes (i.e., 15, 30, 60 etc. minutes), up to the asymptotic state which was approximately 64 hours. This was suggested by Hamill (1987) and supported by Hong et al. (2013). The measurement grid was 5mm × 5mm within the scour area. The elapsed time for data acquisition was measured using a stopwatch. The ship-twin-propeller was paused during the data acquisition, enabling the data to be taken accurately in still water. Temporarily stoppage of the ship-twin-propeller would not affect the overall development of scour geometry profiles as this investigation was conducted in a confined tank without excessive flow and sediment supply towards the experiment environment. Therefore, as suggested by Hamill (1987), it is safe to assume that the scour results would not be affected by turning off the propellers during measurement.

3.6.5 Propeller rotation

Due to the limitation of current model of propeller shaft and controller, the propeller can only rotate in one direction, which is clockwise (towards the right side). The opposite rotational direction will result in backward velocity force, which leads to reversal in the velocity thrust. Therefore the scour impact on the right side tends to be much deeper. Moreover, this rotation also represents the parking movement during ship docking. The pulling of gear case in the same direction will cause the ship to roll over to

the port. Therefore, the longitudinal section view of scour profile shall be obtained from the right side, which has a stronger scour impact especially to the port, and shall be observed through the temporal development of scour profile.

3.7 Regression analysis

Regression is a statistical method used to estimate the relationship between two or more variables, which is commonly represented by the correlation coefficient. In addition, it indicates the relative strength of various independent variables effect on a dependent variable. Regression analysis is commonly used to forecast an effect or future trend prediction. It is used to estimate the best fitted line and equation with minimal prediction error through sets of observed data. The basic equation of a linear regression is as follows:

$$Y = \theta_1 x_1 + \theta_2 x_2 + \cdots + \theta_i x_i + \cdots + \theta_n x_n + \varepsilon \tag{3.13}$$

Where Y is the dependent variable, $\theta_1, \theta_2, \ldots, \theta_{\mathrm{i}}, \ldots, \theta_{\mathrm{n}}$ are the regression coefficients, $x_1, x_2, \ldots, x_{\mathrm{i}}, \ldots, x_{\mathrm{n}}$ are the independent variables, and ε is the random error.

3.7.1 Non-linear Regression

Regression can be used to fit non-linear data where the relationship of the model is represented by curves rather than straight lines, for example, exponential, trigonometric and power functions. Iterative algorithm is used to fit the non-linear regression. The model of a non-linear regression is as follows:

$$\boldsymbol{Y} = \boldsymbol{f}(\mathbf{X}, \beta) + \boldsymbol{\epsilon} \tag{3.14}$$

Where $\boldsymbol{Y}$ is the vector of response variables, $\mathbf{X}$ is a vector of p predictors, β is a vector of k parameters, $\boldsymbol{f}(\cdot)$ is some known regression function, and $\boldsymbol{\epsilon}$ is an error term.

Non-linear regression is capable to accommodate varieties of mean function, which is useful for research, scientific and engineering processes as many of the processes are inherently non-linear. It produces relatively good estimates of the unknown parameters in the model despite having a relatively small number of data sets. However, the parameter estimates are highly dependent on the iterative optimisation procedures, which require an unknown value to be set as the starting value of the iteration. As such, a good starting value of iteration is vital to the regression analysis. Moreover, non-linear regression has high sensitivity to outliers, which may affect the results of the overall analysis.

In current study, non-linear regression was used to estimate the relationship where the response variable, $\boldsymbol{Y}$, is maximum scour depth, and key dependent factors, p, are time, ship-twin-propeller's rotational velocity, the under keel clearances between the seabed and the propeller tip and Froude number.

3.8 Numerical simulation

Numerical simulation is a computational method that uses software instead of laboratory work. The advantages of numerical simulation include the ability to predict some difficult configurations with smaller space consumption as compared to existing experimental methods. Moreover, conventional experiment setup requires large funding and long duration to obtain accurate results. However, as numerical simulation uses software instead of laboratory work, the reliability of results is strongly dependent on the interpretation of experts. Consequently, the accuracy of experimental works is higher than numerical simulation, as numerical simulation solely relies on the interpretation of engineers based on their knowledge and experiences.

There are a few successful simulation cases validated with accurate experimental results which had proven that computational study is reliable. Successful cases include Hamill et al. (2009), which used the artificial neural networks (ANN) as a tool in studying the effects of rudder angle on ship propeller's wash velocities impinged the seabed. Ryan et al. (2013) did further research from Hamill et al. (2009) using ANN method to analyse the velocity distribution from a ship's propeller and the corresponding scour. Lam et al. (2012c) also investigated the turbulence intensity of ship propeller's wash by using Fluent CFD. However, the application of VOF method on the seabed scour induced by propeller wash is still limited.

3.8.1 Selection of CFD software and hardware

From a range of Computational Fluid Dynamic (CFD) products in the market, the selected CFD software must have the capability to analyse the flow regime induced by rotating objects and the capability to model rotational movement of propeller. Therefore, the methods used to model the ship-twin-propeller wash similar to methods applied for single propeller wash. Lam et al., (2010; 2012a) used the CFD method to investigate the velocity distribution field of a single propeller wash. He recommended the appropriate solver, turbulence model and type of mesh which are used for single propeller. Hence, similar method shall provide accurate numerical prediction of the velocity field for ship-twin-propeller wash. On the other hand, the selected software must have the capability to track the particles moving or the alteration of different phases in the simulation. The software is only selected when these two criteria are fulfilled.

An HP Z820 computer workstation with quad core processors Intel Xeon, 2.40 GHz and 32 gigabytes ram was used. This workstation has powerful processors and large memory storage which is able to uphold the simulation process and data storage. The software package selected for current investigation was the ANSYS FLUENT package, version 15.0 (2013), produced by Fluent Incorporate. ANSYS FLUENT is an

engineering computer program for the modelling of fluid in complex geometry with complete mesh flexibility in two or three dimensional meshes (Fluent Inc., 2006). Fluent also has the capabilities in modelling multiple moving frames, free surface and multiphase models for the flow. It has a concise software structure with different functions in different stages:

- In the pre-possessing stage, GAMBIT was used for the geometry modelling and meshes generation, incorporated with different types of filters (translators) for the import of surface and volume meshes such as: ANSYS, Fluent 5/6 and others.
- In the solving and post-processing stage, FLUENT was used as the mesh adapter, solver and also for the post-processing to readable data.

3.8.2 Mesh

Various meshes were built according to the needs of simulation. However, all the created meshes are required to undergo a mesh independent study to ensure the mesh convergence. The mesh size gradually increases by approximately 10 to 20 per cent from the previous mesh. Mesh independent study is completed when the results obtained using finer meshes has a variation of less than two per cent. The simulation works from the subsequent mesh are then used. The mesh independent study was undertaken for two main reasons:

(i) To run the mesh with optimum time while getting the best converged results as other finer mesh.

(ii) To minimise the error margin.

Moreover, as the time required for modelling an unsteady solver was unknown, an optimum time step was selected for the simulation with the consideration on converging trends.

3.8.3 Numerical setup

The propeller simulations were conducted at a bollard pull condition, which is zero advance speed of the ship, as in line with Hamill et al. (1999). Water in simulation tank was set to be shallow still water without channel flow and sediment supply. The vertical gravitational force was also neglected as jet velocity was the only source that caused scour during the simulation.

A test case similar to the experiment work done by Hamill (1987) was set up. Therefore the boundary and initial conditions of the simulation were consistent with Hamill (1987) experiment setup, such as follows: experiment tank size of 3.5m×6.0m×0.7m, a 0.154 m diameter propeller running at its efflux velocity and non-cohesive soil flat bed with density of 1600 kg/m^3.

3.8.4 Multiphase flow: Volume of Fluid (VOF)

Multiphase flow allows different numbers of flows into the nature and forms a mixture of phase. A particular phase can be identified as a particular material or a composition of same materials but with different physical characteristics. Computational fluid mechanics provide insights into the fluid dynamics of multiphase flow in different forms. According to Fluent Inc. (2006), three Euler-Euler available multiphase models are the VOF model, Eulerian model and mixture model.

VOF model is selected in this study due to its capability to resolve difference in density and to observe the tracking of different phases of non-interpenetrating fluid. In VOF model, when medium consists of two types of fluid, the velocity fields for the two types of fluid are assumed to be the same. A volume of fraction was introduced to indicate the changes of each phases, as the changes are not able to be occupied in other phases. The volume of fraction is a continuous function where the sum of all phases equals to 1. The graphical changes at different time and location of the scouring line

were represented by the changes of the advection equation for volume fraction, α. The volume fraction was read in the form of 0 to 1, representing either one of the phases or the mixture of the phases (Fluent Inc, 2006). Consequently, VOF is capable to capture the sediment motion and perform scour prediction by the observation on alpha field at different fraction level. Therefore, accurate settings in each phase are crucial to prevent unnecessary problem. VOF requires at least two different types of phases to run the simulation. These two phases will be defined as water and sediment. The actual sediment particles tracking would not able to be modelled. The moving of different phases can be modelled and using various related equations.

According to Fluent Inc. (2006), equations commonly used in VOF method are volume fraction equation, momentum equation and energy equation, listed as below:

Volume of fraction for q^{th} phase,

$$\frac{1}{\rho_q}[\frac{\partial}{\partial t}(\alpha_q \rho_q + \nabla \cdot (\alpha_q \rho_q \vec{v}_q) = S_{\alpha_q} + \sum_{p=1}^{n}(\dot{m}_{pq} - \dot{m}_{qp})] \quad (3.15)$$

Momentum,

$$\frac{\partial}{\partial t}(\rho\vec{v} + \nabla \cdot (\rho\vec{v}\vec{v}) = -\nabla\rho + \nabla \cdot [\mu(\nabla\vec{v} + \nabla\vec{v}^T)] + \rho\vec{g} + \vec{F} \quad (3.16)$$

Energy among the q^{th} phase,

$$\frac{\partial}{\partial t}(\rho E) + \nabla \cdot (\vec{v}(\rho E + \rho)) = \nabla \cdot (k_{eff} \nabla T) + S_h \quad (3.17)$$

Where, α is the volume of fraction value, E is the energy, T is the temperature, S_h is the source term, k_{eff} is the effective thermal conductivity, ρ is the density,

$\vec{v}$ is the velocity vector, g is the gravitational force. μ is the phase viscosity and $\vec{F}$ is the body force.

When medium consists of two types of fluid, the velocity field for the two types of fluid is assumed to be the same. VOF solves an advection equation for volume fraction, α, which reads in the form of $\partial\alpha/\partial t = 0$. The fraction indicates that the alpha is adverted with the fluid velocity itself and this will give a graphical representation of the alpha field at different time level to indicate the longitudinal scour profile of the ship's propeller wash induced scour.

3.8.4.1 Phase adjustment

Both two-dimensional (2D) and three-dimensional (3D) model were set up. Phase adjustments were made to comply the application of VOF model. Both 2D and 3D dimensional VOF model were set up with the same phase settings. In this model, total of two phases were defined. The phase with lower density is classified as the primary phase whereas the higher density phase is the secondary phase. The water at ambient temperature with a density of 998.2 kg/m3and viscosity of 0.001003 kg/m-s is defined as primary phase. The sand with density weight 1600 kg/m3 and same water viscosity is defined as secondary phase. Both phases of soil and water were assumed to have similar viscosity behaviour. The volume of fraction for primary phase was set to be zero (α=0) whereas the initial flat erodible bed in secondary phase was set as α=1.

3.8.4.2 Two-dimensional VOF: single propeller jet

The simulation tank was initially set to be 6.0m×0.7m. However, after several runs, it was found that the estimation of scour process does not require such a large grid size. In order to optimise simulation time, the tank size was reduced to 3.5m×0.7m. Five clearances were used in this simulation, including 0Dp, 0.31Dp, 0.64Dp, 0.95Dp and 1.32Dp. In line with Hamill (1987), these clearances were chosen to increase the limits

of clearance range for current study. In addition, the changes in scour pattern were visible based on the clearance variation. A two-dimensional model with segregated solver, pressure-velocity coupling by the SIMPLE algorithm, VOF model, standard k-ε turbulence model and equation discretisation by a first-order upwind scheme was set up.

Other boundary conditions include: (i) wall boundary for surroundings, (ii) an interior boundary between both phases, (iii) volume of fraction of 0.5 for boundary layer in secondary phase, (iv) velocity inlet with uniform efflux velocity flow of 2.065 m/s (800 rpm rotating speed), (v) a pressure outlet boundary with zero pressure, (vi) sediment depth of 300 mm, (vii) a zero pressure outlet at the edge of the tank, and (viii) a fan with polynomial pressure jump profile boundary between the inlet and outlet. Besides, the polynomial pressure range was limited to 2.065m/s to ensure that the flow remains constant. Although it was not possible to predict the detailed flow through the fan blades, the model has the capability to estimate the amount of flow through the fan. The influence of ship's propeller geometry on the propeller jet is considered to be insignificant when the ship was stationary or manoeuvring at low speeds (Prosser, 1986). A schematic diagram and the mesh domain are shown in Figure 3.13 and 3.14.

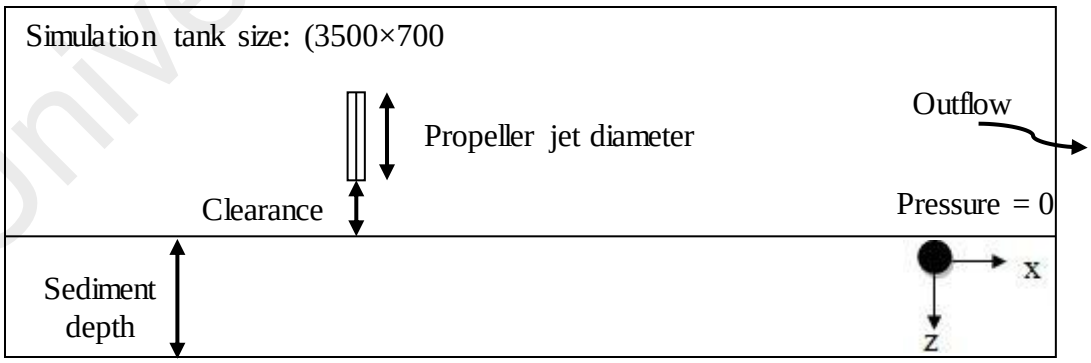

Figure 3.13: Schematic diagram of domain

Figure 3.14: Mesh domain *(From Fluent Inc, 2006)*

3.8.4.3 Three-dimensional VOF: single propeller jet

The initial conditions for 3D VOF simulation were set as follows: (i) a 154mm fan that run under three rotational speeds; 400 rpm, 600 rpm and 800 rpm in two different clearances of $0.31D_p$ and $0.64D_p$; (ii) the sediment density was set to 1600 kg/m^3; (iii) simulation tank mesh was separated into two phases namely water and sediment layer; (iv) a fan-swirling which represents the rotating propeller. A 3D model with segregated solver, pressure-velocity coupling by the SIMPLE algorithm, VOF model, standard k-ε turbulence model and equation discretisation by a first-order upwind scheme was set up.

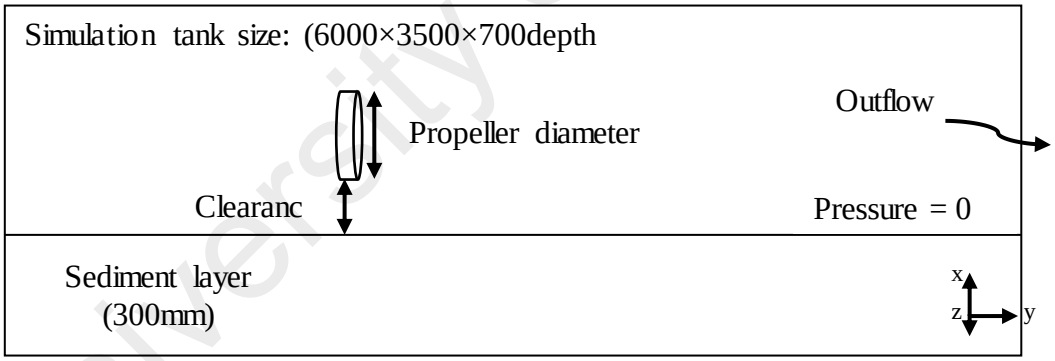

Figure 3.15: Schematic representation of 3-D tank

Figure 3.16: Mesh domain of 3-D simulation

Other boundary conditions of this simulation include the following: (i) volume of fraction of 1 for sediment layer, (ii) a pressure outlet at the edge of tank, (iii) sediment depth of 300 mm, and (iv) fan and fan-swirling setting with polynomial pressure jump profile boundary between the inlet and outlet, the polynomial pressures were limited to 1.032 m/s, 1.549 m/s and 2.065 m/s for each run. Moreover, the swirling effects of the fan modelled in 3D simulation has the capability to remodel the rotating fan features by controlling the pressure difference which leads to the effect of trailing and suction side of a rotating propeller. However, the fan model is unable to predict detailed flow through the fan blades but it is able to estimate the amount of flow through the fan (Fluent Inc., 2006). Prosser (1986) highlighted that the influence of ship's propeller geometry on the propeller jet was insignificant when the ship was stationary or manoeuvring at low speeds. Therefore, consideration on the geometry of the fan blades was neglected in this simulation. The schematic diagram and mesh domain of 3D simulation are shown in Figure 3.15 and 3.16.

3.8.4.4 Three-dimensional VOF: ship-twin-propeller scouring

(a)

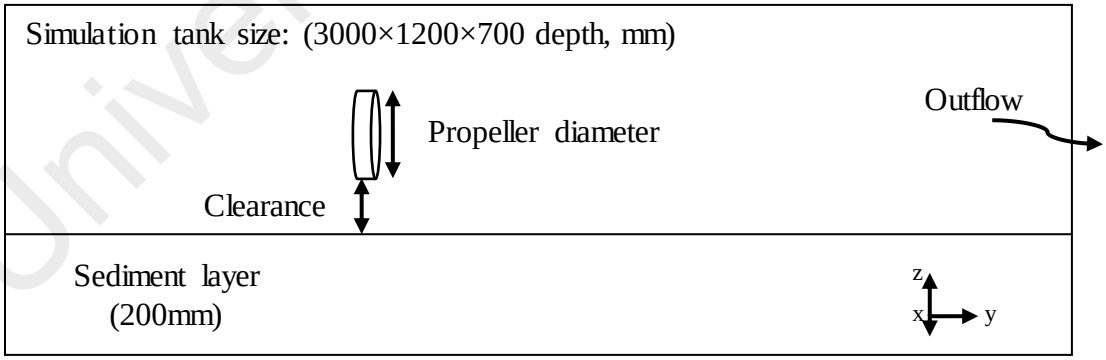

(b)

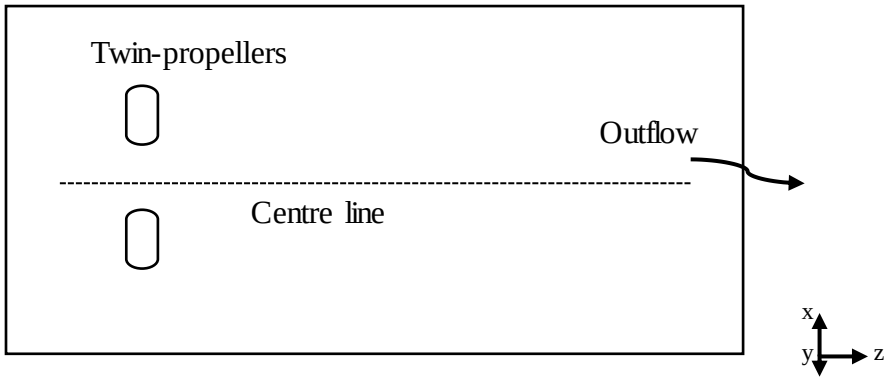

Figure 3.17: Schematic diagram of 3-D ship-twin-propeller simulation (a) side view (b) plan view

The 3D VOF models the ship-twin-propeller scouring experiment works. Using the similar dimension of 3.0 m×1.2 m×1.0 m tank and two propellers P1 with diameter of 220 mm. The soil density was set to be 1600 kg/m^3. Since the water level was merely filled up to 0.7 m, the simulation tank will only consider the depth of 0.7 m instead of 1.0m. Based on the experiment setup, three clearances were used in the simulation.

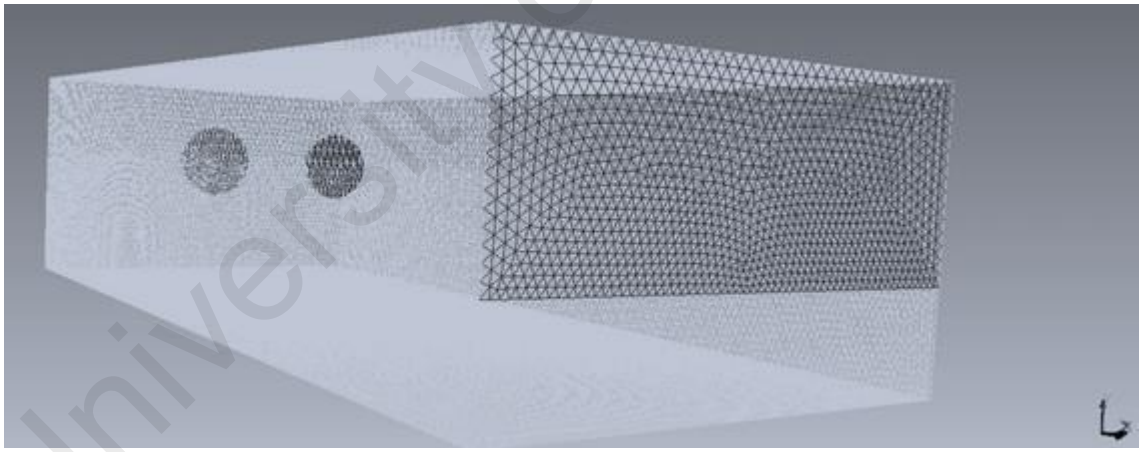

Figure 3.18: Mesh domain of 3-D ship-twin-propeller simulation

A 3D model of ship-twin-propeller was set up with features such as segregated solver, pressure-velocity coupling by the SIMPLE algorithm, VOF model, and equation discretisation by a first-order upwind scheme. Other boundary conditions of the simulation were as follow: (i) volume of fraction of 1.0 for sediment layer, (ii) a pressure outlet at the edge of tank, (iii) sediment depth of 200 mm, and (iv) fan and fan-swirling setting, with polynomial pressure jump profile boundary between the inlet and

outlet. For each simulation, the polynomial pressure range was limited to 1.866 m/s, 2.332 m/s and 2.798 m/s. The schematic diagram and the mesh domain of 3D ship-twin-propeller simulation were relatively similar to single propeller from the side view. Therefore both side and plan views are shown in Figure 3.17 and 3.18.

3.9 Data analysing for experiment and simulation

A brief description on the methodology of data collection and analysis is given in this section. Further explanations are presented in Chapter 4. There are two parts of data obtained through the experiment. Firstly, the validation of ship-twin-propeller with single propeller and its corresponding axial velocity profile. The data was obtained using LDA software and its station files. Then, all the data obtained from the station files was transferred to Microsoft Excel for further analysis such as graph plotting and comparison with previous literature. For part two, which is scour measurement, scour profiles and its dimensions were obtained point by point from the scour hole. Dimensions such as scour depth, area and volume were tabulated and calculated accordingly. Further data analysis was done by contouring the scour profile laterally, longitudinally, as well as in plan view and three-dimensional view. All of these were done to improve the visualisation and estimation of scour profile through analysis. On the other hand, for the simulation section, scour lines and profiles were tabulated and observed from the simulation. The estimation of maximum scour depth was done through the longitudinal section and plan view of scour profile.

3.10 Summary

Methodologies for experiment and numerical setup have been discussed thoroughly in this chapter. Furthermore, all hardware and software used were also justified and explained. Two limitations were highlighted in this chapter. Firstly, the data acquisition of axial velocity flow was completed in the zone of flow establishment, due to the type of velocity produced by propellers which was determined at efflux plane. Secondly, the

investigation on scouring action was performed with uniform sand and fixed plane flat bed. This was done to eliminate velocity distributions other than velocity produced by the ship-twin-propeller. Since the experiment and numerical program were set up, the monitoring of velocities induced by ship-twin-propeller and resulting scouring action was initiated.

CHAPTER 4:RESULTS AND DATA ANALYSIS

Overview

In this chapter the results of data analysis for ship-twin-propeller's wash and its resulting scour are presented. The data were collected and analysed in response to the problems and objectives for this thesis, as stated in chapter 1. The importance and methodology of this study on ship-twin-propeller's wash induced seabed scour have been highlighted in chapter 2 and 3. Since literature had indicated that the ship-twin-propeller's wash induced seabed scour remains limited in this field, the discussion of current chapter will only be focusing on ship-twin-propeller scouring. Outline of this chapter considers the axial velocity profiles by ship-twin-propeller's jet and its resulting scouring action. The experimental investigation on axial velocity profiles of ship-twin-propeller's jet in the zone of flow establishment was analysed and discussed with current literature and existing theories. The axial velocity of ship-twin-propeller's jets and its resulting scour action had been measured throughout this research, experimentally and numerically (only for scour observation). Results from both methodologies have been analysed, discussed and compared in this chapter. Scour dimensions and profiles were also plotted and highlighted in current study for better visualisation view.

4.1 Introduction

When ship's propeller rotates, it draws the water from the back of the propeller and forms the jet. When the jet impinges with the soil and mitigates sediments, it is known as ship's propeller wash. These wash happened in a range of distances of two propeller flow zones as indicated in previous literature. These are zone of established flow and zone of flow establishment. There is no specific limit indicating where the zone ends, but there is literature that shows a good estimation on the zone size. The estimated zone

size is equivalent to two propeller diameters for the zone of established flow as stated in Hamill et al. (1999). Scouring impact within this zone is in particular interest where the highest velocity magnitudes from ship's propellers were induced at this zone.

Scour resulting from ship's propeller wash is due to the velocity magnitudes in contact with seabed layer. The velocity magnitudes depend on the distance of the propeller axis from the bed, as well as the traverse distance from the jet centreline to the point of interest (Hamill, 1987). Therefore, the development of scour is dependent on the velocity magnitudes. The maximum axial velocity is found to be within the zone of flow establishment (Albertson et al., 1950; Hamill, 1987). The maximum flow velocity begins to decay from the end point of the zone and initiates the next zone which is the zone of established flow. Since the efflux velocity has been derived from the zone of flow establishment, the detailed velocity measurement focuses on the particular zone of flow establishment. Moreover, the velocity within this zone must be accurately estimated to enable adequate design on scour protection.

On the other hand, the development of scour profile in relation to time was described in Hamill et al. (1999) and Hong et al. (2013). Therefore, the experiment on the development of scour profiles induced by ship-twin-propeller's wash was monitored at intervals of time, for each experiment, until it achieves the asymptotic condition. Experiments were carried out using ship-twin-propeller, rotating at speeds of 400, 500 and 600 rpm with only non-cohesive sand. Each rotational speed was tested at three clearance distances with same time intervals, as outlined in chapter 3.

The importance of the research on ship's propeller wash induced scour via Computer Fluid Dynamic (CFD) method has been increasing, to improve the understanding of the scouring process induced by ship's propeller wash. CFD is a numerical analysis of flow system by means of computer-based simulation (Versteeg and Malalasekera, 1995). For

current investigation, the results using Volume of Fluid (VOF) method is tabulated and recorded. The functions and procedures of VOF method has been thoroughly stated in Chapter 3.

4.2 Axial velocity of ship's propeller jets

Propellers drew the upstream water into slipstream producing high velocity jets during the rotation which includes axial, radial and tangential velocities. Axial velocity is the main contributor to the total velocity magnitude from the ship's propeller jet and is the key factor in causing scour (Hamill, 1987). The axial velocity profiles from previous literature were estimated using single rotating propellers. These were used to solve the axial momentum equation in reference to Gaussian normal probability function, which was proposed by Albertson et al., (1950). Therefore, these have drawn the attention in investigation of the axial profile from ship-twin-propeller jets profile in order to provide a sound basis for ship-twin-propeller jets scouring action.

In current study, the axial velocities of ship-twin-propeller's jets were investigated through Laser Doppler Anemometry (LDA) system. A scaled ship-twin-propeller with diameter of 220 mm operating in three corresponding rotational speeds of 400 rpm, 500 rpm and 600 rpm was investigated in designated series as mentioned in chapter 3. This was directed to investigate the velocity change of ship-twin-propeller's jets within the zone of flow establishment.

4.3 Axial velocity measured at propeller face whilst ship-twin-propeller running simultaneously

Axial velocity distribution of ship-twin-propeller was firstly measured from single propeller face whilst both propellers running simultaneously (TP). The measured position of current investigation is shown in Figure 4.1. The intersection point of the laser was aimed directly at the jet centreline and proceeded downward to obtain the

decay profile, whereas the cross section profile across the centreline was obtained along the propeller face parallel with the propeller axis. The propeller face is assumed as the horizontal axis of the graph in Figure 4.2 to 4.4 and Figure 4.8.

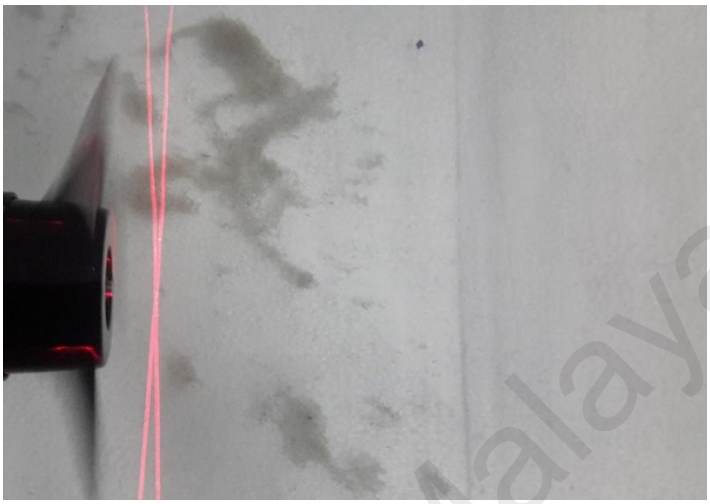

Figure 4.1: Measured position from single propeller face

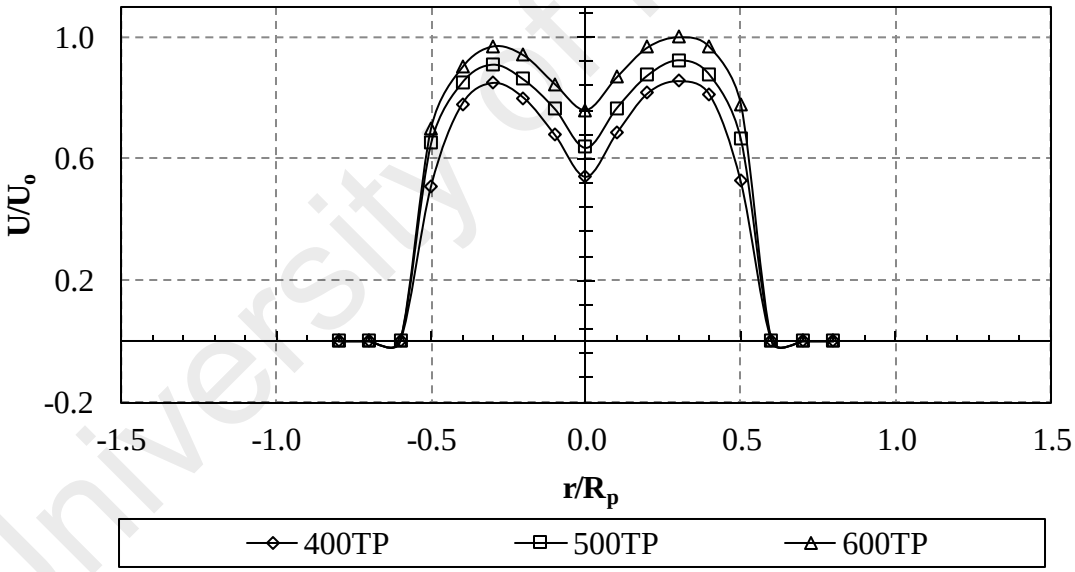

Figure 4.2: Dimensionless axial velocity of running ship-twin-propeller jets measured at single propeller face

A dimensionless axial velocity (U/U_o) in proportion to dimensionless propeller position (r/R_p) is shown in Figure 4.2. A low velocity core was found at the centreline of a single propeller. It has increased in line with the rotational velocity. Two velocity peaks were found at $0.3r/R_p$ on both side of the graph and remained constant despite the increase in rotational speeds. These results showed that the propeller velocity thrust increases in proportion to the given increasing operating speed. Although it was

measured at the single propeller face whilst both propellers were running, the results shared the same characteristics with the results measured from single propeller's face. There were two velocity peaks and a low velocity core at the centreline of propeller as mentioned in Hamill (1987). However, according to Lam et al., (2010), it is possible to have two peaks with different height, and it is acceptable when the difference in height of both peaks is less than 10%.

4.3.1 Experiment validation with previous literature

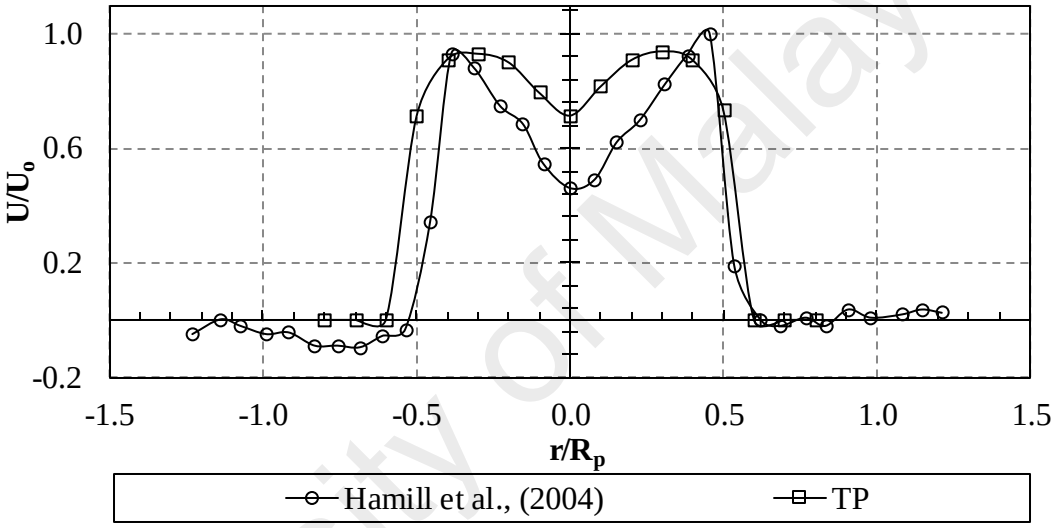

Figure 4.3: Dimensionless axial velocity compared with single rotating propeller

The resulting axial velocity measured from TP was compared with Hamill et al., (2004) at the propeller face (see Figure 4.3). The axial velocity distribution profile has similar curve patterns, which consists of two velocity peaks and a low velocity crest. The velocity of hub was lower than across the blades since the hub does not produce any axial thrust as discussed in Hamill et al. (2004). This is due to the velocity at hub that was lower than other velocity magnitudes across the blades attributed to the hub, which does not produce any axial thrust. Therefore, the velocity at hub is solely dependent on the velocity induced by the propeller blades.

Another experiment was carried out with a single propeller (SP) for validation purposes. A comparison in low-velocity crest has been made between TP, SP and Hamill et al. (2004) as shown in Figure 4.4. TP has the highest crest, which were 58.42% and 15.87% higher than Hamill et al., (2004) and SP, respectively. Moreover, SP was 34.54% higher than Hamill et al. (2004). The difference between SP and Hamill et al., (2004) was attributed to the difference in the blade geometry design of properties. The impact on the rotation of ship-twin-propeller contributed to the higher velocity magnitude at the centre crest, which resulted in higher low-velocity crest magnitude compared to single rotating propeller.

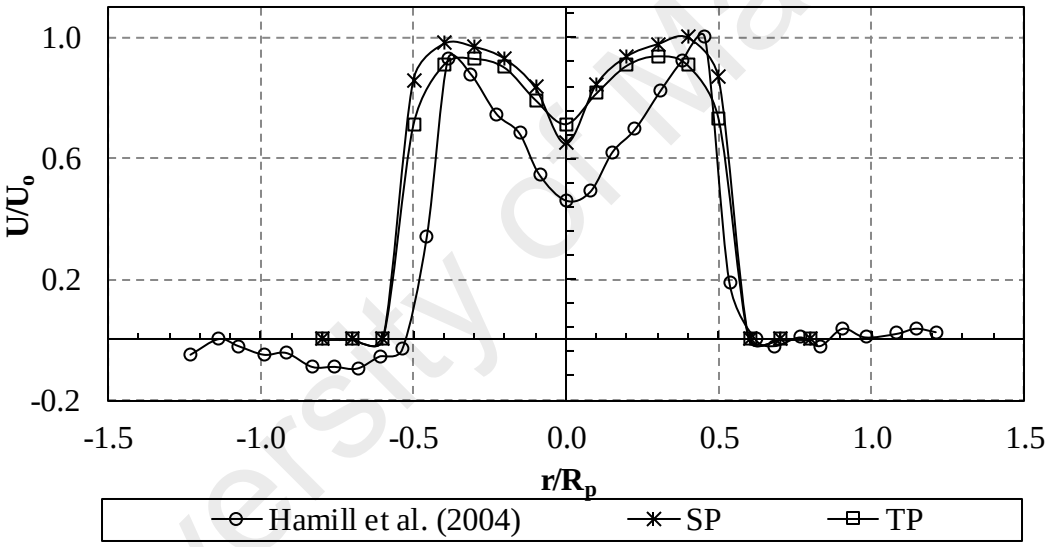

Figure 4.4: Comparison of efflux velocity between TP, SP and literature

Table 4.1: Comparison between single and ship-twin-propeller measured at single propeller face

Properties	**Prediction from theoretical equations [2.24]**	**Single Propeller**	**Single propeller measured from simultaneous running ship-twin-propeller**
Pattern	-	Processed with peaks and a low velocity crest	
No of peaks	-	2	2
Velocity crest	-	Lower	Higher
Position of peak (r/R_p)	0.37	0.45	0.30

Moreover, both velocity magnitude peaks induced from ship-twin-propeller measured along the propeller face were located closer to the hub as compared to single rotating propeller, which were approximately $0.3r/R_p$ and $0.45r/R_p$, respectively. Therefore, the higher concentration was given by the ship-twin-propeller's jets at the centre profile. An overall comparison between single propeller and ship-twin-propeller measured at single propeller face was summarised in Table 4.1.

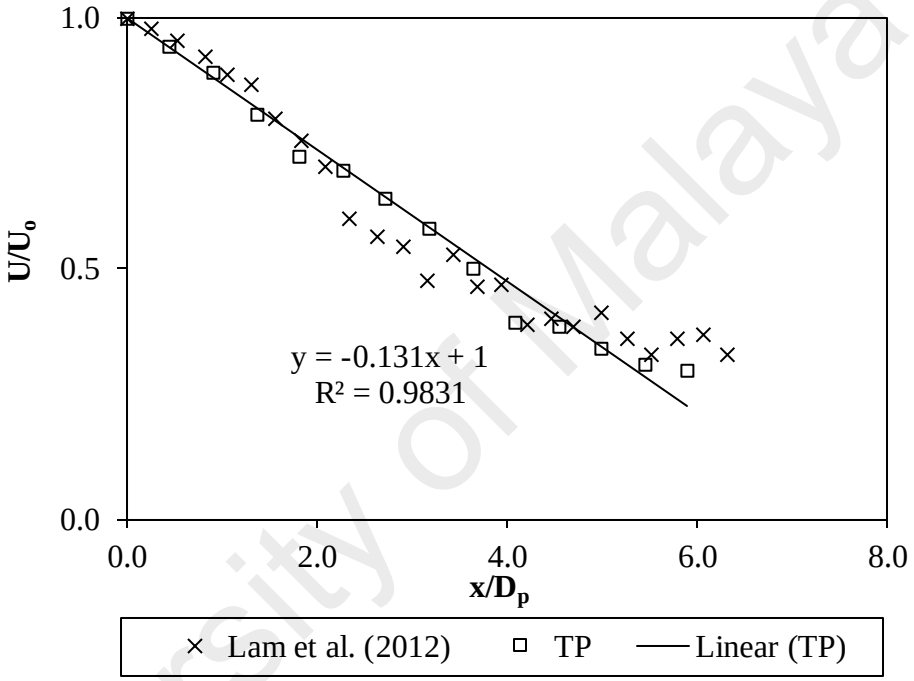

Figure 4.5: Comparison of the dimensionless axial velocity decay at propeller face

A validation measurement of TP was taken and plotted in Figure 4.5, to be compared with the LDA measurement readings by Lam et al. (2011). The x/D_p equals to 0 indicating the propeller face. The pattern and the decay rate of velocity magnitude for TP were similar with the pattern of a single rotating propeller. The maximum axial velocity started to decay immediately after the face of propeller. The linear equation profile has a high R^2 value of 0.9831 and a slope value of 0.131, and the equation is written in the form of $\frac{U_{max}}{U_o} = 1 - 0.131(^{x}/_{D_p})$. The decay velocity profile was further compared with the linear regression model axial velocity along the decay profile,

$\frac{U_{max}}{U_o} = 1 - 0.1592(^{x}/_{D_p})$, proposed by Lam et al. (2011). The slope value difference is merely 0.0282, which is less than 10%. This difference might be due to the contribution factor by another propeller that was rotating simultaneously during the measurement. Moreover, the results were supported by Lam et al. (2011) which indicated that there was no constant maximum axial velocity close to propeller.

4.3.2 Efflux velocity from single propeller face

Efflux velocity is the maximum value of velocity found on the axial distribution profile by a single rotating propeller jet (Hamill et al., 2004). Efflux velocity occurs at the efflux plane, which is located at the immediate downstream of the propeller (Lam et al., 2012). A single peak from the profile was chosen for comparison, as the magnitude profile of propeller jet was asymmetrical (Hamill, 1987; Steward, 1992).

The efflux plane has a similar velocity pattern as the axial velocity profile, but with the highest velocity magnitude peaks near the propeller's centreline. The current measurement of efflux velocity profile of TP was compared with SP and Hamill et al. (2004), as shown in Figure 4.4. It was found that all three curves shared a similar pattern, which consists of a low-velocity crest and two velocity peaks. This indicates that the rotation of an additional propeller did not affect the velocity pattern measured from the single propeller face, as there were still two velocity peaks and a low-velocity crest at the centreline of propeller face. However, the increased number of propellers had influenced the peak velocities across the propeller face. The peak velocities of TP were lower compared to single rotating propeller's peak velocities. This indicates that the highest velocity point did not occur at the propeller face when ship-twin-propeller's jet was powered.

4.3.2.1 Location of efflux velocity

The velocity profile of ship-twin-propeller increased from the propeller hub up to 0.30r/R_p, then gradually decreased to the blade tips. The position differs considerably as compared to Hamill et al. (2004), which were positioned at 0.45r/R_p from the propeller hub (see Figure 4.4). For position of SP measurement, it was located at 0.40r/R_p which is almost similar with Hamill et al. (2004). The position of current study was also compared with theoretical equation proposed by Berger et al. (1981), where the efflux velocity was positioned at R_{mo}=0.67(R_p-R_h). From the theoretical equation, the position of efflux velocity should be located at 0.365r/R_p. Current measurement shown a variation of 8.75% in efflux position, which is less than 10%, indicating that this measurement is acceptable. This might be due to the influence of different blade geometry or shape of the propeller blades, indicated by Hamill et al. (2004). The understanding on propeller locations has been assisting engineers and researchers to understand the point of source that will induce the largest velocity thrust. Therefore, engineers were able to predict the future structures in retaining the coastal line.

4.3.3 Comparison with existing theory

The comparison between the axial momentum theoretical equation, SP and TP is shown in Figure 4.6. The measured efflux velocity of single propeller showed a maximum reading of 3.25 m/s for a single propeller-220 rotating at 600 rpm, whereas the efflux velocity for TP gave a reading of 3.05 m/s with the same propeller running at 600rpm. A value of 2.80 m/s was obtained by substituting the related parameters into the axial momentum theory, $U_o = 1.59nD_p\sqrt{C_t}$, where U_o is efflux velocity, D_p is propeller diameter and C_t coefficient of thrust. The current measurements of SP and TP differed by 13.80% and 8.19% respectively, from the axial momentum theory. The axial momentum theory which was assumed from an actuator disc has resulted in these under predictions.

In addition, when measurement data was inserted in the axial momentum theoretical equation, the results were inconsistent with the theoretical prediction. The SP and TP data showed the linear equations of y=1.91x and y=1.82x, respectively, when all the measurement points were intercepted at the zero point. The coefficient of 1.91 and 1.82 showed that the measurement data were inconsistent in terms of coefficient value when compared with theoretical equation as mentioned in equation [2.24]. These indicated that the data does not perfectly fit into the axial momentum theory. However, R^2 values for both SP and TP were relatively high at 0.96 and 0.95 respectively. The high R^2 values indicate a high data consistency and correlation between the current measurements and the axial momentum theory. The higher R^2 value of SP revealed that the results of SP is more reliable and closer to the axial momentum theory as TP results had been interfered by rotational forces induced by the second rotating propeller. Therefore, the suggested coefficient for measurement at propeller face with both propellers running was 1.82, written in the form of $U_o = 1.82nD_p\sqrt{C_t}$, for the prediction of efflux velocity for TP in this experiment.

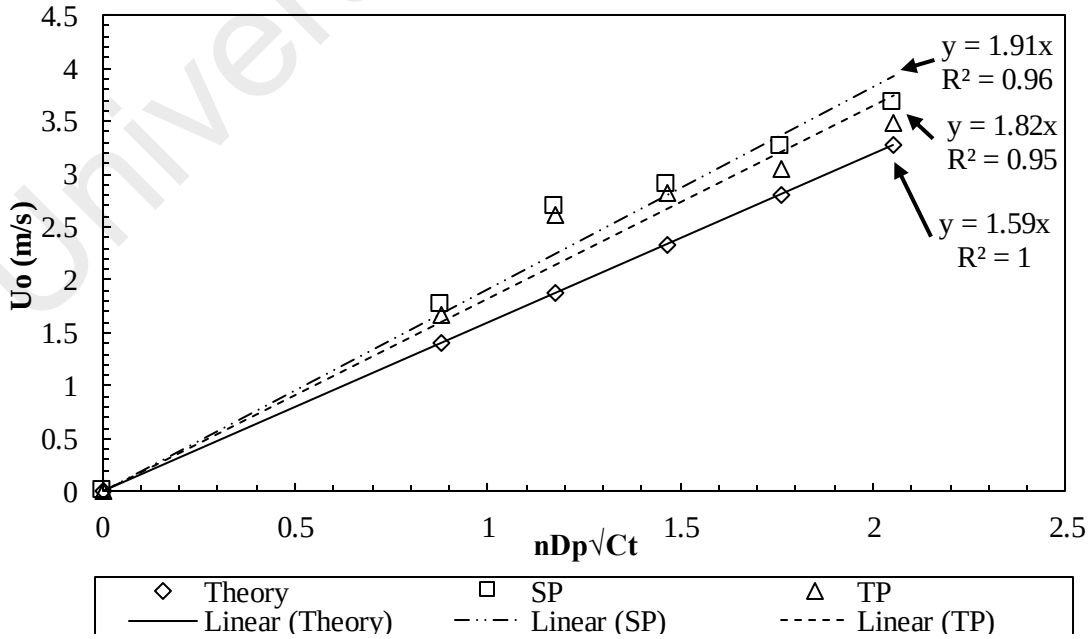

Figure 4.6: Comparison of theoretical equation and measured SP and TP

4.4 Axial velocity measured along the centreline

From previous literature (Steward, 1992; Hamill et al., 2004; Lam et al., 2012), all measured velocity profiles have been plotted across the propeller face. However, the centreline between ship-twin-propeller's jets had drawn attention to the possibly higher magnitude thrust due to the interference of velocity magnitude. Therefore, the profile across the centreline of ship-twin-propeller's jets was investigated and analysed. The position taken across the ship-twin-propeller's profile is shown in Figure 4.7. The intersection point of the laser was aimed directly at the centreline of ship-twin-propeller's jet and proceeded downward to obtain the decay profile whereas, the cross section profile across the centreline was obtained along the ship-twin-propeller face which is parallel with the propeller axis.

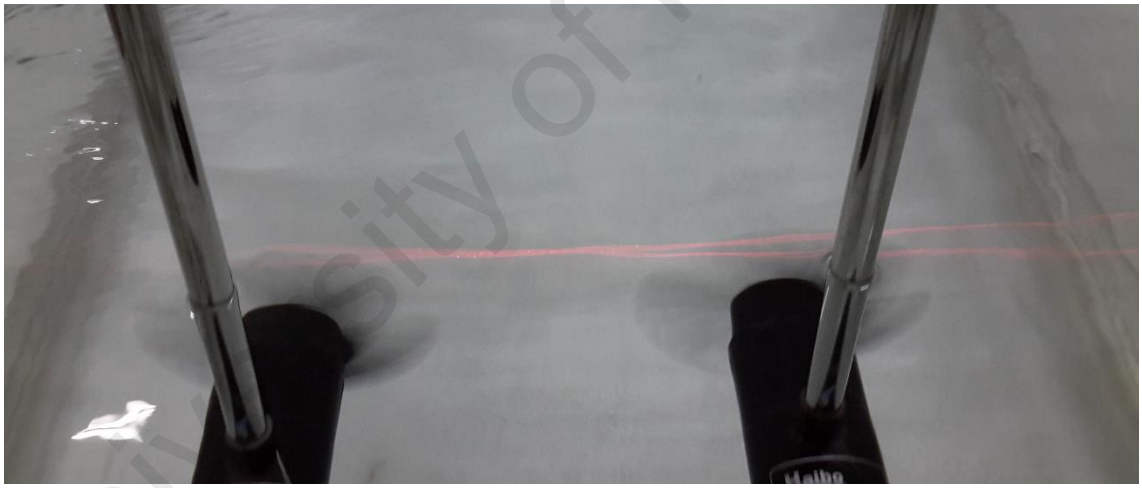

Figure 4.7: Measurement position across ship-twin-propeller jet

Readings from the initial plane across the centreline along ship-twin-propeller jets faces were plotted in Figure 4.8. The centreline of twin-propeller is located at $0r/R_p$. Both points at $1.18r/R_p$ and $-1.18r/R_p$ indicated the ship propeller's hub for both sides. Boundaries of both propellers tips were located at the position of $0.5r/R_p$ and $-0.5r/R_p$, indicating that the two lowest points were near the propeller tip boundary, as suggested by Hamill et al. (2004). As shown in Figure 4.8, the amplitude height of the peak increased with the rotational speed while the locations for both peaks remained constant.

The peak increased gradually from the propeller's hub and started to decrease at the point of $0.91r/R_p$ until the boundary of propeller tip. Thereafter, the velocity magnitudes increased again up to the point of $0.18r/R_p$ which was rather close to the centreline between both propellers.

Overall, initial plan of ship-twin-propeller jets across centreline shares the same pattern with single rotating propeller measured at the propeller face. It has two high velocity magnitudes peaks and a low-velocity crest at the middle point. Both peaks at the centreline were slightly higher than the peaks at the propeller face as compared to single rotating propeller for velocity 500rpm and 600rpm. However, the 400rpm peaks at centreline were similar to the peaks at the propeller face. Therefore, as the propeller rotated at optimum speed of 500rpm or higher, the axial velocity at centreline had a higher peak than the axial velocity measured at the propeller face. By taking the dimension across the efflux plane into consideration, a total of six peaks and three low-velocity crests were formed. Moreover, the axial velocity of ship-twin-propeller measured at centreline was higher than the axial velocity measured at the face, which is important for engineers to identify and reallocate the source of the occurrence of higher velocity thrust whilst both propellers were running. The interferences of both velocity thrust induced by each of the propellers have led to a higher velocity thrust impact at the centreline. As a result, by judging the single propeller's wash that has been inducing severe impact of scour, ship-twin-propeller's wash which induced higher velocity thrust will cause the seabed to be more vulnerable than the velocity thrust induced by ship's propeller wash.

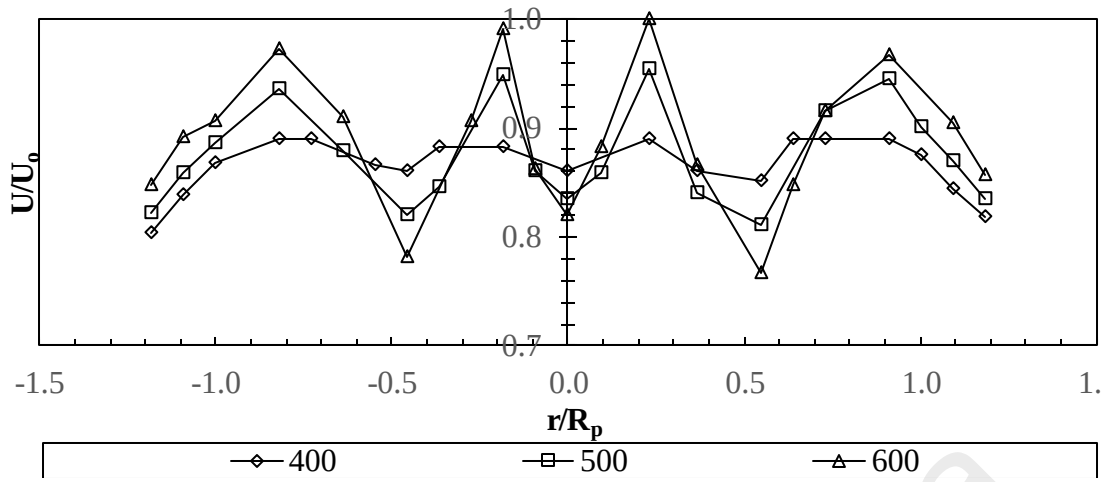

Figure 4.8: Dimensionless axial velocity profile across the propeller face

4.4.1 Location of efflux velocity

The influence of ship-twin-propeller had altered the maximum velocity position and created two efflux velocities, namely primary efflux velocity near the centreline and secondary efflux velocity along propeller face. For the propeller plane across the centreline, the highest velocity magnitudes were revealed at the centreline instead of the propeller face. This is relatively different from single rotating propeller as analysed in previous literature. Moreover, the velocity profile decreased from the position of 0.18r/Rp to 0.5r/Rp, and subsequently inclined to the secondary efflux velocity, which was located at the propeller face positioned at $0.91r/R_p$, as shown in Figure 4.8. The relocation of efflux velocity is possibly due to the interference of the velocity thrust induced from the ship-twin-propeller's wash. On the other hand, the location of both peaks at the centreline was asymmetrical. It was skewed to the right hand side at $0.23r/R_p$, whereas the left hand side was at $-0.18r/R_p$. This was due to the features of current analysis, whereby both propellers were constrained to rotate clockwise. Thorough details on the velocity profiles shall be evaluated in future research.

4.4.2 Evaluation the existing method for current investigation

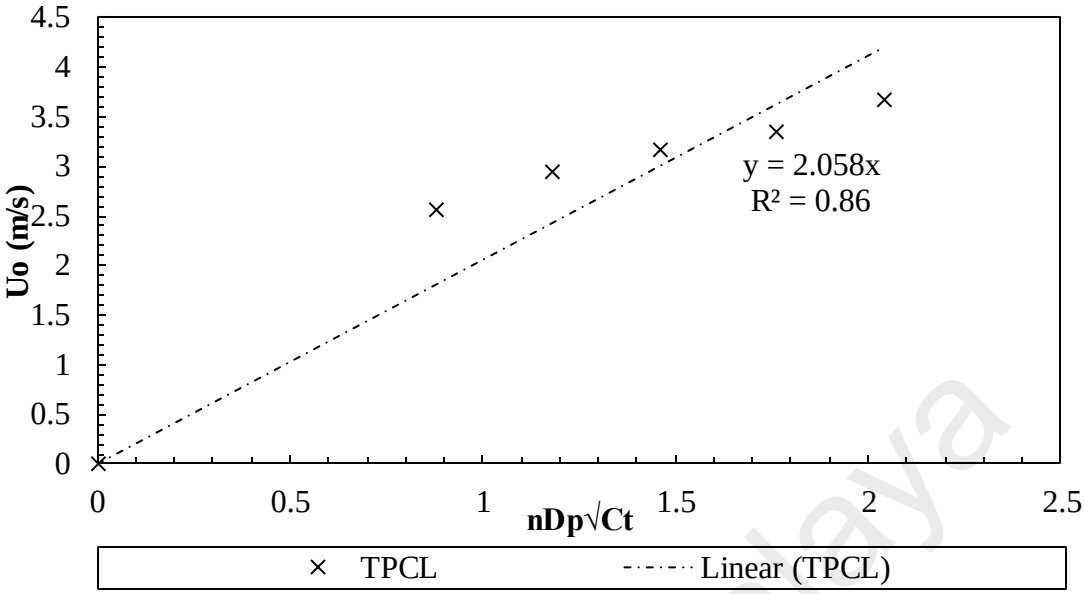

Figure 4.9: Relationship of Uo and nDp$\sqrt{C_t}$ for TPCL

Linear regression test was performed to check the correlation between axial momentum theory and the axial velocity profile of ship-twin-propellers measured across centreline (TPCL). Correlation, R^2 of TPCL found from the linear regression of U_o versus $nD_p\sqrt{C_t}$ for rotating ship-twin-propeller was 0.86, as shown in Figure 4.9. The relatively high R^2 value indicated that the current equation for the measurement is reliable. Therefore, the axial momentum theoretical equation can be practiced for ship-twin-propeller across the centreline but with lower accuracy. Consequently, the current investigation requires further research on the axial velocity distribution at the centreline to improve the results and the correlation value with the axial momentum theory. By using data correlation analysis, a coefficient was suggested to improve the accuracy predicted by theoretical equation. The suggested coefficient for the prediction of efflux velocity at the centreline was 2.058, written in the form of:

$$U_o = 2.058nD_p\sqrt{C_t} \tag{4.1}$$

4.5 Velocity decay in Zone of Established Flow

As the axial velocity exerts from the initial plane of propeller, the velocity will gradually reduce and form velocity decay. Previous literature indicated the importance of decay zone for the understanding of the impact of area according to the velocity magnitudes. Higher velocity magnitude will result in higher scour impacts as compared to the lower velocity magnitude. Moreover, the decay profile also indicates the possible location of maximum scour depth. Literature (Hamill, 1987; Steward, 1992) believed that there is no maximum velocity decay close to the propeller face. Hamill (1987) stated that there is no maximum axial velocity decay up to a length of $0.35x/D_p$ from propeller face. However, Lam et al. (2011) furthered this study and found that there is no constant maximum axial velocity close to propeller which is contradictory to previous literature (Fuehrer and Römisch, 1977; Blaauw and van de Kaa, 1978; Berger et al., 1981; Verhey, 1983). The validation of current measurement is shown in Figure 4.5 and had been discussed in section 4.3.1.

4.5.1 Ship-twin-propeller jets decay profile

Steward (1992) and Hashmi (1993) proposed that the axial velocity decays longitudinally from propeller face. Therefore, the ship-twin-propeller's decay profile has been plotted longitudinally along the centreline ($0r/R_p$), which was located between both propellers (Figure 4.10). The velocity magnitudes increased from propeller face up to the first peak at $0.05x/D_p$, measured from the propeller face. Afterward, it decreased gradually to $2.0x/D_p$ and increased again up to the second peak at $2.8x/D_p$, which was measured from the propeller face. Subsequently, it decreased again until the end of zone of flow establishment.

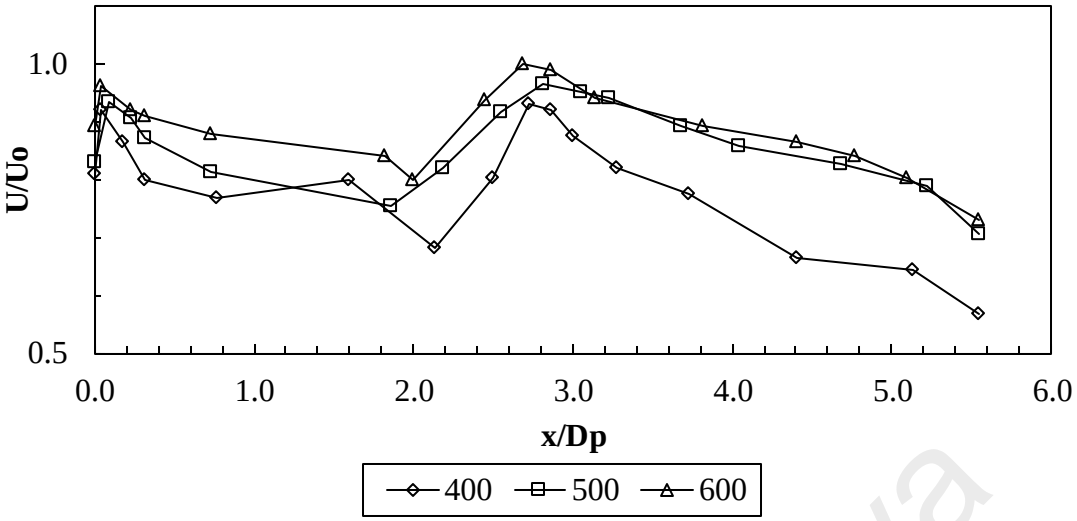

Figure 4.10: Longitudinal decay profile of ship-twin-propeller along the centreline

The longitudinal profile of ship-twin-propeller jets showed the two peaks towards downstream, which one peak was located near propeller face and the other located down forward at a position of $2.8x/D_p$, which falls within the zone of flow establishment ($x/D_p<3.25$). This indicates that the two direct scour impact zones induced by ship-twin-propeller's wash may form a larger scour hole as compared to single rotating propeller's wash. Therefore the decay pattern has given an insight of the possible occurrences of larger scour hole before $2.8x/D_p$, which is approximately 60cm from the propeller face. This relationship is further discussed in the later sections on the formation of scour induced by ship-twin-propeller's wash. However, since the main objective of current study is to analyse the scour formation induced by ship-twin-propeller's wash, the further analysis of decay profile across centreline shall be conducted in future research.

4.6 Summary of axial velocity flow of ship-twin-propeller jets

The overall comparison between ship-twin-propeller jets and single propeller jet in terms of efflux velocity and axial velocity decay is tabulated in Table 4.2. Single propeller has two peaks when measured at propeller face, whereas ship-twin-propeller's jet has a total six peaks when measured across the centreline. The six peaks comprised two peaks from each of the two propeller faces and another two peaks at the centreline

between both propellers. There are two peaks which located at the most left and most right is not shown in Figure 4.8, as in this figure only focus on the centre line profile. The positions of efflux velocity for both single and ship-twin-propeller were also different as the efflux velocity position had altered its location from propeller face to the centre of ship-twin-propeller. Based on current study, the correlation coefficient to predict the ship-twin-propeller's jet was suggested, as stated in equation [4.1]. Similar experiment with different propeller geometries is recommended to refine the practicability of current analysis.

On the other hand, for the decay profile, the number of peaks along the longitudinal decay profile of axial velocity for ship-twin-propeller jets was higher compared to single propeller which only has one peak. Two peaks occurred after the efflux plane and another located at $2.8x/D_p$. These two peaks indicated that it is possible to have two scour holes at different location. These two locations would subsequently merge into a large scour hole as the scour time prolonged. It is believed that STP creates higher velocity thrust only at the merging point. However, when the distance between both propellers is far enough, it will behave like single propeller. Further research was carried out to investigate the scour profile resulted by the ship-twin-propellers' jets.

Table 4.2: Comparisons between single and ship-twin-propeller measured along propellers' face

Properties	**Theoretical**	**Measurement at single propeller**	**Twin-propellers measured across the centreline (TPCL)**
Efflux plane			
No of peaks	2	2	6
Position of efflux velocity	At propeller face		At centreline
Position of efflux velocity, R_{mo}	$0.67(R_p-R_h)$	$0.55(R_p-R_h)$ (TP)	-
Coefficient with axial momentum theory	1.59 (Verhey,1983)	1.91 (SP)	2.058
	1.33 (Hamill,1988)	1.82 (TP)	

Properties	Theoretical	Measurement at single propeller	Twin-propellers measured across the centreline (TPCL)
Decay profile			
No of peaks	1	1	2
Decay pattern	No constant maximum velocity at face		
Decay position	After the efflux plane		After the efflux plane ($0.05x/D_p$) and at the position of $2.8x/D_p$

4.7 Scour induced by ship-twin-propeller jets

The investigation on scour induced by ship's propeller wash was initiated by Blaauw et al. (1978) and Verhey (1983), to study the relationship of the impingement of velocity flow induced by a two-dimensional propeller jet on the surface of seabed. No relationship was found to describe the temporal development of scour induced by ship's propeller wash. The development of scour profiles were then monitored and studied by Hamill (1987) and in the later works of Hong et al. (2013). The temporal development of scour gave insights in describing the maximum eroded depth at any instant of time, until asymptotic stages were reached.

As mentioned in Chapter 2, the scour profile from the initial ship-twin-propeller's wash remains unveiled. The development of scour profiles of ship-twin-propeller was then monitored at a series of time intervals for each experiment. Experiments were carried out using propeller (P1) at rotational speed of 400rpm, 500rpm and 600rpm. Only one type of sand was used in the experiments and the sand level was adjusted to three different clearance distances, as outlined in Chapter 3. The overall scour geometry was plotted in plan and longitudinal view, as shown in the later sections.

The final time duration for each experiment to achieve its asymptotic state was approximately seven days including the set up procedures. Despite only 64 hours were required to reach the asymptotic stage as mentioned in Hamill (1987) and Hong et al. (2013), the ship-twin-propeller system was not continuously run to prevent overheating

on the motor system and causing the irregular rotational speed to occur. Therefore, a longer duration was considered to retain the accuracy of results.

4.7.1 Dimensional consideration

Dimensional consideration improves the understanding on the influence of all determining variables for the formation of maximum scour depth. Therefore, factors that affect the maximum scour depth of the ship-twin-propeller are written in the form of,

$$\varepsilon_{max} = f_1(U_o, D_p, C, d_{50}, g.\rho, \rho_s, \upsilon, N, D_p, \mathrm{t}) \tag{4.2}$$

where,

U_o = Efflux velocity
D_p = Diameter of ship's propeller
C = Clearance between propeller's tip and surface of sand bed
d_{50} = Mean sediment grain size
g = Gravitational acceleration, 9.81 m/s^2
ρ = Fluid density
ρ_s = Sediment density
t = Time
υ = Kinematic viscosity
N = Number of propellers

As mentioned in previous literature (Hamill, 1987; Hamill et al., 1999; Hong et al., 2013), Froude number, F_o, is the inertial force to gravity for flow with a free surface, which is extremely important in determining the maximum scour depth. It is written in the form of,

$$F_o = \frac{U_o}{\sqrt{g\, d_{50}\, \Delta\rho/\rho}} \tag{4.3}$$

Previous work by Rajarathnam (1981) on the erosion of plain wall jet, showed that when the Reynolds number, R_{ej} is larger than 10^4, the viscosity effect of flow could be neglected. The Reynolds number is written in the form of,

$$R_{ej} = \frac{U_o D_p}{\upsilon} \tag{4.4}$$

Since the Reynolds numbers of proposed rotational speed range falls between 3.6×10^5 and 5.3×10^5, the viscosity effect flow is neglected. By using the Buckingham Pi Theorem, equation [4.2] and [4.3] were inserted into equation [4.1], which is then reduced to

$$\frac{\varepsilon_{max}}{D_p} = f_2(F_o, R_{ej}, \frac{D_p}{d_{50}}, \frac{C}{D_p}, N, t)$$

Showing that the maximum depth of scour is dependent on:

i. The densimetric Froude number, F_o
ii. The ratio of the propeller diameter to the mean sediment grain size
iii. The ratio of clearance to the mean sediment grain size, and
iv. The number of propellers
v. Time of scouring

4.7.1.1 Dependency on Froude number coefficients, velocity thrust and tip clearances

For current experiment, the ship-twin-propellers were continuously run to scour the sediment bed until the asymptotic state. The profile of dimensionless maximum erosion depth was compared with different clearances at different rotating velocity as shown in Figure 4.11. The experimental data of current investigation on the correlation of data used is shown in Table 4.3.

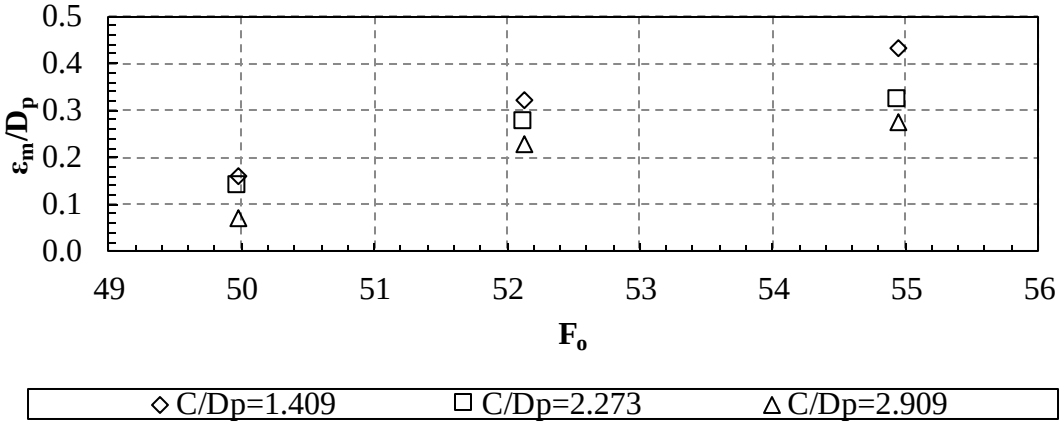

Figure 4.11: Relationship of F_o with Scour Depth at Different ratio of C/Dp

Moreover, Hamill, (1987) mentioned that the dependency on ε_m/D_p is different with the existence of F_o, which is supported by current investigation. Therefore there is no further validation test on the sediment size, while the sediment size used in current investigation remained as constant. Other constant parameters of current investigation are as follows:

D_p = 22 cm
d_{50} = 0.1 cm
g = 9.81 m/s^2
ρ = 998.2 kg/m^3
ρ_s = 1590 kg/m^3

The densimetric Froude number, F_o, has shown significant increment as the rotating velocity speed increases and the clearance value decreases. However, the increasing rate was not proportionate to F_o. The increased clearances have led to a distinction between the maximum depths of scour. However, there were no obvious changes on F_o value. Therefore, for current study, efflux velocity thrust and clearance play an active role in the investigation on ship-twin-propeller's wash induced seabed scouring profile.

Table 4.3: Data of current investigation for correlation investigation

Rotational velocity (rpm)	ε_m/D_p	C/D_p	F_o
400	0.273	1.409	54.943
500	0.545		52.130
600	0.545		49.979
400	0.227	2.273	54.973
500	0.273		52.130
600	0.318		49.979
400	0.045	2.909	54.943
500	0.227		52.130
600	0.318		49.979

4.7.2 Development of scour profile induced by ship-twin-propeller wash

Scour profiles induced by ship-twin-propeller's wash were plotted in longitudinal and plan forms, to observe the temporal variations. The scour profile developed slowly with the progress of time. There are four stages throughout the temporal development of ship-twin-propeller's wash induced seabed scour, as described below:

(i) Initial stage

The sediment began to be transported from its initial location, along with the direction of ship-twin-propeller's wash. No obvious scour is formed at this stage. Only two small scour holes were formed individually in front of both propellers with two small ridges located at both head and tail of the scour hole.

(ii) Developing stage

Both individual scour holes deepened at this stage. The height and length of ridges increased in line with the deepening of scour, resulting in the increase in length of scour plane. The width of scour expanded both horizontally and vertically, but the scour holes have yet to merge at this stage.

(iii) Merging stage

This is the most significant stage where both individual scour holes and scour ridges merged and formed a large scour hole with a continuous circle scour ridge. Both scour holes were measured individually to observe the dimension changes. The scour depth and width continued to increase during this stage.

(iv) Asymptotic stage

The maximum scour depth was achieved and the scour dimension remained unchanged at this stage. It is also believed that the changes on scour and scouring rate at and beyond this stage are minimal.

The schematic diagram for stages of scour induced by ship-twin-propeller wash under a constant clearance and rotational speed are shown in Figure 4.12 (longitudinal view) and Figure 4.13 (plan view). The rotating ship-twin-propeller was positioned at 0 on y-axis for longitudinal view. For plan view, the scour profile was plotted right at the point of the formation of scour hole. Current measurement showed that the scour formed two holes initially, and subsequently combined into a large hole with two ridges located at scour head and tail.

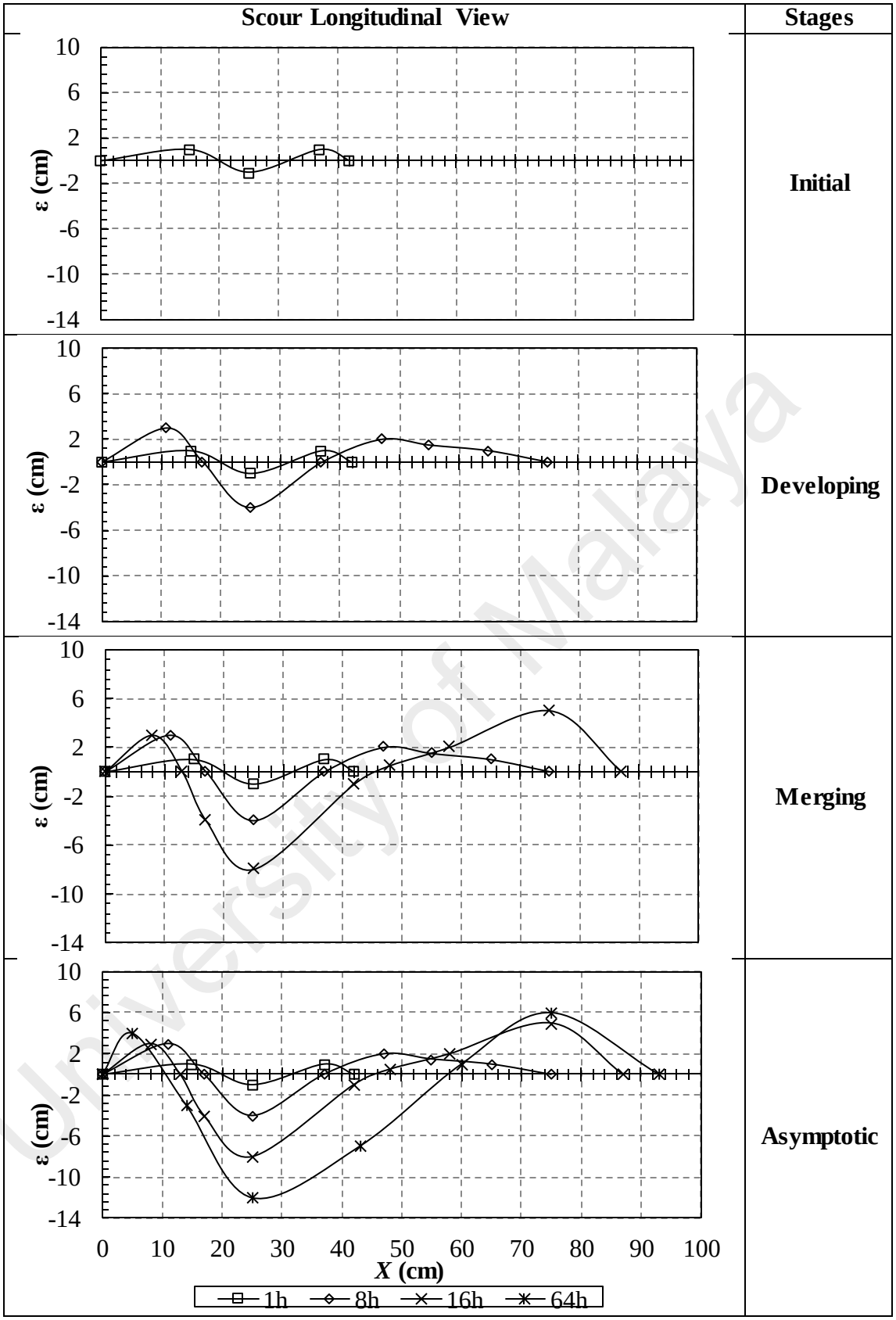

Figure 4.12: Schematic diagram of stages of scour (longitudinal view) induced by ship-twin-propeller wash (C1, 600rpm)

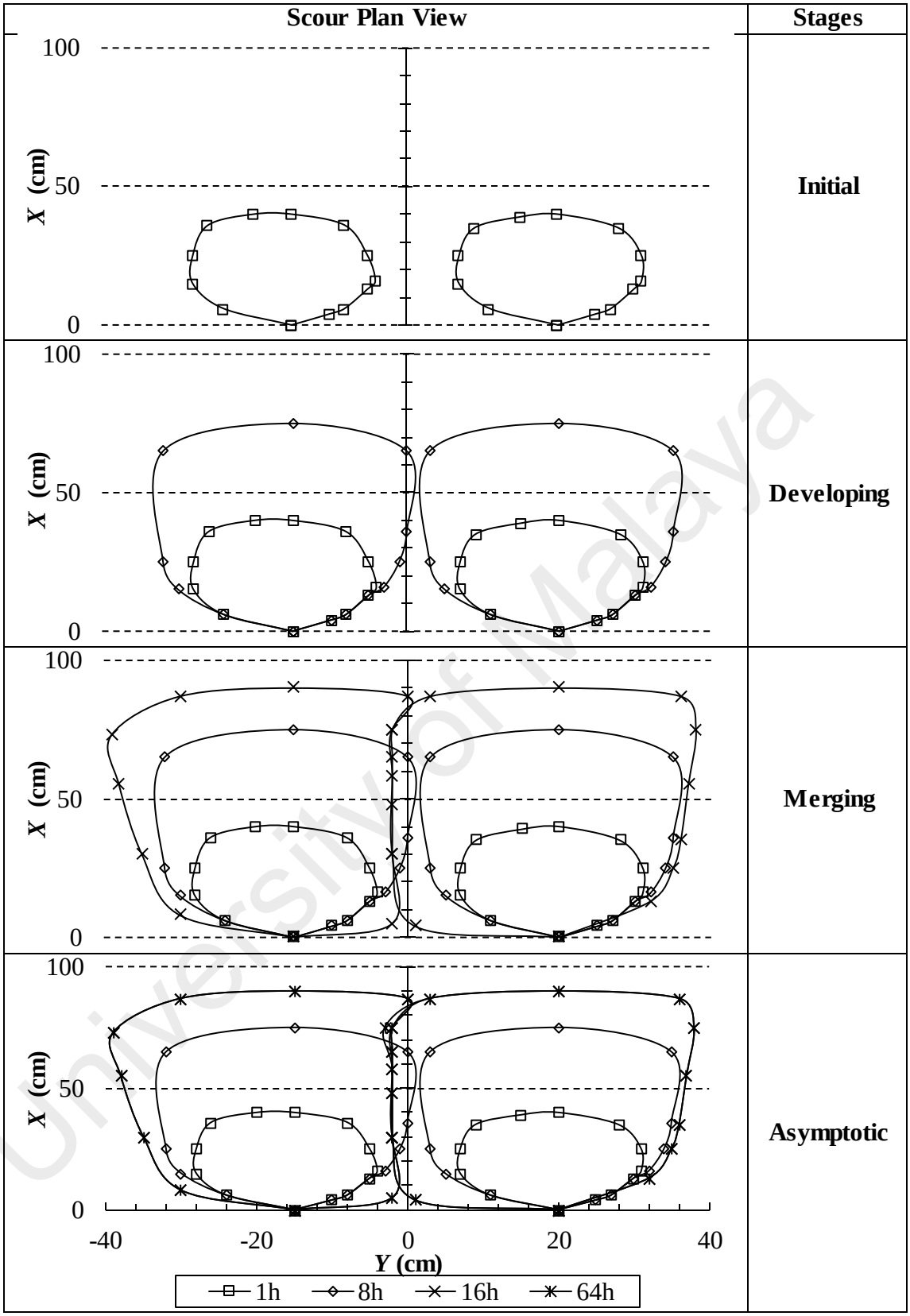

Figure 4.13: Schematic diagram of stages of scour (plan view) induced by ship-twin-propeller wash (C1, 600rpm)

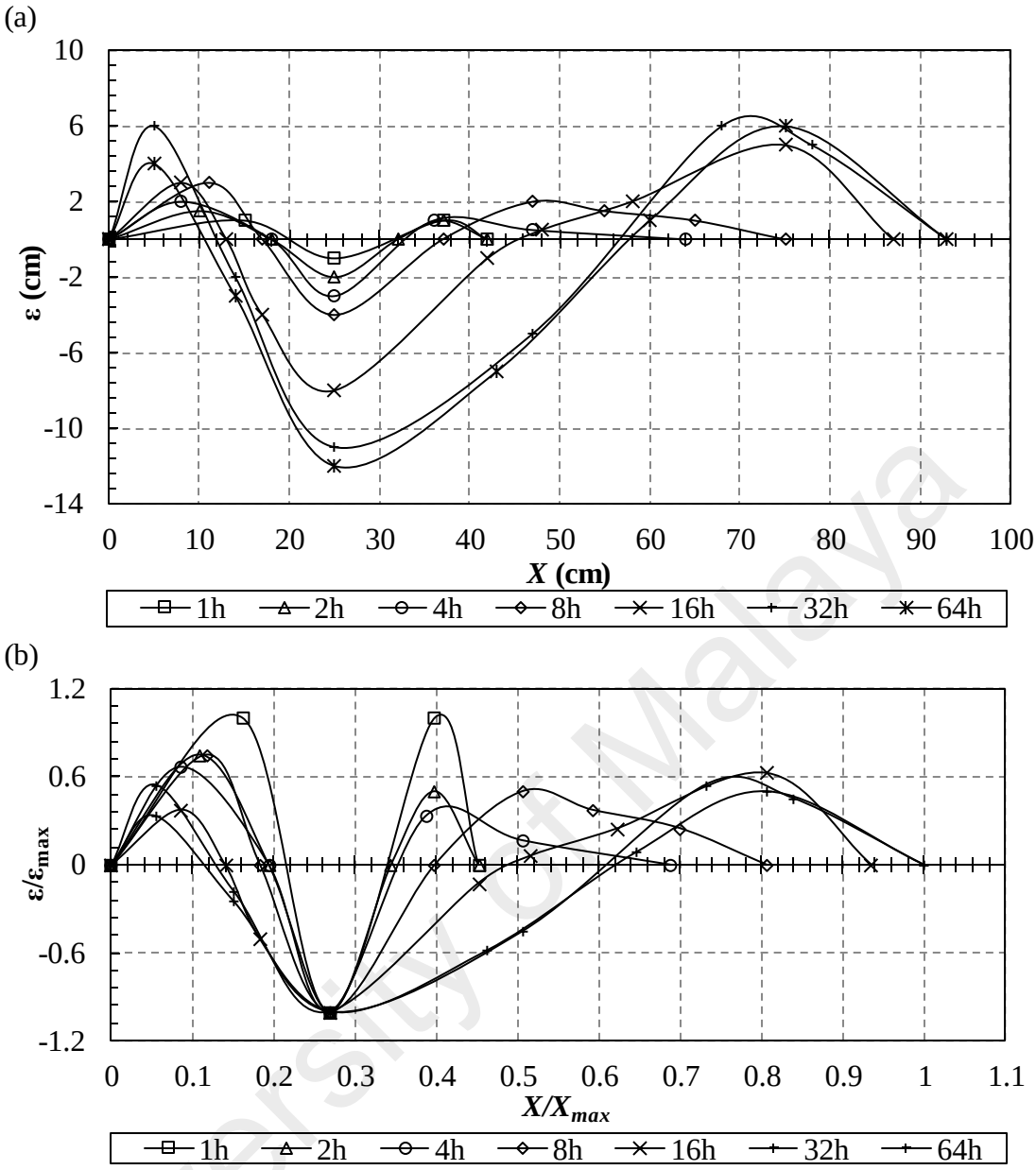

Figure 4.14: Typical scour profile at different times: (a) dimensional and (b) non-dimensional (C1, 600rpm)

Typical scour profiles induced by ship-twin-propeller wash measured along the longitudinal section were plotted dimensionally and non-dimensionally in Figure 4.14. The non-dimensional profile utilised ε_{max} and X_{max} to normalise variables for the vertical and horizontal dimensions of the typical scour holes, respectively. The non-dimensional graph was plotted to observe the development of temporal scour holes and ridges at different times. As shown in Figure 4.14, the scour ridge developed rapidly at the early stage, which was prior to 8h. Then, the scour ridge area spread from point 0.34 to 0.81.

The scour ridge area widened until 32h and subsequently changes of ridge was minimal until 64h.

The scour depth also deepened and widen quickly at the early stage. The changes of scour width increased tremendously until 16h. Then, the development of scour width and depth slowed down up to 32h and remained constant with minimal changes up to 64h. These temporal variation indicated that the scour profiles were uncertain at the early stage, while the scouring rate reduced gradually at the later developing stage until minimal changes. When the variations of scour depth and width are minimal, it is considerably in asymptotic condition.

4.7.2.1 Longitudinal view of scour profile

The final eroded profiles at 64 hours for different clearances and speeds were plotted in dimensional form from Figure 4.15 to Figure 4.19. The right hand side longitudinal view was considered in the analysis due to the limitation of propeller and in view that the scour impact on the right hand side will be higher. This is due to the constraint of current analysis which limits both propellers to rotate towards right hand side for the docking effect. Therefore the right side longitudinal view has been plotted for current analysis. The propeller face was located at 0 on the x-axis. It is noticeable that different clearances and rotational speed will give different sizes of scour hole and height of scour ridge. The shape of the scour hole and its resulting ridges are similar to a sinus curve from the side view. Ship-twin-propeller's wash induced scouring has the sequence of a smaller ridge deposited at the scour head and scour hole, then a larger scour ridge is deposited at the scour tail. It has a deepest point where the maximum scour depth, ε_{max} and its location, X_{max} were measured. The ridge occurred before the scour head is R_1 whereas the ridge deposited at the scour tail is R_2. The highest point of R_1 and R_2 were considered for the comparison.

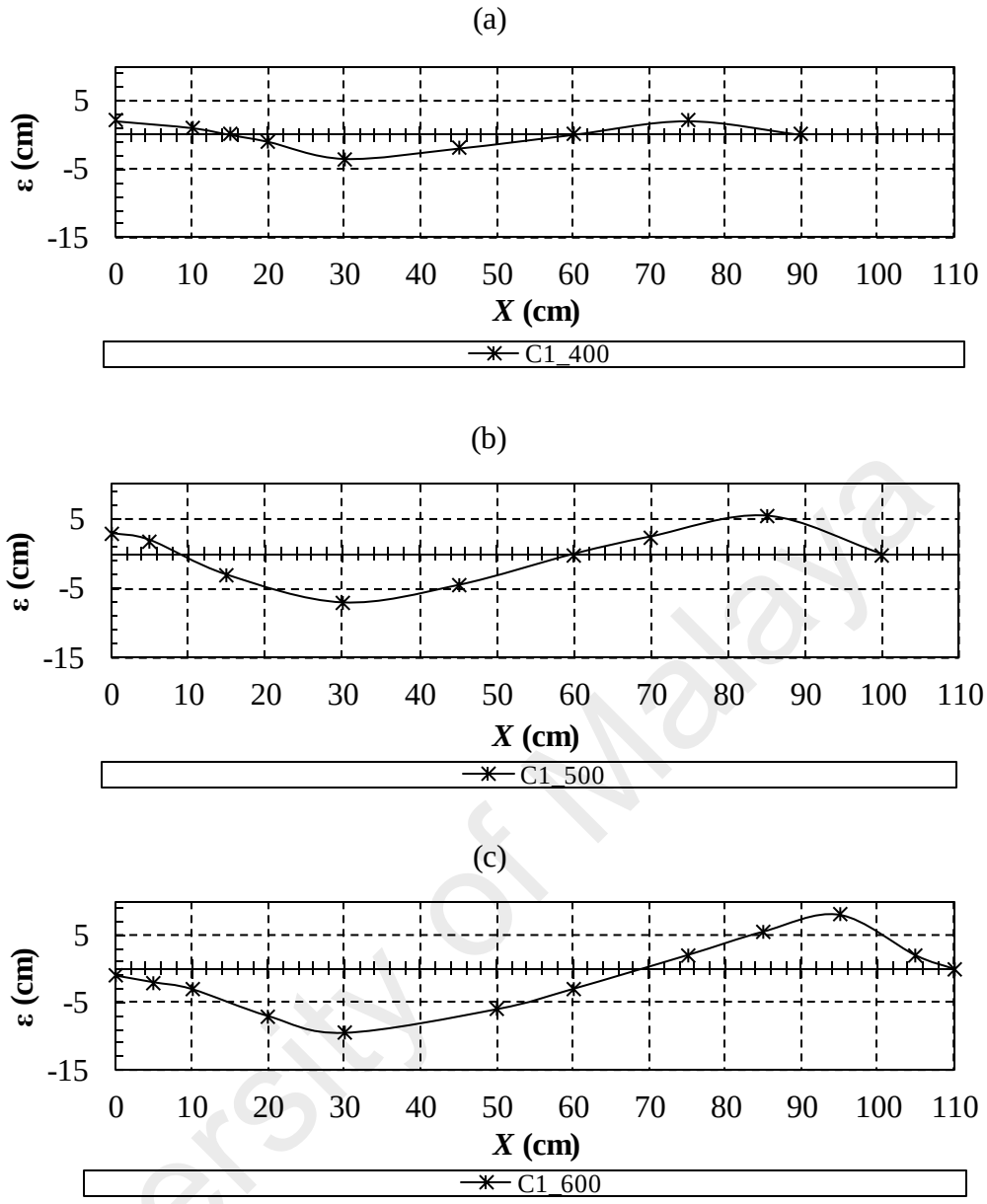

Figure 4.15: Longitudinal view of scour profile at clearance of 0.31Dp (C1): (a) 400rpm; (b) 500rpm and (c) 600rpm

For clearance of $0.31D_p$, which is referred to as C1, it has the closest value of clearance between ship's propeller and the surface of soil bed. Therefore it is expected to have the highest value of maximum scour depth when compared to other clearances, as the forces induced from ship-twin-propeller wash will require the least travel distance to reach the surface of soil bed. Therefore the forces have the least decay value, which implied the largest erosive power when it impinged towards the soil bed. On the other hand, as discussed in section 4.5.1, the second decay initiated at $2.8x/D_{p,}$ which is

approximately 60cm from the propeller face. Therefore it is predicted that another formation of maximum wash shall occur before $2.8x/D_p$.

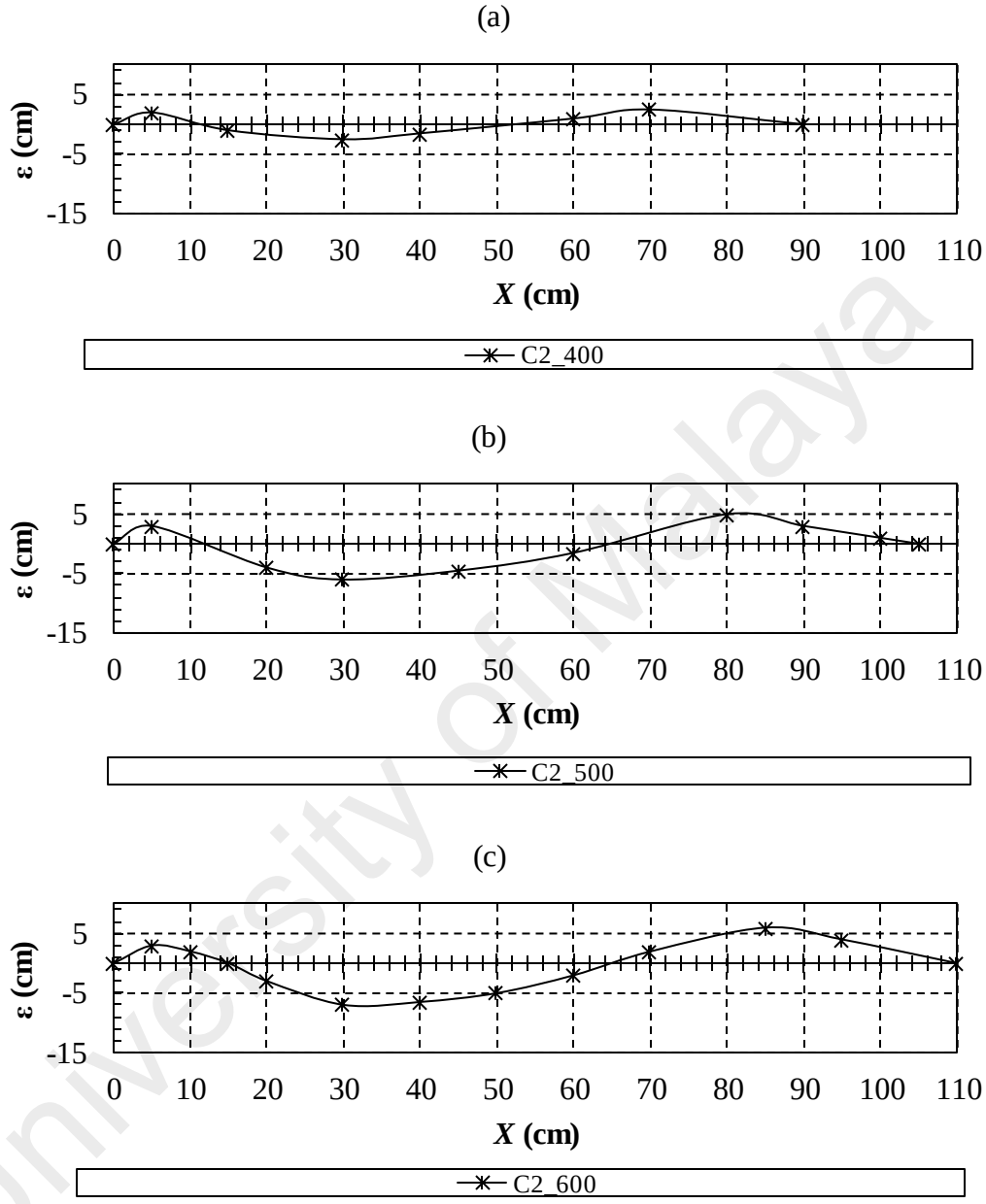

Figure 4.16: Longitudinal view of scour profile at clearance of 0.50Dp (C2): (a) 400rpm; (b) 500rpm and (c) 600rpm

The longitudinal view of scour profile of C1 with different rotational speed is plotted in Figure 4.15 with the axis of scour depth, ε, against the distance from the propeller face, *X*. Therefore it can be concluded that the lower clearance, C, induced higher scour. Based on Figure 4.15, the highest rotational speed has the deepest maximum scour depth, ε_{max}, where ε_{max} is 9.5cm. Therefore, the scour hole is more critical with low

under keel clearance or high rotational speed. Scour profiles for the two other clearances with the respective rotational speed are plotted in Figure 4.16 and Figure 4.17.

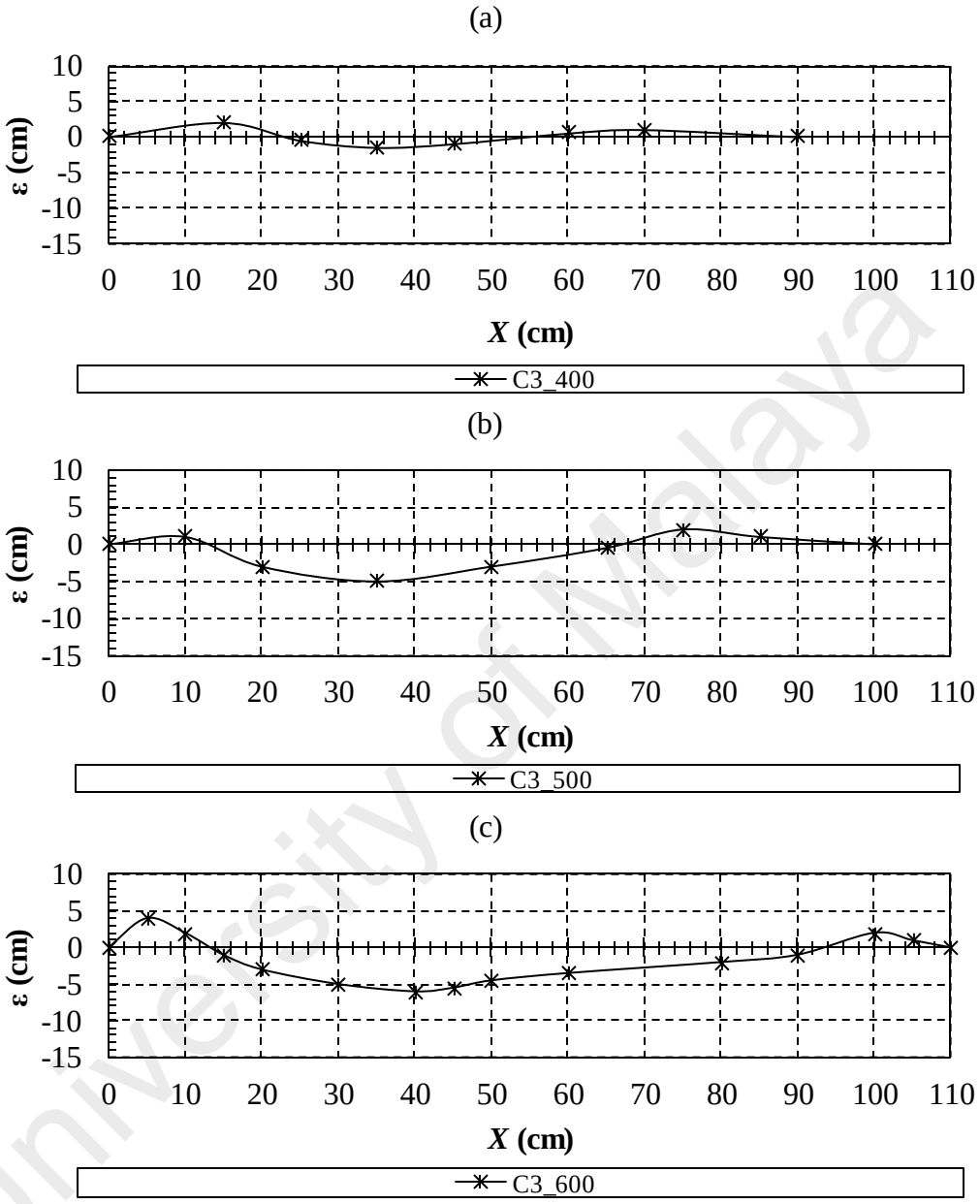

Figure 4.17: Longitudinal view of scour profile at clearance of 0.64Dp (C3): (a) 400rpm; (b) 500rpm and (c) 600rpm

Comparisons have been made between constant clearance and velocity as showed in Figure 4.18 and 4.19. Six aspects have been compared between constant clearance and velocity, specifically. (i) the maximum scour depth, ε_{max}; (ii) the location of maximum scour depth, X_{max}; (iii) scour size, W; (iv) scour head ridge location, X_{R1}; (v) scour tail ridge location, X_{R2} and (vi) Scour ridge height for both ridges, R_1 and R_2 as shown in Table 4.4.

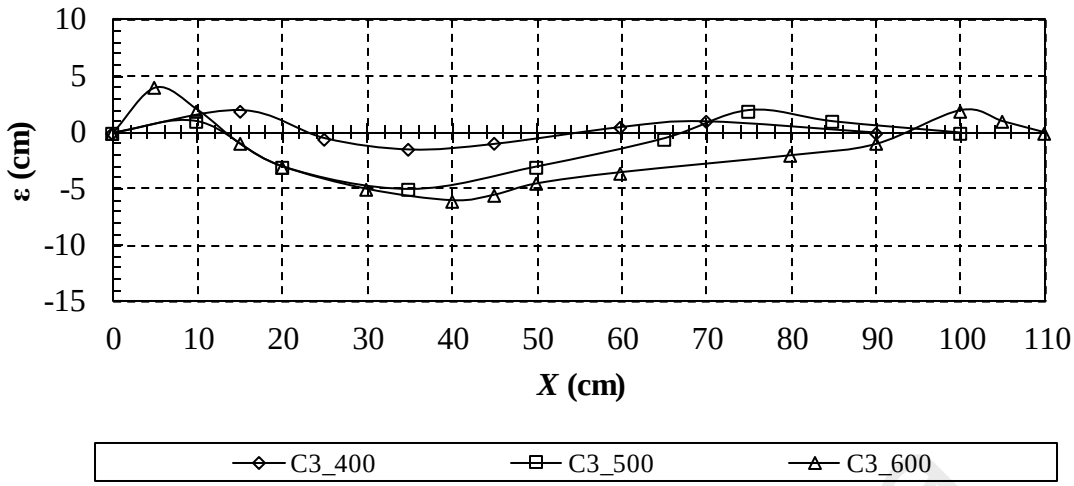

Figure 4.18: Comparison of longitudinal scour profiles at constant clearance

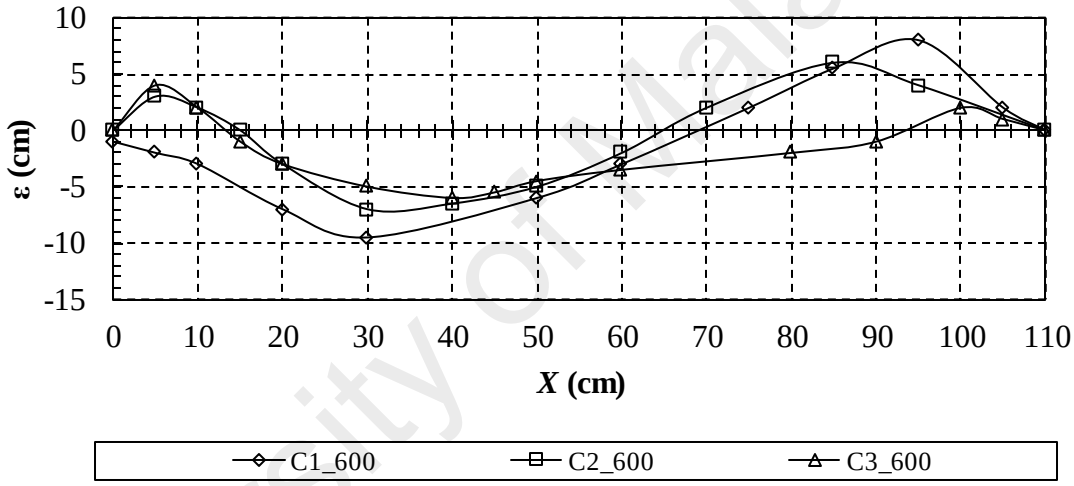

Figure 4.19: Comparison of longitudinal scour profiles at constant rotational velocity

The ε_{max} was low at the lower rotational speed, which increased in line with the increase of rotational speed, while the clearance remained constant. Meanwhile, the ε_{max} and the height for both ridges increased as the clearance decreases, assuming that the rotational velocity is constant. X_{max} moved further from the propeller face as the rotational speed and clearance ratio increase. Therefore, it is believed that the location of maximum depth is dependent on the velocity thrust driven from the ship-twin-propeller's jet. The ridge location moved forward and further from the propeller face as the rotational velocity speed and clearance increased. Based on the comparison in Table 4.4, it was found that ε_{max} increased with increasing velocity and decreased with

increasing clearances. X_{max} remained relatively constant despite the increasing velocity, and only increased slightly as the clearance increased. The scour width, W increased when the velocity and clearances increased. However, changes in scour size did not affect the scour impact, whereas scour depth reduced whilst clearance increased. Therefore, W was shown as an indicator on the scour area caused by ship-twin-propeller's wash. The ridge height value R_1 gradually increased as the rotational speed increased, whereas it decreased when clearance increased.

Table 4.4: Comparison between (i) constant clearance and (ii) constant rpm

(i) Constant clearance *(all units in cm)*			
Properties	400rpm	500rpm	600rpm
ε_{max}	1.5	5	7
X_{max}	35	35	40
W	32	54	81
R_1	2	2	4
X_{R1}	15	10	5
R_2	2	2	3
X_{R2}	70	85	100
(ii) Constant rpm *(all units in cm)*			
	C1	C2	C3
ε_{max}	7	6	5
X_{max}	30	30	40
W	35	52	54
R_1	3	3	2
X_{R1}	0	5	10
R_2	5.5	5	2
X_{R2}	85	80	85

The trend of height for R_2 at scour tail is similar to R_1 when rotational speed increased. However, R_2 decreased when the clearance increased, as an increase in clearance will reduce the wash impact forces impinges toward the seabed, and therefore result in smaller ridge when the scour hole impact is smaller. The location of R_1 was closer to the propeller face when the rotational speed increased or clearance decreased. However, the location of R_2 increased with rotational speed but is not affected by the clearance differences.

4.7.2.2 Plan view of scour profile

The plan view profile was plotted at the view of x-y plane. The graphs were plotted along the ship-twin-propeller faces (x-axis), and the side with the scour profile (y-axis) were observed. The solid line represents the scour hole where the sand bed level was below the initial bed level, while the dash line profile represents the scour profile including the scour ridge. The scour plan view profile for two typical clearances was plotted in Figure 4.20 and 4.21. The comparison of the scour plan view profile at constant clearance and constant rotational velocity were plotted in Figure 4.22 and 4.23.

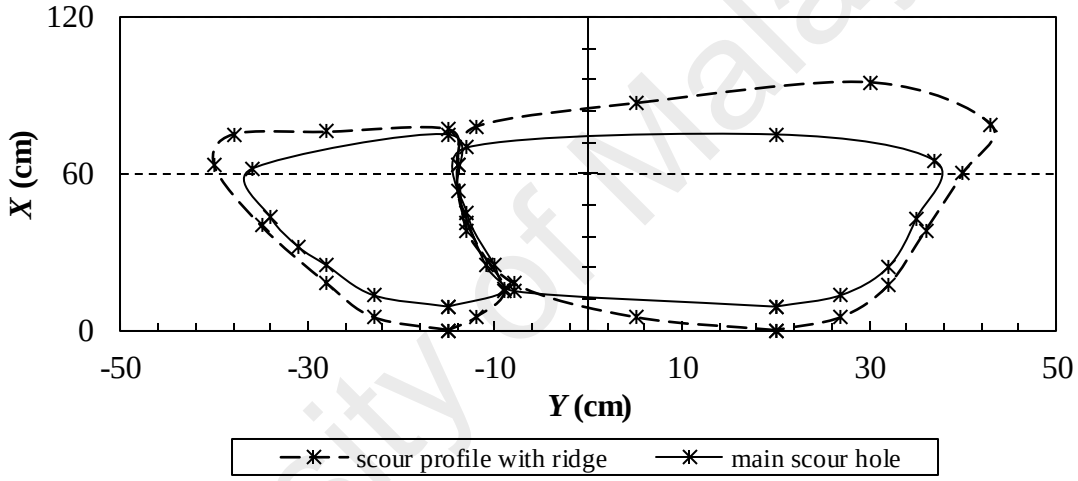

Figure 4.20: Plan view of scour profiles at asymptotic state: 0.31Dp clearance running at 600rpm

From the results, the right side has a larger scour impact as compared to the left side. The right side has been expected to have larger scour impact as discussed in Chapter 3 and aforementioned sections. Therefore the right scour hole dominates the scour profile. There were ridges surrounding the scour hole, firstly the two independent scour holes, then the merged scour hole. The typical scour plan view extracted from this experiment is shown in Figure 4.20 and 4.21. The merged scour hole profile occurred for all clearances and rotational speed other than C1 600rpm and C2 600rpm, can be referred in Appendix A.

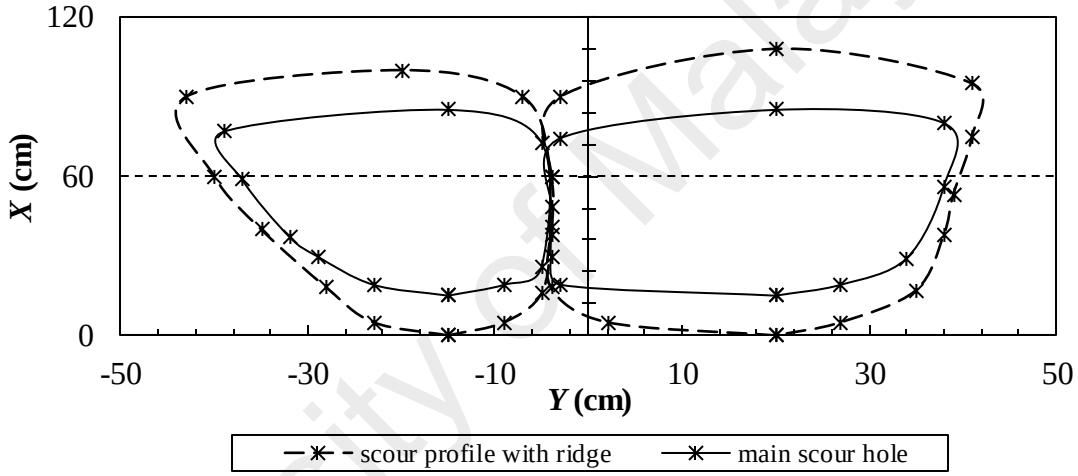

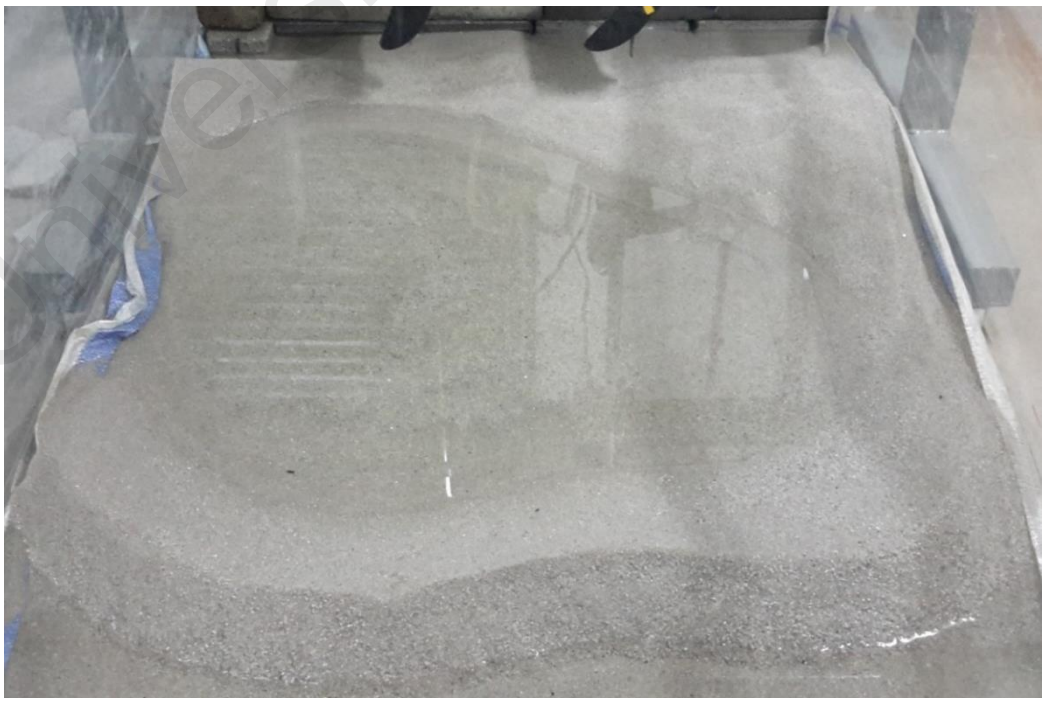

Figure 4.21: Plan view of scour profiles at asymptotic state: 0.50Dp clearance running at 600rpm

The longitudinal scour profile for C1 600rpm has the most severe scour impact. Therefore, the scour plan profile has the largest merged scour hole and highest ridge at scour tail as shown in Figure 4.20. The development of scour profile showed that the entire scour profile will enlarge at constant clearance when the rotational speed increases. However, at constant velocity, the scour hole size fluctuated and the scour size continuously widen when the clearances increased. This can be assumed that the higher clearance will result in an increase of the scour impact area, whereas the higher rotational velocity will result in an increase of the forward impact of the ship-twin-propeller wash.

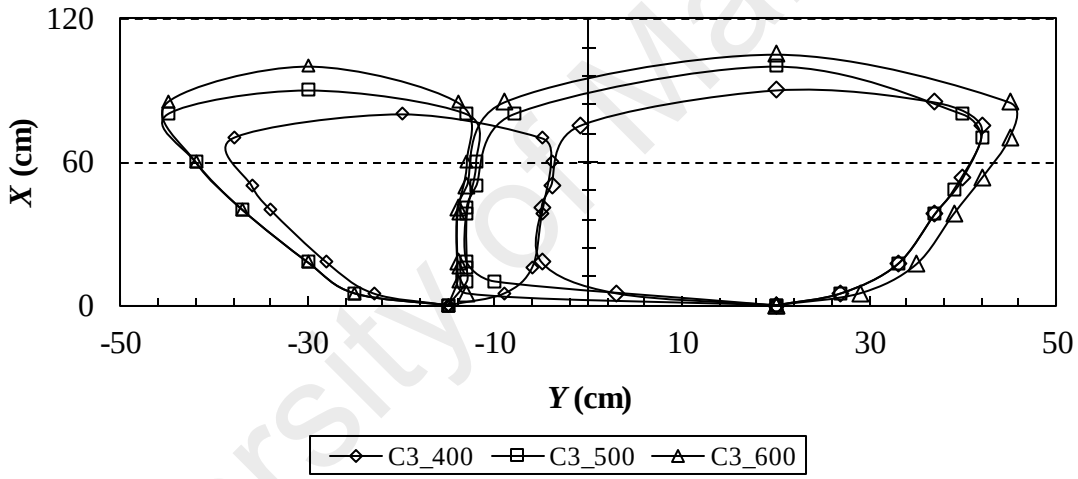

Figure 4.22: Comparison of plan view scour profiles at constant clearance

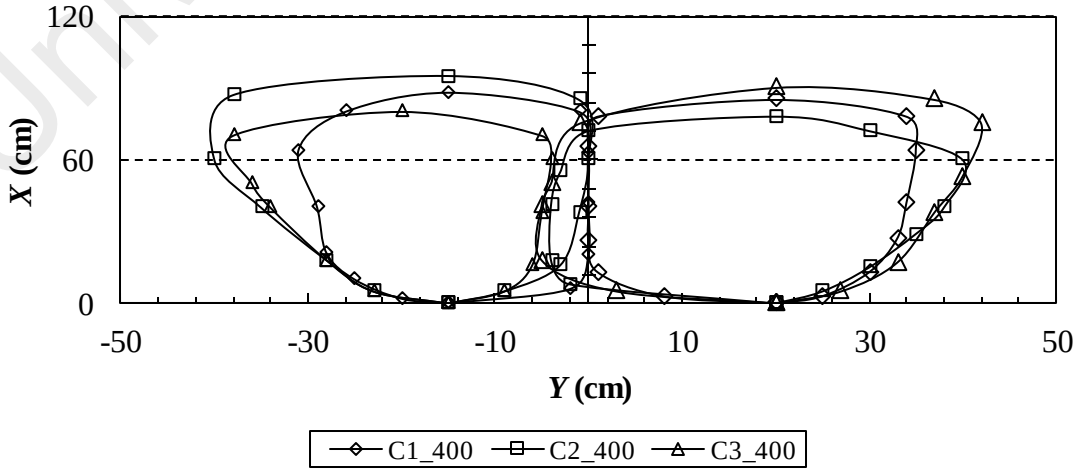

Figure 4.23: Comparison of plan view scour profiles at constant rotational velocity

4.7.2.3 Estimation of scour profile

The schematic diagram of scour profile induced by a ship-twin-propeller's wash under asymptotic condition of current analysis is depicted in Figure 4.24. The location of scour profile including all the parameters in current study is labelled according to their type of view.

In current study, the location of maximum scour depth induced by ship-twin-propeller's wash, $X_{max,}$ has gone through a series of trial and error prior to the formation of the equation. The equation was proposed as follows:

$$X_{max} = {F_o}^{0.909}(\frac{C}{D_p})^{0.193} \tag{4.5}$$

The above equation was suggested as it has the lowest root mean square error, *S* equals to 2.119% which is less than 2.5%. This indicates that it has a low standard error and the confidence level was above 95%. The application of current equation is proposed to be in the range of $x \geq 0.31D_p$, where $0D_p$ clearance is expected to occur directly beneath the ship-twin-propellers' tips.

The correlation data of maximum scour depth induced by ship-twin-propeller's wash, ε_{max} of current study was suggested as follows:

$$\varepsilon_{max} = \mathrm{k}(\log t)^{0.0231} \tag{4.6}$$

$$k = \left(\frac{C}{D_p}\right)^{-0.488}(\frac{U_o t}{C})^{0.241}.$$

Where,

t	=	time in seconds
C	=	Clearance difference between the seabed and propeller tip
D_p	=	Propeller diameter
U_o	=	Efflux velocity
ε_{max}	=	Maximum scour depth in cm
X_{max}	=	Location of maximum scour depth in cm

The equation was suggested based on the highest correlation agreement between all the dependent factors analysed using non-regression method. It has a low root mean square error at 1.46, which indicated that the data has a high confidence level of 97%. The applicability of the proposed equation was tested based on the correlation between the predicted ε_{max} and the observed ε_{max} as shown in Figure 4.25. The comparison also showed that the proposed equation has a high correlation with experiment data, where R^2 value equals to 0.909. The range of application of this equation is only for $t \geq 1s$. The equation expects that at 0 seconds there is no physical velocity to initiate any scouring impact. Moreover, it is not applicable for $0D_p$ clearance level as it is assumed that the scour will happen directly below the propeller tip.

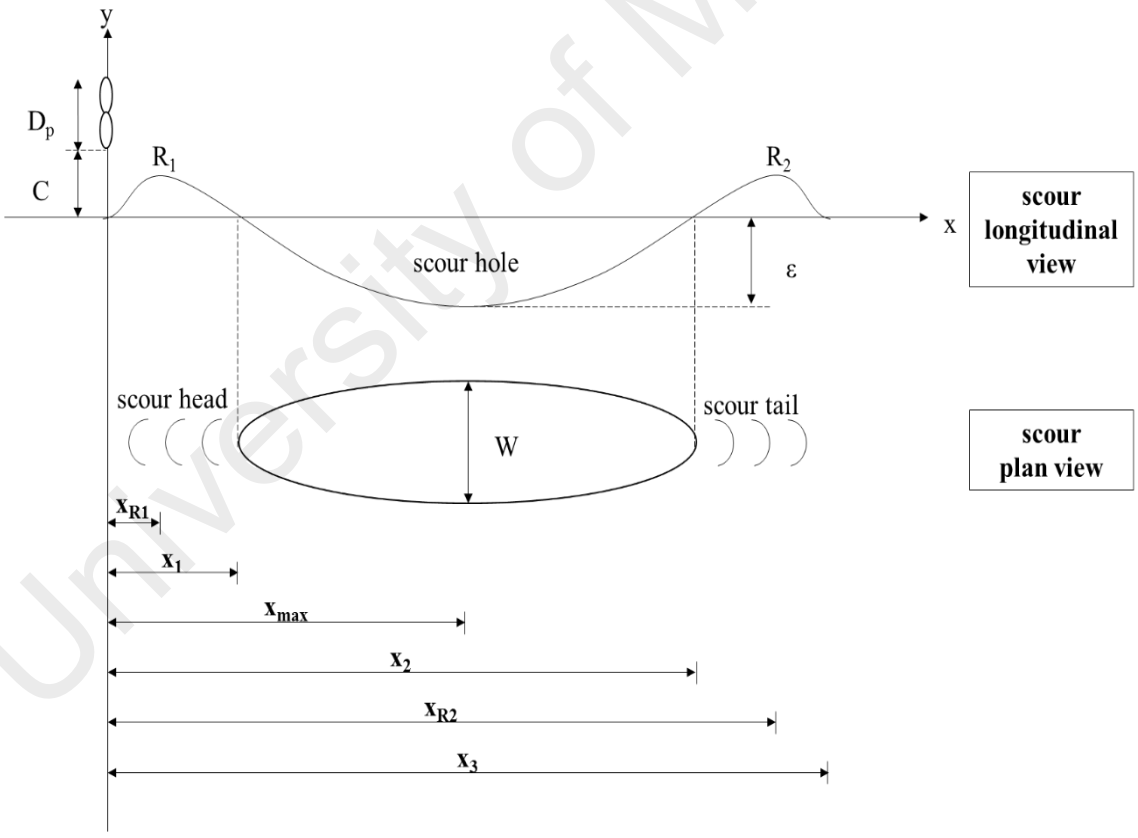

Figure 4.24: The schematic diagram of scour profile under asymptotic condition induced by ship-twin-propellers' wash

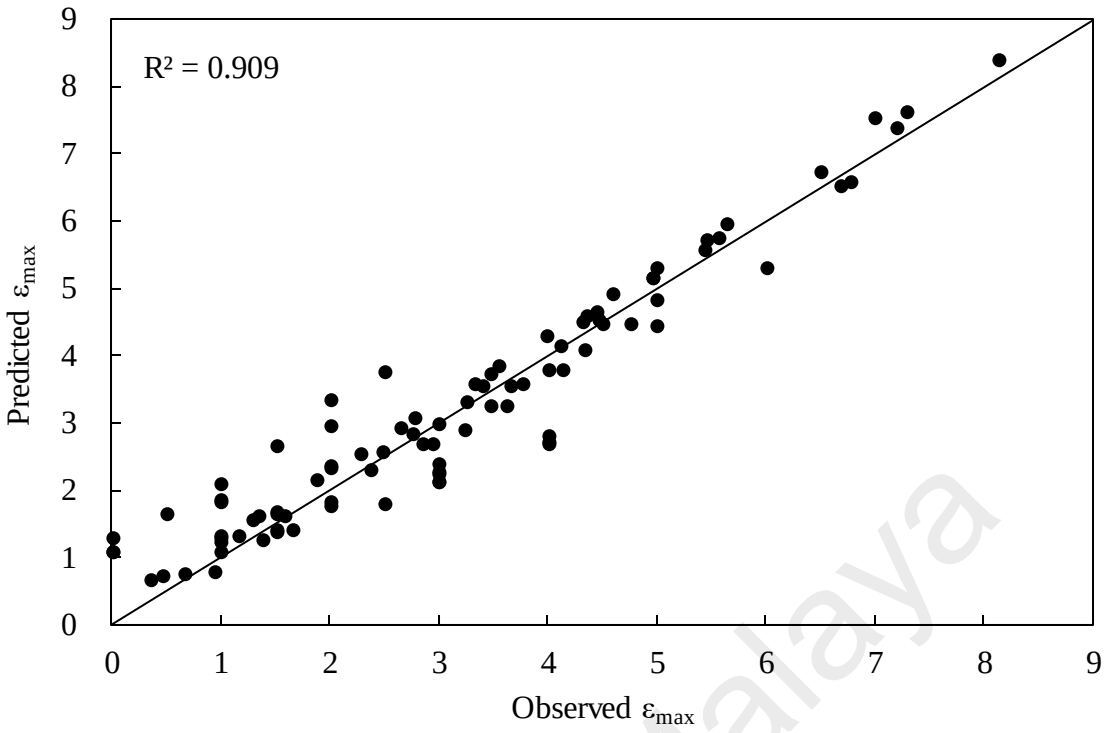

Figure 4.25: Comparison between observed and predicted ε_{max} using the proposed model above

4.8 Impact of ship-twin-propeller's wash induced seabed scouring

The scour pattern induced by STP wash was then compared with single rotating propeller to have an overview on the differences. The number of scour holes occurred was slightly different. Single rotating propeller will only produce one scour hole at any time, but STP will induce two scour holes at the early stage of scour. This condition maintained when the STP is under low rotational speed or with a high clearance gap. From previous literature by Hamill et al. (1999), X_{max} is equivalent to $F_o^{0.94}C$. The current experiment showed that the equation of X_{max} induced by ship-twin-propeller's wash is $X_{max} = F_o^{0.9098}(\frac{C}{D_p})^{0.1932}$, as stated in equation [4.5]. On the other hand, equation [4.6] which was proposed based on current study, is less complicated as compared to scour predicting equation by Hamill et al., (1999) and Hong et al., (2013). This is due to the focus of current study, which is emphasised on the relationship between ship-twin-propeller's wash induced scour, rotational speed and under keel clearance. Therefore, it can be concluded that the relationship between the estimation of

X_{max} and ε_{max} are similar, which are highly dependent on the clearance level, rotational velocity and Froude number.

4.9 Simulation works

Simulation works were initiated to observe the scour pattern through Computer Fluid Dynamic (CFD) software. Volume of Fluid (VOF) was chosen for the simulation as discussed in Chapter 3. VOF has been used on single propeller two dimensionally (2D) and three dimensionally (3D), for validation purpose. Then, it is used to observe the scour pattern induced by ship-twin-propeller wash.

Ever since, numerical simulation is able to provide the necessary data as an input for predictive equations of scour depth and pattern. In consistent with Hamill et al., (1999) and Hong et al., (2013), two key parameters for scour pattern prediction were collected, namely time consumption and scour positions for single propeller, to generate the validation. Time consumption is used to predict scour depth, whereas scour position is used to estimate the scour pattern. The ship-twin-propeller numerical model follows the experiment done by current experimental study. All results and discussion relating to simulation are discussed in the following sections.

4.9.1 Volume of Fluid (VOF) validation

The simulation was first observed with single propeller using two dimensional (2D) and three dimensional (3D) VOF. This is to validate that the results produced by VOF were in line with previous literature. Previous work done by Hamill (1987) was used to compare with the VOF simulation results. The setup of boundary and initial condition of the simulation were consistent with Hamill (1987) experiment setup as discussed in Chapter 3. Longitudinal scour profile, scouring depth (ε) and scour location (X_s) for both dimensional simulations were considered in current analysis. Results were compared and it was found that the predicted results were in line with previous literature.

Therefore, VOF was used for subsequent works for estimation and observation of ship-twin-propeller wash induced seabed scour.

4.9.1.1 Two-dimensional (2D) VOF observation with single propeller

A 2D fan setting has suppressed a 3D propeller jet to represent a 2D propeller jet. The polynomial pressures were limited to 1.032 m/s, 1.549 m/s and 2.065 m/s for each run. Two forces were highlighted from the vector velocity profile; axial (forward) and tangential (downward) forces (Figure 4.26). These two forces were used in 2D analysis as they represent two of the most important forces from the propeller which had been discussed by Lam et al. (2012a). The axial velocity is the main contributor to the velocity induced by propeller jet, whereas, the radial velocity is 14% of the axial velocity thrust, as suggested by Lam et al. (2011). These two forces are exerted from the velocity inlet and flow towards two pressure outlets. One of these pressure outlets is at the edge of tank, while the other is at the back of the propeller. The pressure outlet at the back of the propeller jet allows reflow from the fan to the velocity inlet, thus forming the rotating propeller feature.

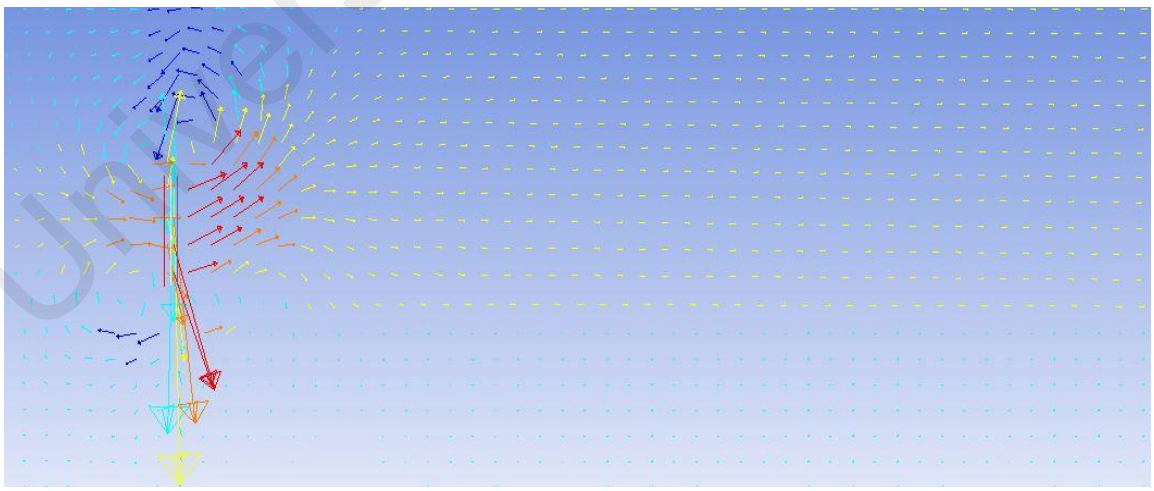

Figure 4.26: Velocity vector plot (m/s) from the 2D propeller jet with a magnificent of ×7

Mesh independence study

The mesh condition was simulated by 2D structured mesh using Gambit 2.2.30. Qualilateral mesh type is used for mesh construction in current study. Convergence of

the constructed mesh was tested by gradually decreasing the interval size between mesh nodes. The mesh size for Mesh 1 is 8241. The size of each simulation mesh increased by approximately 10% compared to previous mesh. Based on the convergence of mesh independence study (see Figure 4.27) it was found that the scour pattern calculated by mesh no. 1 does not have distinct difference with mesh no. 2 and 3. Therefore, mesh no. 1, which requires less time consumption, was used for further simulation. As the time required to model an unsteady solver is unknown, an optimum time step was selected for the simulation by taking the converging trends into consideration. Another attempt was made to run this simulation in steady state, where the final asymptotic scour profile was obtained at such state in minimal time step.

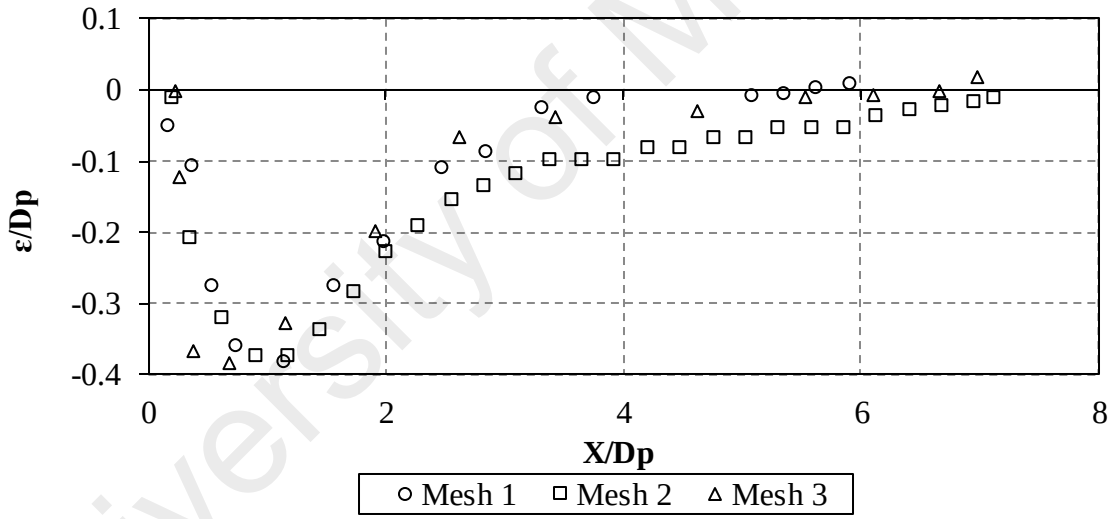

Figure 4.27: Convergence of mesh independence study

The physical time for scour profile to achieve steady-state condition is 200s (2000Δt, where Δt = 0.1s) for 2D VOF model. The scour parameters that were studied in this simulation are shown in Figure 4.28. Scour profile under asymptotic condition did not show any changes in scour depth. The interaction of propeller jet flow with sediment layer resulted in changes in phase number and development of the scour hole. The formation of scour holes developed gradually, and the depth increased until it reached the asymptotic state.

These phases' changes are indicated by volume of fraction value. When the fraction value is equivalent to zero, it indicates that the water continuum does not have any interaction with the sediment layer. On the other hand, fraction value of 1.00 indicates that there are no changes in phase interaction between sediment layer and water layer. The VOF numbers between 0.00 and 1.00 indicate that there are changes due to velocity forces (Figure 4.29). The asymptotic scour profile is plotted based on the scour line where VOF equals to l. Figure 4.27 shows the asymptotic state of scour profile for current study.

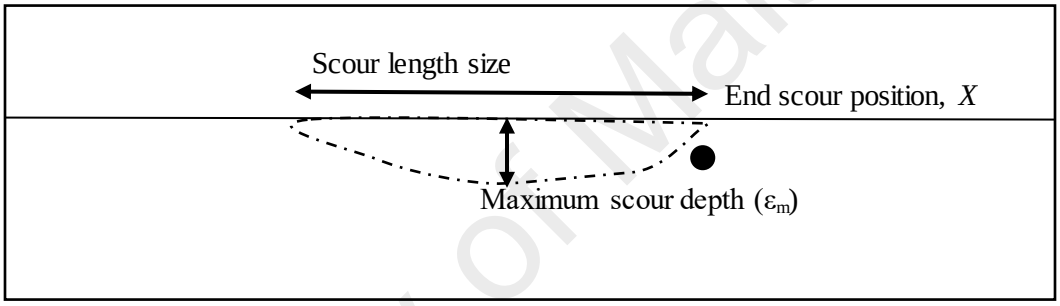

Figure 4.28: Scour parameters studied in a 2D VOF model

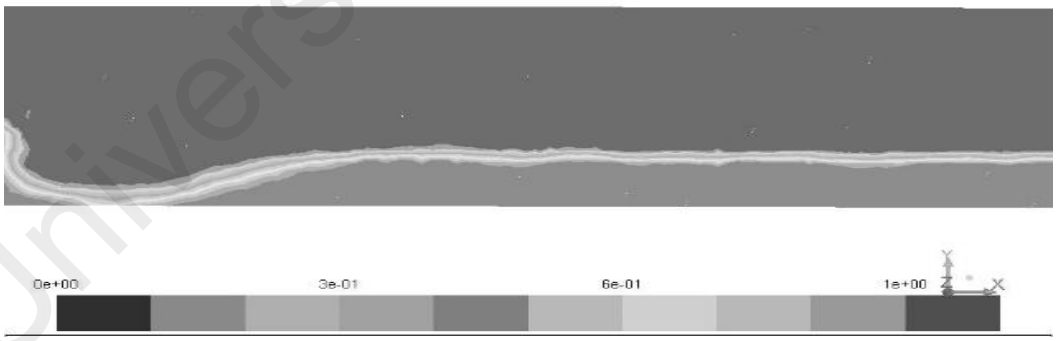

Figure 4.29: Example of 2D volume of fraction (VOF) profile

The depth of scour decreased gradually as the horizontal distance from the propeller jet face increased. Clearance of $0D_p$ represents the most critical scour depth as compared to others. Clearance of $1.32D_p$ had the least impact on scour, indicated that the scour decreased when the clearance between the tip of propeller jet and the sediment layer

increased. The case of $0D_p$ in this study showed that it is slightly more critical when compared with $0.31D_p$.

The overall scour pattern of $0D_p$ is relatively similar to $0.31D_p$ clearance. For other clearances ranging from $0.64D_p$ to $1.32D_p$, the scour location moved forward from the propeller jet face as the clearance increased. The ship's propeller wash interacted with seabed moved forward as the source of flow height increased. Therefore higher source of flow is associated with lower scour depth and further scour hole. The scour widths of the simulated scour hole ranged between 3 and $5X/D_p$. For clearance of $1.32D_p$, wider scour widths of approximately 8X/Dp was developed, but with low scour depth. Table 4.5 shows the scour parameters of each clearance.

Table 4.5: Examples of scour parameters of all clearances from simulation at 800rpm

Clearances, C (z/D_p)	**Maximum scour depth, (ε_m/D_p)**	**Scour position**		**Scour width (X/D_p)**
		Initial (X_1/D_p)	**End (X_2/D_p)**	
0	0.3895	0.345	4.456	4.111
0.31	0.3836	0.025	3.900	3.875
0.64	0.1739	0.944	6.605	5.661
0.95	0.1688	1.111	5.222	6.111
1.32	0.1335	1.020	9.859	8.839

4.9.1.2 Further analysis on 2D VOF

The scour pattern trend between the observed pattern and the predicted pattern by Hamill (1987) had similar trends as shown in Figure 4.30 from a qualitative comparison between observed pattern and pattern plotted using Hamill (1987) data. However, 2D simulation scour pattern was just 50% of the actual experiment data at steady state condition or asymptotic stage by using both experiments data equation, as proposed by Hamill et al., (1999) and Hong et al., (2013). The average shortfall in predicting the line is 60% of the predicted data by Hamill (1987). The under prediction was caused by the

mesh construction of 2D modelling, which is less refined. However, the error was reduced and appeared more comparable with literature as the clearance height increased.

Therefore, another attempt was made to compare the simulation results with the semi-empirical equations. Semi-empirical equations proposed by Hamill et al. (1999) and Hong et al. (2013) were used to estimate maximum scour depth. Besides, longitudinal scour cross sections were re-produced using VOF method, coupled with the empirical equations. The location of longitudinal scour cross section was predicted in correlation with $X/X_{\max}$. The semi-empirical equation proposed by Hamill et al. (1999) was as below:

$$\varepsilon_m = k\Omega[\ln(t)]^{\Gamma} \tag{4.7}$$

Where,

k = 38.97 is a constant proposed by Hamill et al. (1999)

t = time in seconds

$\Gamma = (\frac{C}{d_{50}})^{0.94}(\frac{D_P}{d_{50}})^{-0.48}F_o^{-0.53}$ and,

$\Omega = \Gamma^{-6.38}$

Furthermore, the following equation was proposed by Hong et al., (2013).

$$\varepsilon_m = 0.105 D_p F_o^{0.852}(\frac{d_{50}}{D_p})^{0.315}(\frac{U_o t}{D_p})^{0.168} \tag{4.8}$$

Other parameters include gravitational force, g, median size of sediment particles, d_{50} which is 0.1 mm in this study, fluid density, ρ, and mass density differences between fluid and sediment, $\Delta\rho$. According to their researches, the higher the Densimetric Froude number indicates a stronger impact of ship's propeller scour. Efflux velocity U_o is calculated using $U_o = 1.59nD_p\sqrt{C_t}$, where n is the rotational speed of

the propeller in revolution per second (rps) and C_t is the thrust coefficient of propeller. In consistent with Lam et al., (2010), C_t was chosen to be 0.4 for current simulation.

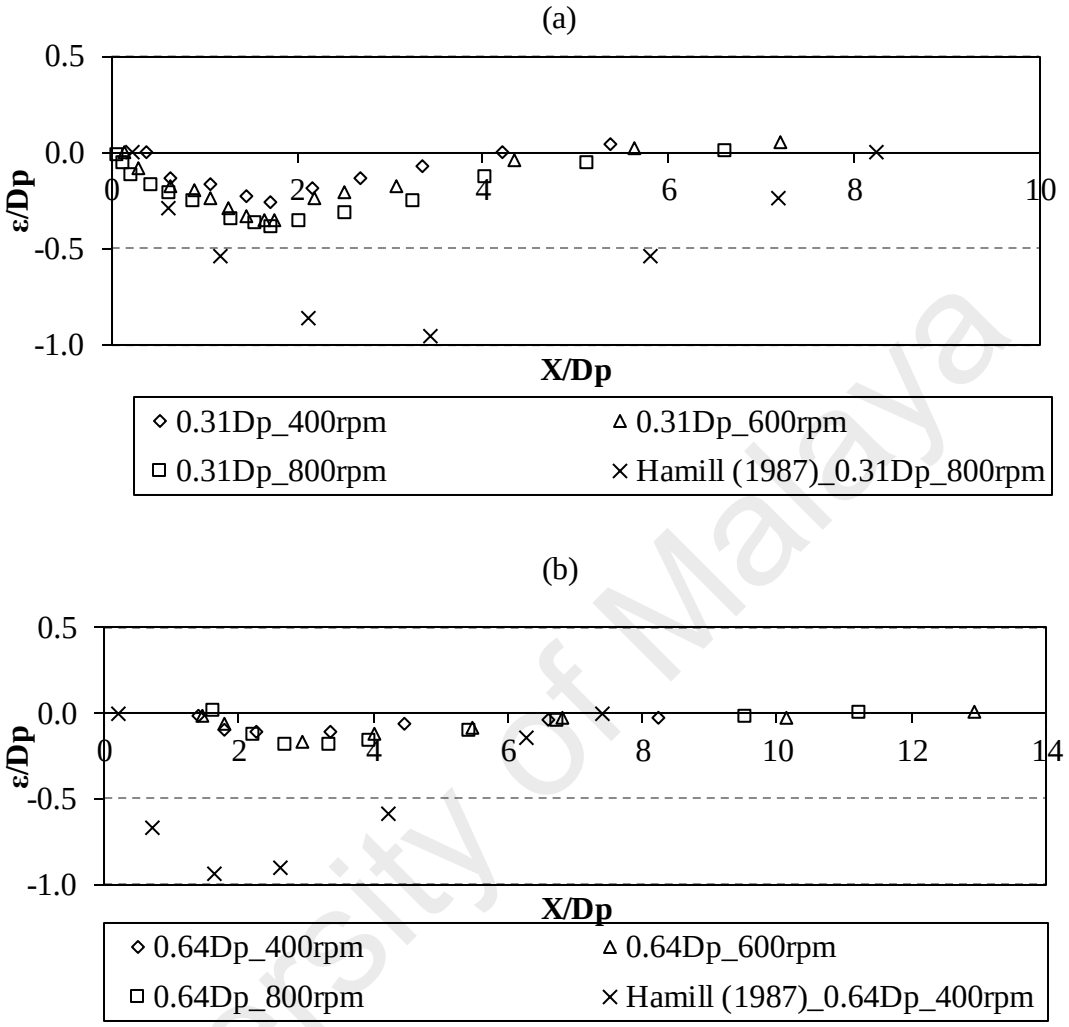

Figure 4.30: 2D scour pattern in asymptotic state: (a) clearance 0.31Dp and (b) clearance 0.64Dp

Moreover, it was observed that the CFD data incorporated from the empirical equation [4.8] was unable to produce longitudinal scour cross section. Comparison between maximum scour depths predicted by equation [4.8] was done, and results shown that the most critical scour impact occurred at $0.31D_p$. The clearance and scour depth were then decreased for the later clearances. However, it was not possible to predict maximum scour depth at 0Dp. Equation [4.8] also gave over prediction for maximum scour depth at $0.31D_p$, Therefore, these two clearances were not considered in the comparison. Validity range of scour depth was in line with Hamill et al., (1999)

findings. Consequently, equation [4.8] cannot be applied for $0D_p$ and $0.31D_p$ clearances. Trend of comparison of maximum scour depth predicted by equation [4.7] showed that the maximum scour depth increased from $0D_p$ to $0.31D_p$ and then decreased from $0.31D_p$ onwards. This result showed that the equation is reasonable and applicable for all ranges of clearance as suggested by Hong et al (2013).

Comparison of these two equations showed that both methods require a few main parameters for the prediction, including D_p, t, F_r and d_{50}. Figure 4.31 showed that both equations and 2D simulation predicted the same scour pattern despite the predicted scour depths were different. There were some limitations for both methods. Equation [4.8] was only applicable for the range of $0.5D_p \leq C \leq 2.5D_p$ whereas equation [4.7] was applicable for all the tested clearances in a range of $0D_p \leq C \leq 1.32D_p$. Maximum scour pattern predicted by both equations were compared with 2D simulation results as tabulated in Figure 4.31. A detailed dimensional comparison of maximum scour depth predicted by both equations was compared with 2D simulation results as tabulated in Figure 4.32.

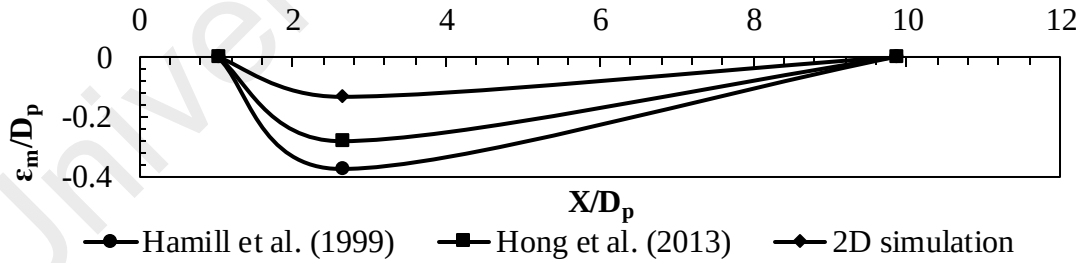

Figure 4.31: Example scours line with proposed coupled method

After qualitative comparison, 2D simulation using VOF method showed an acceptable agreement with scour development when rotational speed is constant. 2D simulation only considers two-dimensional impacts from propeller jet flow. Moreover, CFD model does not consider the non-Newtonian effect of the sediments, and hence there were differences between simulations and semi-empirical predictions. However,

the increased clearances exhibited an increase in accuracy of results, which showed that 2D VOF has better ability in predicting higher clearance of scour.

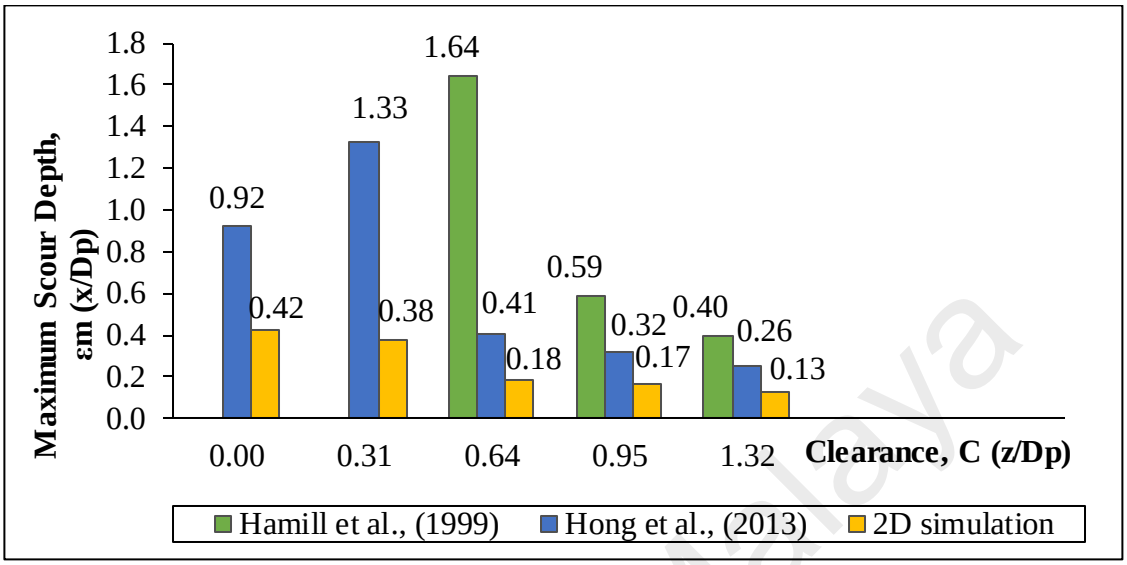

Figure 4.32: Comparison of 2D simulation results with theoretical equations

4.9.2 Three-dimensional VOF observation with single rotating propeller

In 3D simulation, the rotating ship propeller's wash was modelled with the fan swirling setting. All three directional forces (axial, radial and tangential forces) were reproduced with the fan swirling method in application of velocity inlet and pressure outlet boundary on the next layer of the fan swirling boundaries. The blade effects were not considered in fan swirling method. The velocity vector induced from the modelled ship's propeller has been plotted in Figure 4.33.

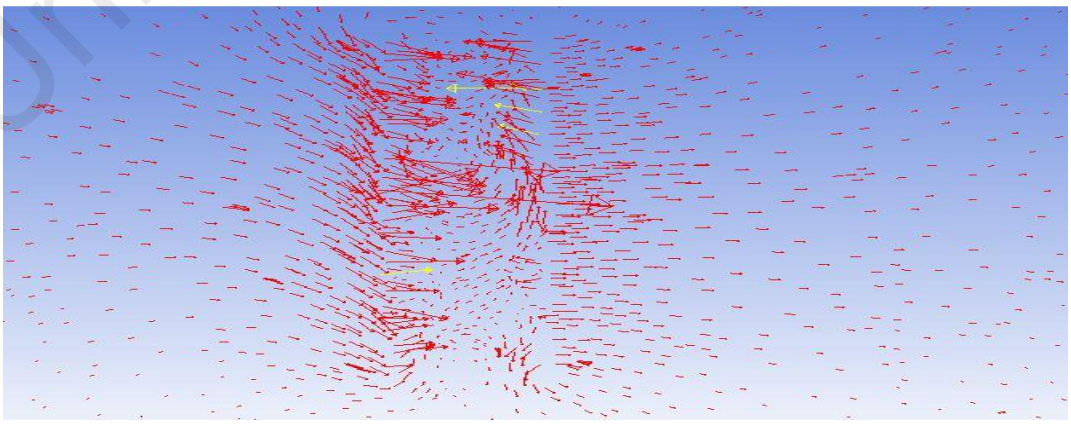

Figure 4.33: Vector plot with magnification ×7of a 3D simulation ×7

Mesh Independence Study

Different 3D mesh resolutions of the scour profile are shown in Figure 4.34. The quality of mesh resolution increased in line with the mesh count, by 10-20% of the preceding coarser mesh count. Only 2% variation of the scour depth results was accepted for the complement of mesh independent study. The mesh independent study details are reported in Table 4.6.

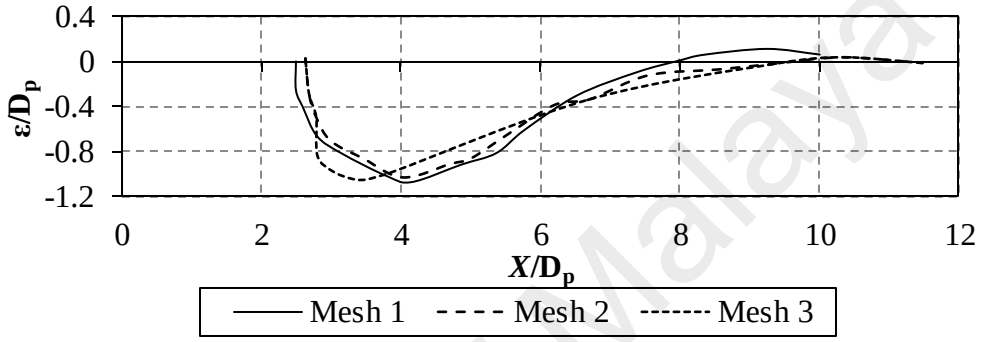

Figure 4.34: Mesh independence study curve for 3D simulation (single propeller)

The physical time for scour profile to achieve the steady-state condition was 3800s. The scour parameters studied in this simulation are shown in Figure 4.36. The scour patterns for 3D simulation were plotted in the form of ε/D_p versus X/D_p, where ε is the scour depth at asymptotic state and X is the location of the developed scour. Table 4.7 shows the summary of scour parameters in 3D simulation. The example of 3D VOF fraction profile observed from longitudinal view is also shown in Figure 4.36.

Table 4.6: Scour parameters for 3D simulation

Parameters	**$0.31D_p$ clearance**		**$0.64D_p$ clearance**
Types of scour hole	Initial	Main	Main
Maximum scour depth (ε/D_p)	0.23 - 0.25	1.16 - 1.26	1.07 – 1.12
Location of maximum scour depth (x/Dp)	0.38 – 0.48	3.01 – 3.26	1.88 – 2.23
Width (mm)	68	844	883

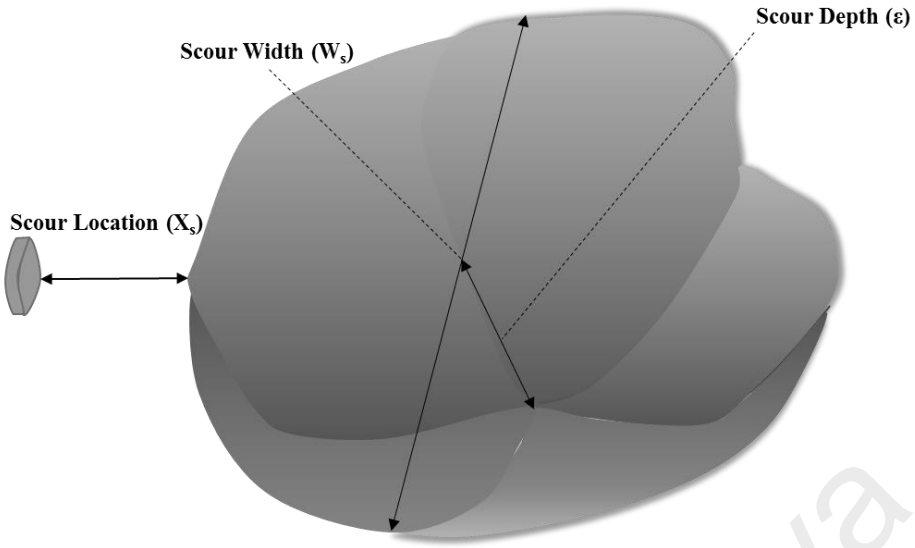

Figure 4.35: Scour parameters studied in a 3D VOF model

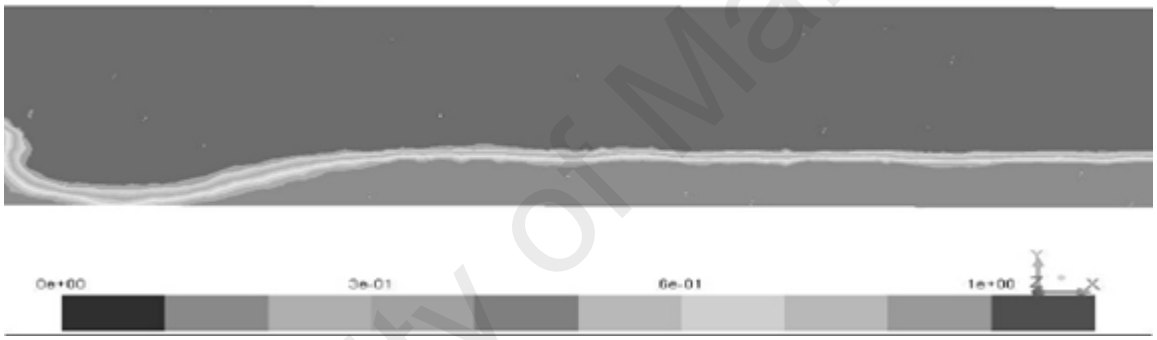

Figure 4.36: Example of 3D volume of fraction (VOF) profile

Figure 4.37 showed that any increase in clearance will reduce the scour depth. Scour has formed further from the propeller jet as clearance increased. Clearance $0.31D_p$ has given deeper scour depth compared to clearance of $0.64D_p$. Moreover, the large in contact forces from the wash caused the location of main scour hole for $0.31D_p$ to be further from the propeller face compared to $0.64D_p$. On the other hand, $0.64D_p$ has given a wider scour than the $0.31D_p$ in 3D VOF scour plot.

Both 2D and 3D indicated that an increase in clearance will result in a decrease in scour depth. This is attributed to the shorter distance of wash contact which has a larger force on the erodible soil bed. Furthermore, Figure 4.38 showed the typical scour profiles from VOF for 3D simulation at xy-plane. The scour width simulated from the

VOF showed a mere difference of 4% from results by Hamill (1987). The xy-plane showed that the maximum scour positions moved further from the propeller face as the jet speed increased. It is shown that a bigger clearance result in a shallower scour hole. Although the profiles showed a similar form of scour, the maximum scour positions moved further from the propeller face when the speed increases. This was attributed to an increase in velocity forces impinged to the soil as the rotational speed increases. The scour estimation of current study is in line with Hamill (1987), Hamill et al. (1999) and Hong et al. (2013).

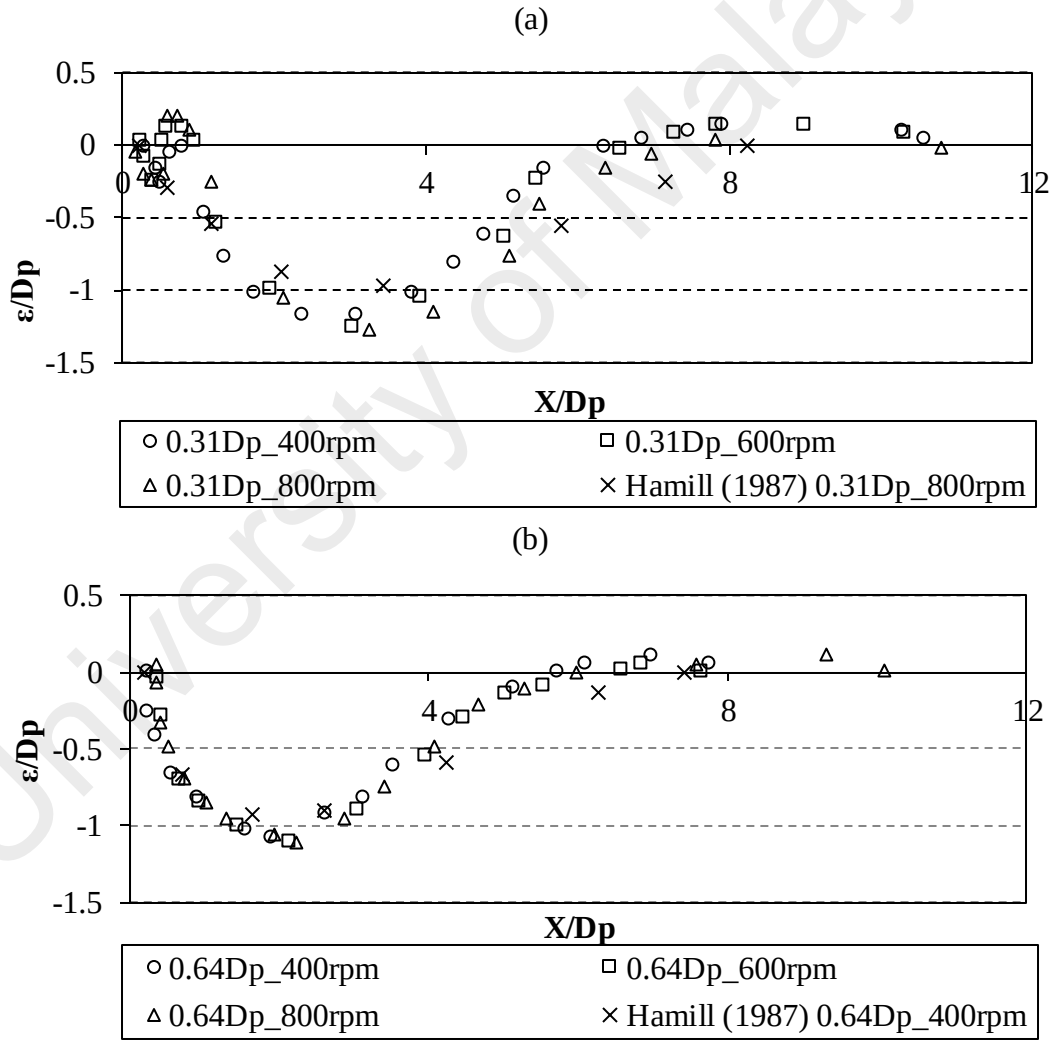

Figure 4.37: 3D scour pattern in asymptotic state: (a) clearance $0.31D_p$ and (b) clearance $0.64D_p$

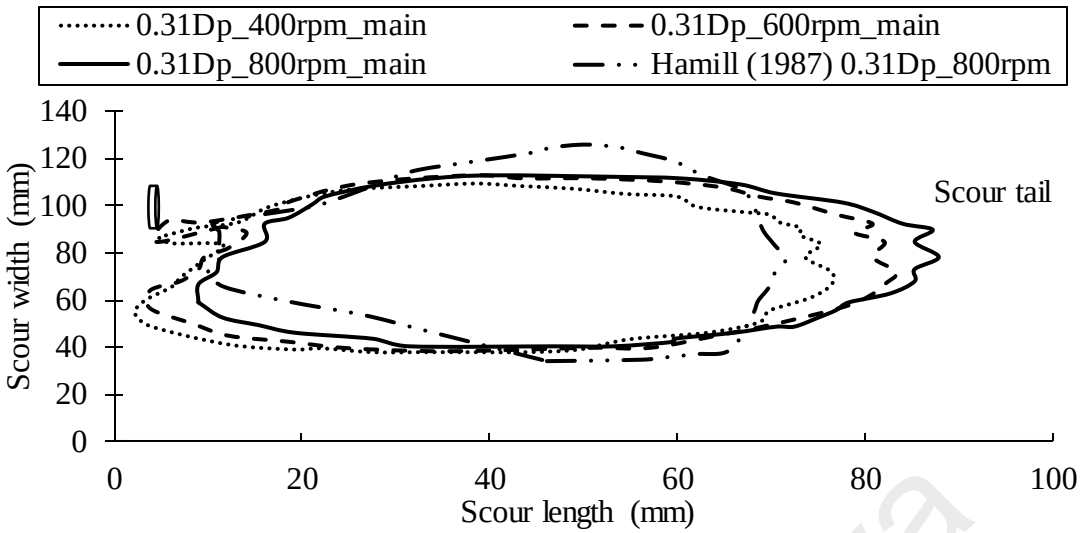

Figure 4.38: Typical scour profiles (x-y plane) increased with speed

Table 4.7: Comparison of 2D, 3D and experiment data

Differences in term of maximum scour depth				
	$0.31D_p$_800rpm		**$0.64D_p$_400rpm**	
	2D	**3D**	**2D**	**3D**
3D	69%	-	89%	-
Experiment (Hamill,1987)	60%	23%	87%	12%
Experiment formula (Hong et al., 2013)	67%	6%	81%	45%
Differences in term of location for maximum scour depth				
	$0.31D_p$_800rpm		**$0.64D_p$_400rpm**	
	2D	**3D**	**2D**	**3D**
3D	47%	-	16%	-
Experiment (Hamill,1987)	50%	5%	27%	12%

In summary, both 2D and 3D simulation results predicted a similar pattern of scour profile, i.e. the 'U' shaped curve below the horizontal axis as shown in Table 4.7. The differences between 2D simulation and experiment results were relatively high with approximately 73% difference on the prediction of maximum scour depth. Meanwhile, 3D simulation was able to predict the maximum scour depth at higher accuracy with an average of 17% difference for both clearances. However, it was observed that the 3D simulation is capable to predict higher accuracy results when the rotational speed is low. This may be due to the fan setting where the detailed blade effect was not taken into consideration. Therefore, an increase in rotational speed will result in higher occurrence

of error. However, since the bollard pull condition for propeller has a low range of speed, which is less than 200rpm, the propeller speed range is practical to be applied. Moreover, the 3D simulation has accurately predicted the location of maximum scour with a slight variation of 8% from the experimental data. Overall, the scour width observed by Hamill (1987) is wider than the scour holes predicted using 3D simulations.

4.10 Estimation of ship-twin-propeller's scour with VOF

Mesh independence study

From the past validation simulation, it was found that 3D simulation has higher accuracy and produces higher correlated data. Therefore, only 3D simulation was used to model the ship-twin-propellers. Mesh independence study was repeated for each new simulation run. The mesh independence curve for ship-twin-propeller simulation was reported in scour depth perpendicular to the distance in *X*, as shown in Figure 4.39. The mesh count gradually increased by 15-25% of the preceding mesh count of coarser mesh as shown in Table 4.8. Mesh independence study is completed when the scour profile and maximum depth have been obtained using finer meshes with variations less than 2%. Therefore, the M2 mesh was chosen to use in the later simulation as it requires shorter simulation time and produces quality work which is equivalent to other finer meshes.

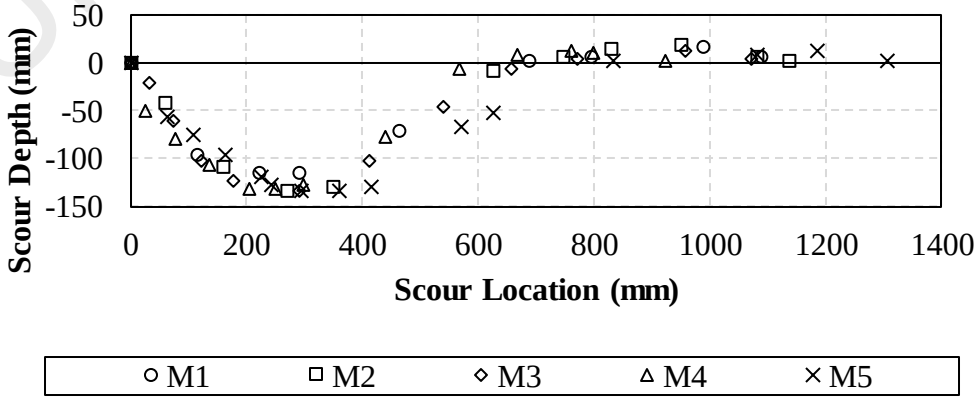

Figure 4.39: Mesh independence curve for 3D ship-twin-propeller meshes

Table 4.8: Mesh independence for 3D mesh (twin-propeller)

Properties	Meshes				
	M1	M2	M3	M4	M5
Grid cells	4,070,779	4,254,634	4,541,318	4,871,111	5,314,089
Increment (%)	-	17.17	22.85	21.39	23.67
Maximum scour depth, (mm)	114.78	134.69	134.73	133.90	134.04

4.10.1 Three-dimensional observation with twin rotating propeller

The ship-twin-propeller was remodelled using Fluent 15.0, as outlined in Chapter 3. In section 4.9.2, the rotating ship propeller's wash was modelled with the fan swirling setting. Therefore, the vector profile of ship-twin-propeller is relatively similar to single rotating propeller. However, since the modelling of ship-twin-propeller's hydrodynamic properties was not considered in current study, the details of hydrodynamic properties of ship-twin-propeller jets were not observed. As a result, only scour profile induced by ship-twin-propeller's wash was plotted and analysed. Scour profiles based on three clearances ($0.31D_p$, C1; $0.5D_p$, C2; and $0.64D_p$, C3) and three rotational speed (400, 500 and 600rpm) were studied. Three section views, which are the longitudinal view, x-y plan view and the x-z plan view, were plotted to observe the simulated results. X-z plan view was used to observe the cross section of scour hole. The example of simulation modelling induced from ship-twin-propeller's wash, before plotting into graph, is shown in Figure 4.40.

Figure 4.40: Example of simulation modelling induced from ship-twin-propeller wash (from x-z view)

4.10.1.1 Longitudinal view

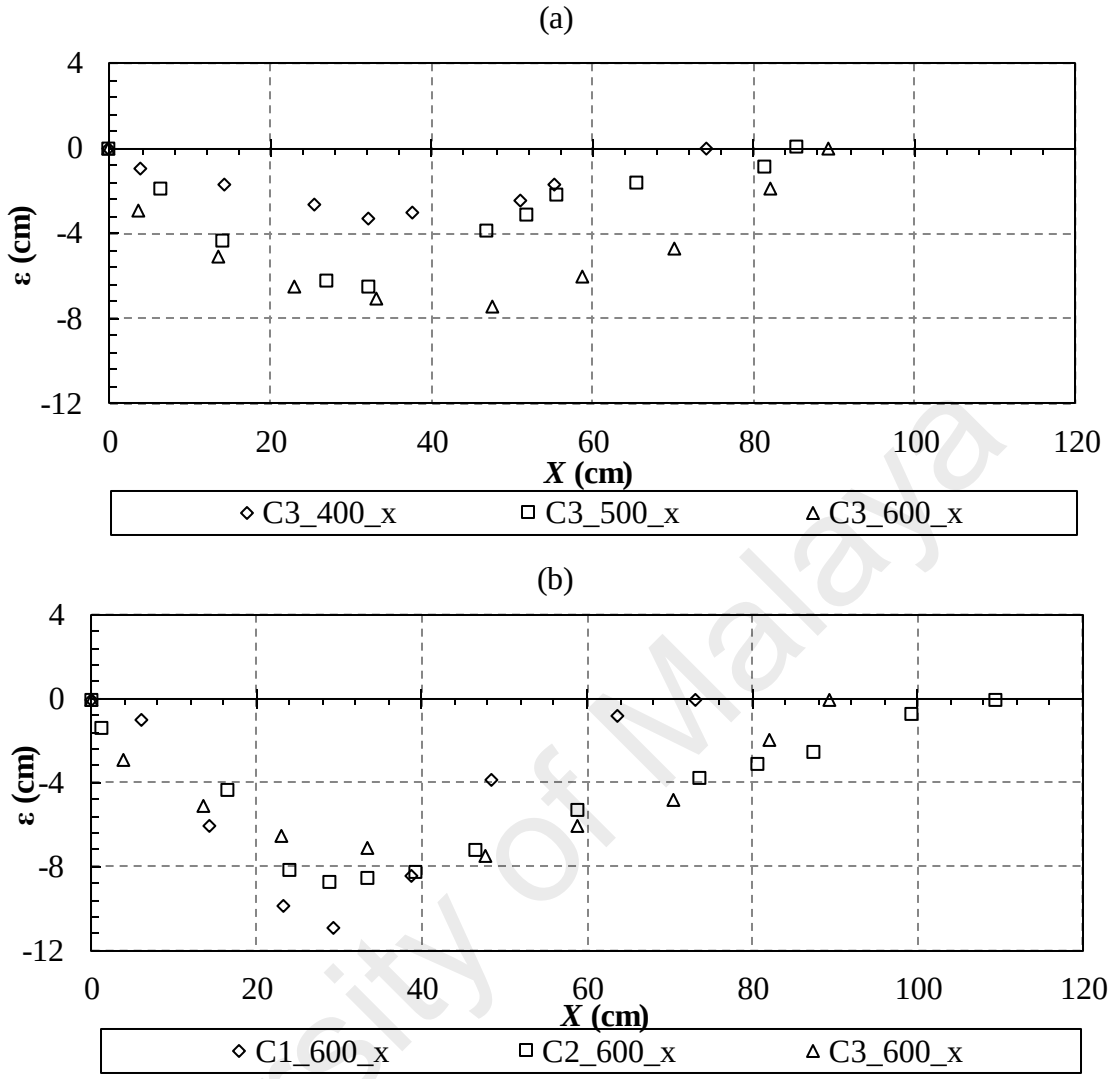

Figure 4.41: Longitudinal section of 3D scours profile induced by ship-twin-propeller's wash: (a) constant clearance and (b) constant rotational speed

In order to obtain results which are comparable with experiment results, only the right side scour longitudinal profile was observed and analysed in current simulation as shown in Figure 4.41. It is found that the scour hole of lower clearance gave a deeper scour with smaller scour hole at constant clearance. An increase in clearance will result in decrease of scour depth but an increase in the size of scour hole. Conversely, the increasing clearance at constant rotational speed showed that the higher rotational speed will result in deeper and larger scour.

4.10.1.2 Plan view (x-y plane)

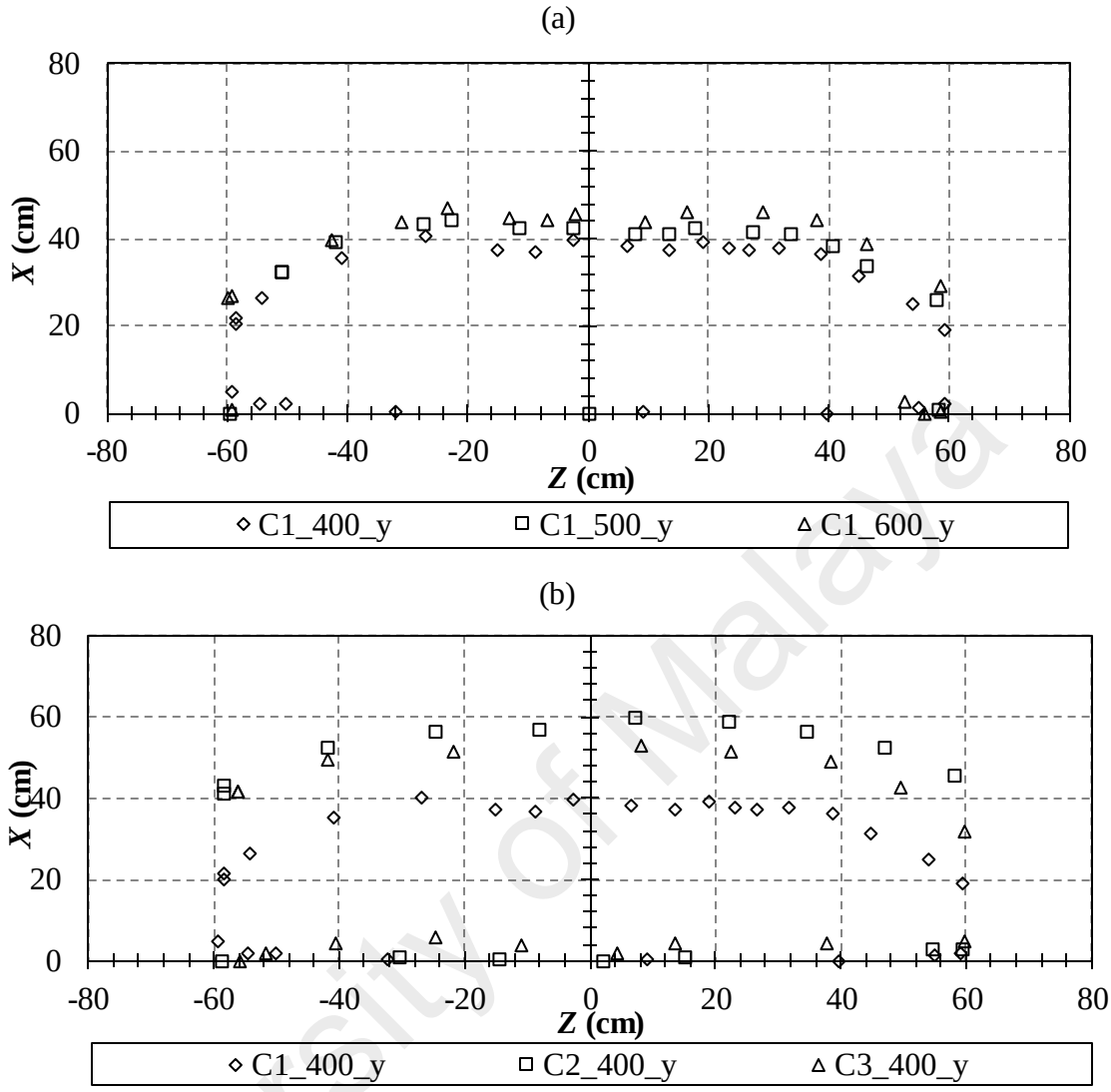

Figure 4.42: X-Y section of 3D scours profile induced by ship-twin-propeller's wash: (a) constant clearance and (b) constant rotational speed

The plan view section of x-y plan was plotted in Figure 4.42. At constant clearance, the scour width increases in line with rotational speed and clearance height. However, based on current simulation, the scour at C2 was wider than C3. Subsequently, C2 is the optimum level of clearance in inducing scour hole for such case.

4.10.1.3 Plan view (x-z plane)

The x-z plan showed the cross section of scour depth induced by ship-twin-propeller's wash. Based on Figure 4.43, the scour depth increased in line with rotational speed despite a decline in clearance.

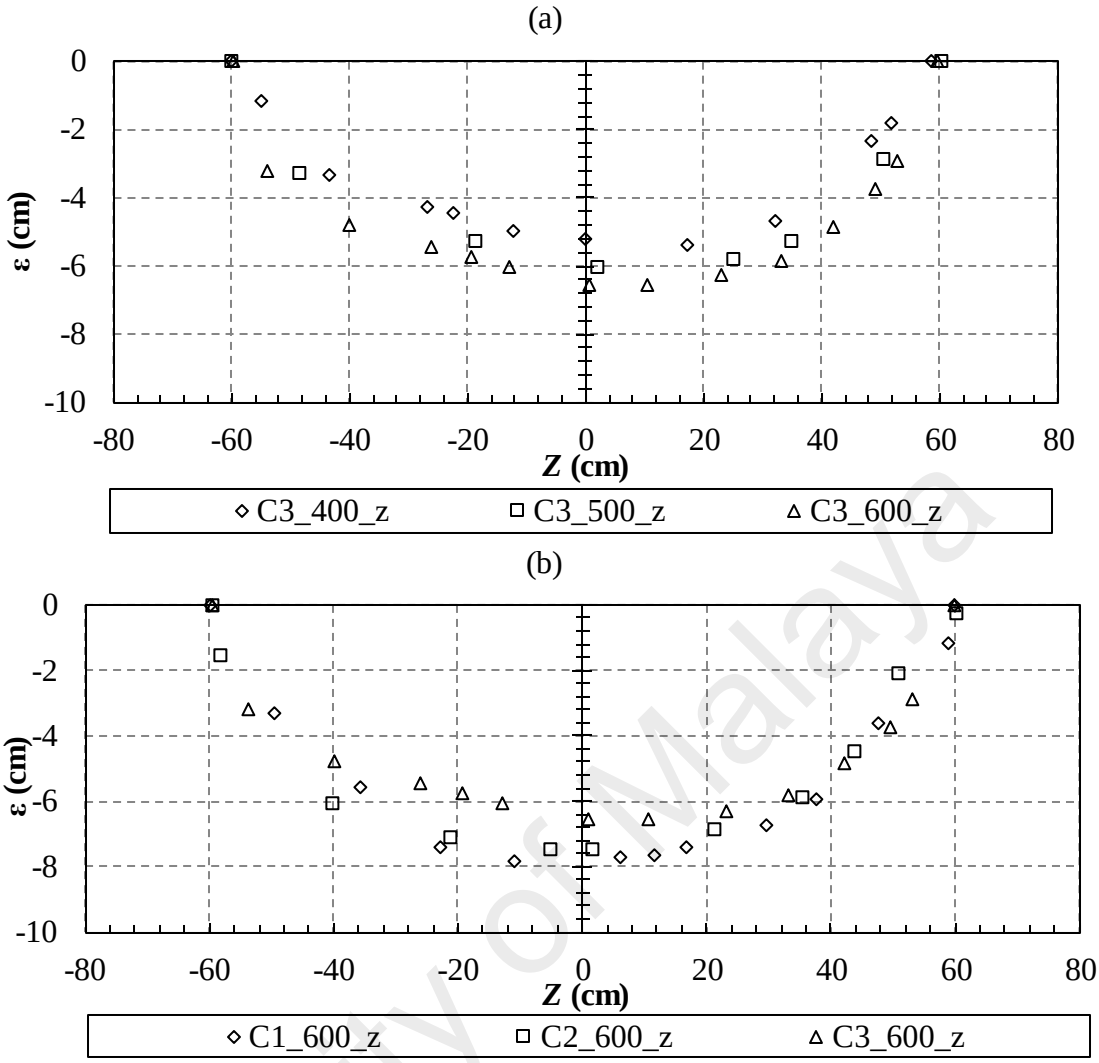

Figure 4.43: X-Z section of 3D scours profile induced by ship-twin-propeller's wash: (a) constant clearance and (b) constant rotational speed

4.10.2 Validation with experiment data

The example of simulation results was compared with experiment data, as shown in Figure 4.44 and 4.45. The simulation results do not include the scour ridge. However, the simulation scour results induced by ship-twin-propeller showed a similar pattern with experiment results. The simulation patterns included the maximum scour depth, maximum scour depth location, as well as the scour width. The differences between simulation results and experiment data fell within a range of 5-30%. This is possibly due to the series which was generated until converged state, where extra time step may be taken to consider further development of the scour depth. Series with lower

rotational speed has higher differences when compared to experimental data, where the propeller modelling is required to be improved.

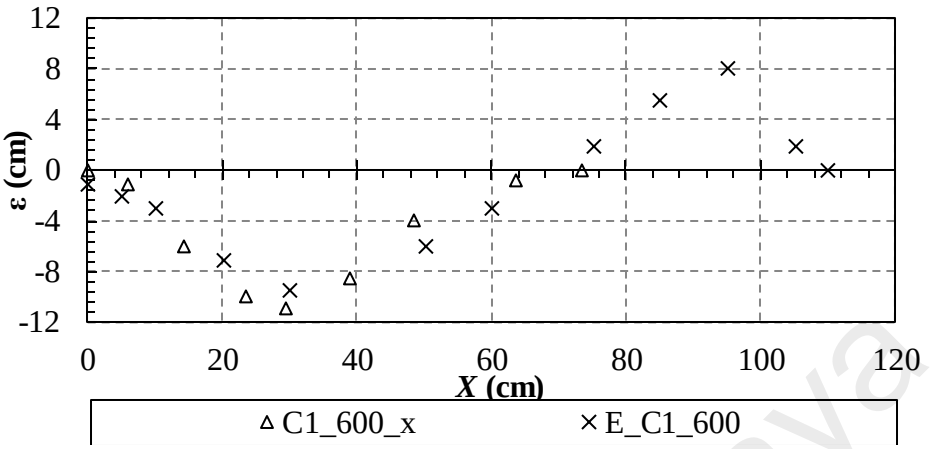

Figure 4.44: Comparison of scour pattern of simulation with experiment data of current study

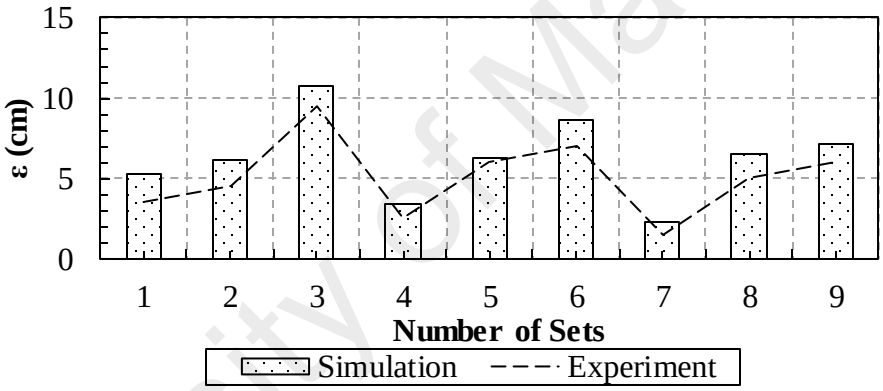

Figure 4.45: Comparison of maximum scour depth simulation with experiment data of current study

4.11 Summary

Throughout the literature reviews outlined in Chapter 2, it was found that the ship-twin-propellers' jet induced seabed scouring has yet to be revealed from the past researches. Current study focuses on the relationship of ship-twin-propellers wash in relation to various clearances and rotational speed. This study is preliminary which requires future works to improve its practicability. The relationship between ship-twin-propellers' jet, clearances and rotational speed was suggested as per equation [4.1], which is $U_o = 2.058nD_p\sqrt{C_t}$. The overall results indicated that there are differences between STP's jets and single propeller jets in terms of axial velocity profile and its

resulting decay pattern as summarised in section 4.6. Therefore, it is considerably a new outcome from STP investigation. The velocity decay profile has altered its usual pattern from single peak to double peak where the second peak is located at $2.8X/D_p$. The second peak indicates another possible location of maximum scour depth, which should happen before $2.8X/D_p$. Therefore, based on this analysis, the maximum scour depth of current study is located between $0X/D_p$ and $2.8X/D_p$.

The STP's wash showed that two small scour hole will be induced at the initial state of scour development. When the scour prolonged, both scour holes will emerge and form a large scour hole. There are exceptional cases where both scour holes do not emerge into a large scour hole, which only happens when the scour clearance is high, under the condition of STP running at low velocity speed i.e. less than 400rpm, for current study. With the help of non-linear regression, the maximum scour location was suggested to be $X_{max} = {F_o}^{0.909}(\frac{C}{D_p})^{0.193}$. Further investigation on the prediction of maximum scour depth was also carried out. Based on the data obtained from the experiment, which focuses on the relationship between rotational velocity and under keel clearance, the proposed equation has been stated in equation [4.6].

Simulation results using VOF method was first validated using single rotating propeller, and then compared with previous literature works. It was found that 3D modelling has a highly correlated profile, in terms of scour pattern and scour depth prediction. Therefore, consideration on running the STP model was only limited to 3D modelling. The results showed a slightly higher prediction for scour depth and size. CFD works had been given advantages which are more time and cost effective. However, future works are still required to improve the simulation prediction, which will be discussed in Chapter 5.

CHAPTER 5: CONCLUSION AND RECOMMENDATION

5.1 Conclusion

Based on literature review, it was found that there are limited experimental works performed on ship-twin-propeller's wash and its resulting scour. Therefore it was decided that a study on ship-twin-propeller's wash induced scour should be carried out. Laboratory and simulation works were performed to achieve all three objectives of current study. The first objective was to identify the source and pattern of axial velocity impinging the seabed which was induced by ship-twin-propeller's wash. The second objective was to determine the temporal development of scour induced by ship-twin-propeller's wash by investigating the seabed scouring pattern. The third objective was simulation of seabed scour pattern induced by ship-twin-propeller's wash. Overall, this research shows the relationship between the axial velocities of STP impinged onto the soil bed. This is found to be necessary before any further application onto the field study conducted.

Experimental methods for the investigation of parameters of ship-twin-propeller's wash and its resulting scour were developed. Axial velocity and scour measurements from the series of experiments were tested and analysed. The analyses are revealed as follows,

i. The source of axial velocity of ship-twin-propeller was found at both sides of the propeller blade, which is similar to single rotating propeller. The combination forces of each side of the blade caused an increase in the axial velocity thrust and resulted in higher impact of scour.

ii. The experiment on measurement of axial velocity suggested that the axial velocity of ship-twin-propeller shall be calculated using the formula of $U_o = 2.058 D_p \sqrt{C_t}$, which was based on the axial momentum theory.

iii. There are forces interferences at the centre line of ship-twin-propeller with distance of one propeller diameter in between. This has resulted in different decay profile which consists of two peaks, specifically decay at initial plan and another decay at the location of $2.8X/D_p$. The second decay profile indicated that the range of maximum scour should be located between $0X/D_p$ and $2.8X/D_p$.

iv. Ship-twin-propeller has shown that the two scour holes at the initial stage subsequently emerged to a large scour hole at the later stage. Ship-twin-propeller with high level of under keel clearance, rotating at 400rpm or less, remained with two single scour holes until the asymptotic stage.

v. The temporal development of scour was observed experimentally. All investigated scour parameters in current study were plotted as shown in Figure 4.25, where the key parameters were X_{max} and ε_{max}.

vi. The maximum scour location has been suggested to be calculated using the formula of $X_{max} = {F_o}^{0.9098} (\frac{C}{D_p})^{0.1932}$. This formula was proposed based on the lowest root mean square value with confidence level of 95%.

vii. The estimation of maximum scour depth in relation to the rotational speed, clearances and time was suggested based on highest confidence level of data and lowest root mean square which is,

$$\varepsilon_{max} = \mathrm{k}(\log t)^{0.0231}$$

$$k = \left(\frac{C}{D_p}\right)^{-0.488} (\frac{U_o t}{C})^{0.241}$$

This equation also has a high R^2 value of 0.909 when both observed value and predicted value were compared.

viii. The current twin-propeller scour analysis has given an insight on the high impact of scour would occurred when the under keel clearance is low and bollard pull rotating speed is high. Therefore, to overcome the damage of scouring action, sea bathymetry need to be always maintained to ensure the bathymetry level is low.

ix. VOF model was firstly modelled in single propeller form to validate the simulation. It was found that 3D modelling has a highly correlated profile in both scour pattern and scour depth prediction as compared to 2D modelling. As a result, only 3D simulation was modelled in scour prediction on ship-twin-propeller's wash induced seabed scouring.

x. The 3D simulation of ship-twin-propeller was performed and compared with the experiment data. It was found that it has higher prediction on the maximum scour depth as compared to the experimental data obtained from current study. However, current model only limits in the scour formation prediction, actual scour depth still required further validation and will be further discussed in the later section. Simulation study has advantages on time and cost effectiveness which can be practiced by engineers and port authorities in order to improve design in minimising scouring effect induced by ship-twin-propeller's wash.

5.2 Limitation and suggestion for further research

Despite the contribution of current study, there are still a number of areas which have to be investigated further in order to improve the existing knowledge on the ship-twin-propeller's wash induced seabed scour.

i. The proposed coefficient as mentioned in equation [4.1] requires further verification with different types and geometry of propeller as this is the initial step in investigating ship-twin-propeller's jet. Since internal space between both propellers was limited to 1.0 propeller diameter in current study, space variation should also be considered in improving the existing coefficient.

ii. Only axial velocity and its resulting decay profiles were studied in current works which only provides a preliminary investigation on the ship-twin-propeller's jet velocity components. Therefore, to provide a strong methodology in predicting the ship-twin-propeller's jet, other hydrodynamic properties of ship-twin-propeller should also be considered in future works.

iii. On the other hand, the scour development induced by ship-twin-propeller's wash requires further verification with propellers of other geometry and other types of soil, to improve the correlation data in equation [4.5] and [4.6] for usage under all situations.

iv. Simulation works using different sets of data with similar test settings are required for further validation. In addition, detailed propeller geometry should be considered in future analysis.

v. Field works should be considered in future, in order to validate the laboratory results, particularly on the investigation of scour development with the existence of harbour structures.

REFERENCES

Abramovich, G.N. (1963). "Theory of Turbulent Jets", M.I.T. Press, Cambridge, Massachausetts.

Abramowicz-Gerigk, T. (2008). Experimental Study on the Hydrodynamic Forces Induced by a ship-twin-propeller Ferry during Berthing. *Ocean Engineering*, *35*(3/4), pp. 323-332. doi:10.1016/j.oceaneng.2007.10.009

Albertson, M.L., Dai, Y.B., Jensen, R.A., Rouse, H. (1950). Diffusion of Submerged Jets. Transcript of the A.S.C.E., Paper No. 2409, 115, 639–697.

Andrew, J. M. (Ed.). (2013) Sediment Transport and Their Modelling Applications. Croatia: InTech.

Balachandar, R., & Kells, J. A. (1997). Local channel scour in uniformly graded sediments: the time-scale problem. *Canadian Journal of Civil Engineering*, 24(5), 799-807.

Balachandar, R., Kells, J. A., & Thiessen, R. J. (2000). The Effect of Tailwater Depth on the Dynamics of Local Scour. *Canadian Journal of Civil Engineering*, *27*(1), 138-150.

BAW (2010). Principles for the Design of Bank and Bottom Protection for Inland Waterway. Bundesanstalt für Wasserbau (BAW).

Berger, W., FelKel K., Hager, M., Oebius, H., Schale, E. (1981). Courant provoque par les bateaux protection des berges et solution pour eviter l'erosion du lit du Haut Rhin, P.I.A.N.C., 25 Congress, Endinburgh, 1981, Section I-1.

Blaauw, H. G., Kaa, E. J. van de (1978). ''Erosion of Bottom and Sloping Banks Caused by the Screw Race of the Manoeuvering Ships.'' Publ. No. 202, Delft Hydraulics Laboratory, Delft, The Netherlands.

Brewster, P. M. (1997). "Modelling the Wash from a Ship's Propeller". Thesis submitted to the Queen's University of Belfast for the degree of Doctor of Philosophy.

Chang, F. M., Simons, D. B. and Richardson, E.V. (1965). "Total Bed-material Discharge in Alluvial Channels", U.S. Geological Survey Water-Supply Paper 1498-I.

Chang, F.M., Simons, D.B. and Richardson, E.V. (1967). "Total bed material discharge in alluvial channels". In *Proceedings of 12th Congress IAHR*, Vol. I, Colorado: Fort Collins.

Choudhury, D. (1993). Introduction to the Renormalization Group Method and Turbulence Modelling, Fluent Inc. Technical Memorandum TM-107.

Cihan, K., Ozan, A.Y., Yülsel, Y., 2011. The effect of slope angle on propeller jet erosion near quays. Proceedings of the ICE – Maritime Engineering, Volume 165, June 2012, Issue MA2, pages 81-92, 2011.

Coraddu, A., Dubbioso, G., Mauro, S., Viviani, M. (2013). Analysis of twin screw ships' asymmetric propeller behaviour by means of free running model tests. Ocean Engineering 68. pp. 47-64.

Dubbioso, G., Viviani, M. (2012). Aspects of twin screw ships semi-empirical maneuvering models. Ocean Engineering 48. pp. 69-80.

DuBoys, M.P. (1879). "Le Rhone et les Riveres a Lit affouillable, Annales de Ponts et Chausses, Sec. 5, vol. 18, pp. 141-195.

Einstein, H.A. (1942). "Formula for the Transportation of Bed-Load", Transactions of the ASCE, vol. 107.

Einstein, H.A. (1950). "The Bed-Load Functions for Sediment Transportation in Open Channel Flows", U.S. Department of Agriculture, Soil Conservation Service, Technical Bulletin no. 1026.

EN-ISO-3715-1. (2004). Ships and Marine Technology, Propulsion Plants for Ships, Part 1: Vocabulary for Geometry of Propellers. Technical Report, European Committee for Standardisation.

Fluent User Manual. (2003). "Fluent User's Guide." Fluent Inc, Lebanon, USA.

Fuehrer, M., Römisch, K. (1977). "Effects of Modern Ship Traffic on Islands and Ocean Waterway and their Structures." In: proceedings of P.I.A.N.C., Leningrad, 1977, Sections 1-3.

Fuehrer, M., Pohl, H., Römisch, K. (1987). "Propeller Jet Erosion and Stability Criteria for Bottom Protection of Various Constructions", In Proceedings of P.I.A.N.C., Bulletin No. 58, 1987.

Gaythwaite, J. (2004). Design of Marine Facilities for the Berthing, Mooring, and Repair of Vessels. ASCE Publications, ISBN: 0784407266 531 pages.

Gerr, D. (2001).Propeller Handbook, The complete Reference for Choosing, Installing and Understanding Boat Propellers. International Marine, Camden.

Hamill, G.A. (1987). "Characteristics of the Screw Wash of a Manoeuvring Ship and the Resulting Bed Scour. Thesis submitted to the Queen's University of Belfast for the degree of Doctor of Philosophy.

Hamill, G. A. (1988). ''The Scouring Action of the Propeller Jet Produced by a slowly Manoeuvring Ship.'' Bull. No. 62, Permanent International Association of Navigation Congresses, 85-110.

Hamill, G.A., Johnston, H.T. (1993). The descay of maximum velocity within the initial stages of a propeller wash. *Journal of Hydraulic Research*, 31(5), pp. 605-613

Hamill, G. A., McGarvey, J. A., and Mackinnon, P. A. (1998). "A method for estimating the bed velocities produced by a ship's propeller wash influenced by a rudder." Proc., 26th Int. Conf. on Coastal Engineering, Copenhagen, Denmark, 3, 3624–3633.

Hamill, G.A., Johnston, H.T., Stewart D.P. (1999). Propeller Wash Scour near Quay Walls. Journal of Waterway, Port, Coastal and Ocean Engineering, July/August, 1999.

Hamill, G.A., McGarvey, J.A., Hughes, D.A.B. (2004). Determination of the Efflux Velocity from a Ship's Propeller. Proceedings of the Institution of Civil Engineers: Maritime Engineering 157 (2), 83–91.

Hashmi, H.N. (1993). "Erosion of a granular Bed at a Quay Wall by a Ship's Screw Wash." Ph.D. Thesis, Thesis submitted to the Queen's University of Belfast for the degree of Doctor of Philosophy.

Hinze, J. O., (1957). "Turbulence", Mc Graw Hill Series in Mechanical Engineering.

Hirt, C.W., Nichols, B.D. (1981). Volume of Fluid (VOF) Method for the Dynamics of Free Boundaries. *Journal of Computational Physics*, 39 (1), pp. 201–225.

Hoffmans, G. and Verheij H. (2011). Jet scour. Proceedings of the ICE – Maritime Engineering 164, Issue MA4, December 2011, pages 185-193.

Hong, J.H., Chiew, Y.M., Susanto, I., Cheng N.S. (2013). Evolution of Scour Induced by Propeller Wash. *Journal of Hydraulic Engineering*, 139(9), pp. 1003-1012.

Ishii, M., Hibiki, T. (2006). Thermo-fluid dynamics of two-phase flow, Springer.

Jensen, K. D. (2004). Flow Measurements. *Journal of the Brazilian Society of Mechanical Sciences and Engineering*, 26(4), pp. 1678-5878.

Johnston, H.T., Elsawy, E.M., Hamill, G.A., McKillen, H.G., (1985). A Study of Scour and Deposition near a Berth Structure Caused by the Propulsion Action of Manoeuvring Ships. International Association for Hydraulic Research, 21st Congress, Melbourne, Australia.

Johnston, H.T., Hamill, G.A., Wilson, P.R., Ryan, D. (2013). Influence of a boundary on the development of a propeller wash. Ocean Eng. 61, 50-55

Kalinske, A. A. (1947). "Movement of Sediment as Bed-Load in Rivers, Transactions of the American Geophysical Union, vol. 28, no. 4.

Kang, D.H., Nagarajan, V., Hasegawa, K. (2008). Mathematical Model of Single-Propeller Twin-Rudder Ship. Journal Marine Science Technology 13:207-222.

Kang, D.H., Nagarajan, V., Gonno, Y. (2011). Installing Single Propeller Twin-Rudder System with Less Asymmetric Manoeuvring Motions. Ocean Engineering 38:1184-1196.

Keenan, L. and Chapin O. (2009). "Laser Doppler Velocimetry." Final Report, Physic 173: Biophysic Laboratory. Retrieved from: https://physics.ucsd.edu/neurophysics/courses/physics_173_273/173_paper_final.pdf

Kim, Y.G., Kim, S.Y., Kim, H.T., Lee, S.K., Yu, B.S. (2007). Prediction of the maneuverability of a large container ship with twin propeller and twin rudders. *Journal of Marine Science and Technology 12*. pp. 130-138.

Lam, W. H., Hamill, G.A., Robinson, D.J., Raghunathan, S. (2010). Observations of the Initial 3D Flow from a Ships Propeller. Ocean Eng. 37, 1380–1388.

Lam, W. H., Hamill, G.A., Song, Y.C., Robinson, D.J., Raghunathan, S. (2011a). A Review of the Equations Used to Predict the Velocity Distribution within a Ship's Propeller Jet. Ocean Eng. 38 (1), 1–10.

Lam, W., Hamill, G.A., Song, Y.C., Robinson, D.J., Raghunathan, S. (2011b). Experimental Investigation of the Decay from a Ship's Propeller. China Ocean Eng., 252 (2).

Lam, W.H., Song, Y., Raghunathan, S., Hamill, G., Robinson, D. (2011c). Investigation of a Ship's Propeller Jet using Momentum Decay and Energy Decay. *Canadian Journal of Civil Engineering*, 38 (1-11), 6, 1-6.

Lam, W.H., Hamill, G.A., Robinson, D., Raghunathan, S., Song, Y.C. (2012a). Analysis of the 3D Zone of Flow Establishment from a Ship's Propeller. *KSCE Journal of Civil Engineering*, 16(4), 465-477.

Lam, W.H., Hamill, G.A., Robinson, D.J., Raghunathan, S. (2012b). Semi-empirical Methods for Determining the Efflux Velocity from a Ship's Propeller. Appl. Ocean Res. 35, 14–24.

Lam, W.H., Robinson, D.J., Hamill, G.A., Zhao, J.F., Jia, M. (2012c). Time-averaged velocity and turbulence intensity at the initial downstream flow from a six-bladed ship propeller. Ocean Eng. 51, 85–93.

Lam, W.H., Robinson, D.J., Hamill, G.A., Johnston, H.T. (2012d). An Effective Method for Comparing the Turbulence Intensity from LDA Measurements and CFD Predictions within a Ship Propeller Jet. Ocean Engineering, 52, 105-124.

Lee, S.K., Fujino M., Fukasawa T. (1988). A Study on the Manoeuvring Mathematical Model for a Twin-Propeller Twin-Rudder Ship. Journal Soc. Nav. Archit. Japan 163:109-118

Lee S.K., Fujino M. (2003). Assessment of Mathematical Model for the manoeuvring Motion of a Twin-Propeller Twin-Rudder Ship. ISP50:109-123.

Launder, B.E., Reece, G.J. (1975). Progress in The Development of a Reynolds-stress Turbulence Closure. *Journal of Fluid Mechanics*, 68(3), pp. 537-566.

Launder, B.E., Spalding, D.B. (1972). Lectures in Mathematical Models of Turbulence. Academic Press, London, England.

McGarvey, J.A., (1996). "The Influence of The Rudder on The Hydrodynamics and The Resulting Bed Scour, of a Ship's Screw Wash," Ph.D. Thesis, Thesis submitted to the Queen's University of Belfast for the degree of Doctor of Philosophy.

Mohamed, M.S., and McCorquodale, J.A. (1992). Short-term Local Scour. *J. Hydr. Res.*, 30(5), 685-699.

Pantan, R. L., (1984). "Incompressible Flow." John Wiley & sons. p. 712.

Petersson, P., Larson, M., Johnsson, L. (1996). "Measurements of The Velocity Field Downstream of an Impeller", Journal of Fluids Engineering Centre, Cranfield.

PIANC. (2015). Report n° 180 - 2015 Guidelines for protecting berthing structures from scour caused by ships.

Pierson, Thomas C. (2005). "Hyperconcentrated flow—transitional process between water flow and debris flow." Debris-flow hazards and related phenomena, pp. 159-202.

Prosser, M. (1986). Propeller Induced Scour. Technical Report, BHRA Project RP A01415, The Fluid Engineering Centre, Cranfield.

Qurrain, R. (1994). Influence of the sea bed geometry and berth geometry on the hydrodynamics of the wash from a ships propeller,'' PhD thesis, Queens University of Belfast.

Rajaratnam, N. and Berry, B. (1977). Erosion By Circular Turbulent Wall Jets. *Journal of Hydraulic Research*, 15(3), 277-289.

Rajaratnam, N. (1981). Erosion by Plane Turbulent Jets. *Journal of Hydraulic Research*, 19(4), 339-358.

Ryan, D. (2002). "Methods for Determining Propeller Wash Induced Scour in Harbours." Ph.D. Thesis. Thesis submitted to the Queen's University of Belfast for the degree of Doctor of Philosophy.

Shields, A. (1936). "Anwendung der Ahnlichkeitsmechanik und Turbulenz forschung auf die Geschiebebewegung", Mitteil, Preuss, Versuchsanst. Wasser, Erd, Schiffsbau, Berlin, Nr. 26.

Shih, T. H., and Liou, W. W. (1995). A New k-ε Eddy-Viscosity Model for High Reynolds Number Turbulent Flows-Model Development and Validation. Computer Fluids, 24(3), 227-238.

Spalart, P., and Allmaras, S. (1992). " An One-equation Turbulence Model for Aerodynamic Flows." Technical Report AIAA-92-0439, American Institute of Aeronautics and Astronautics.

Steward, D. P. J., Hamill, G.A., Johnston, H.T. (1991). "Velocities in a Ship's Wash". In Proceedings of International Symposium on Environmental Hydraulics, Rotterdam.

Steward, D. P. J. (1992). "Characteristics of a Ship's Screw Wash and the Influence of Quay Wall proximity". Thesis submitted to the Queen's University of Belfast for the degree of doctor of philosophy.

Stoye, T. (2011) Propeller Design and Propulsion concepts for Ship Operation in Off-Design Condition. Second International Symposium on marine Propulsors smp'11, Hamburg, Germany, June 2011.

Sui, J., Faruque, M.A.A., Balachandar. R. (2008). Influence of channel width and tailwater depth on local scour caused by square jets. *J. Hydro-Environment Res.* 2(1), 39–45.

Sumer, B.M., Fredsøe, J. (2002). The Mechanics of Scour in the Marine Environment. World Scientific Publisher, ISBN: 9810249306, 552p.

Techet, A.H. (2004). Hydrodynamic for Ocean Engineers: Reading: Propelelrs. Retrieved from: http://web.mit.edu/13.012/www/handouts/propellers_reading.pdf

Verhey, H.J. (1983). "The Stability of Bottom and Bank Subjected to the Velocities in the Propeller Jet Behind Ships." Delft Publication No 303, April 1983, Delft Hydraulics Laboratory, Netherlands.

Verhey, H. J., et al. (1987). ''Experiences in The Netherlands with quay structures subjected to velocities created by bow thrusters and main propellers of mooring and unmooring ships.'' *PIANC, Bull. No. 58*, 69–88.

Whitehouse, R. (1998). "Scour at Marine Structures: A Manual for Practical Applications." Thomas Telford Publisher, ISBN: 0727726552.

Wilcox, D.C. (1998). "Turbulence Modelling for CFD." DCW Industries, Inc, La Canada, California.

LIST OF PUBLICATIONS AND PAPERS PRESENTED

Manuscript List

No	Penerbitan/ Journal	Tajuk Penerbitan/ Title of Journal	Status
1.	Journal of Engineering Research	Estimation of Ship's Propeller Wash Induced Scour using VOF Method	Under Review
2.	Journal of Chinese Institute of Engineers	Experimental Investigation on Axial Velocity Distribution for Ship-Twin-Propeller Jets	Revision submitted
3.	Journal of waterway, port, coastal and ocean engineering	Experimental Investigation of Ship-Twin-Propeller Wash Induced Scour	Revision submitted

Attended Conferences

No	Conference	Title	Status
1.	ICCOEE 2014	Seabed Condition from Single beam Echo Sounder from Penang Port, Malaysia	Published
2.	IJAS 2016	Estimation of Ship-Propeller Wash Induced Seabed Scour with VOF	Published